Post-combustion CO_2 Capture Using Polyethylenimine Impregnated Mesoporous Cellular Foams

by

Zhengyi Liu

A thesis submitted in partial fulfillment of the requirements for the degree of

Master of Science
in
Chemical Engineering

Department of Chemical and Materials Engineering
University of Alberta

Abstract

In this work, mesoporous cellular foams (MCFs) were synthesized and impregnated with different weight percentage of polyethylenimine (PEI) using wet impregnation method. The synthesized adsorbents were characterized using nitrogen adsorption/desorption, SEM, TEM, and FTIR analysis. The CO_2 adsorption capacity of PEI-impregnated MCFs was measured using thermogravimetric analyzer (TGA). The effects of PEI loadings, adsorption temperatures, and CO_2 partial pressures on CO_2 adsorption performance using PEI-impregnated MCFs were explored. 70 wt % PEI loading was found to be the optimum for the highest CO_2 adsorption capacity of about 5 mmol/g in 95% CO_2/5% N_2 gas mixture and 4 mmol/g in 10% CO2/90% N_2 gas mixture, at 75 °C. The effect of moisture on the CO_2 adsorption performance in simulated flue gases was studied. It was found the CO_2 adsorption performance of PEI-impregnated MCFs can be improved with the presence of moisture, especially at low adsorption temperatures. The adsorbent with optimum PEI loading was then tested for multi-cycle stability and adsorption/desorption kinetics in both humid and dry conditions. Good stability of the adsorbent in multi-cycle tests was found as no significant change in CO_2 adsorption capacity was observed. Various equilibrium adsorption isotherms, such as Langmuir and Freundlich adsorption isotherms, were applied to describe the CO_2 adsorption behavior. Different kinetic models were developed to study the CO_2 adsorption kinetics of this type of adsorbents. John-Mehl-Avrami (JMA) model was found to be well fitted with the experimental data, indicating another possible way to describe the kinetics of CO_2 adsorption process under isothermal conditions. The heat of adsorption of CO_2 adsorption process using PEI-impregnated MCFs was also calculated.

Acknowledgements

I would like to extend my sincere gratitude to my research supervisors, Prof. Rajender Gupta and Prof. Chad Liu, for their countless help and support throughout my course of research. This would not have happened without their continuous help in every phase of my research work.

I also would like to express my thanks to Dr. Deepak Pudasainee and Dr. Arunkumar Samanta for their continuous assistance and support in helping me with the research work. My research work would not have gone smoothly without their wholehearted support.

I would like to thank Dr. Moshfiqur Rahman for his help for my research work. I would like to thank my colleagues, An Zhao, Donghai Lin, Xiaotian Zhang, Nikhil Mittal, Navjot Kaur Sandu, and Mehdi Alipour, for their technical assistance. I would like to express my thanks to all the group members for their cooperation and help in creating a wonderful working environment.

I would like to acknowledge the financial support of Canadian Center for Clean Coal/Carbon and Mineral Processing Technology (C^5MPT).

Table of Contents

List of Figures

List of Tables

Abbreviations

AC	Activated carbon
AN	Acrylonitrile
AAPD(%)	Average absolute percentage deviations
APTES	3-aminopropyl-triethoxysilane
BET	Brunauer Emmett Teller
BJH	Barrett Joyner Halenda
B_2CNTs	boron carbon nanotubes
Btu	British thermal units
CCS	Carbon Capture and Storage
CFCMS	Carbon fiber composite molecular sieves
CPAHCL	3-chloropropylamine- hydrochloride
CMS	Carbon molecular sieves
CNT	Carbon nanotube
DEA	Diethanolamine
DETA	Diethylentriamine
ECH	Epichlorohydrin
EIA	Energy Information Administration
EP	Epoxy resin
FTIR	Fourier transform infrared spectroscopy
IG-MWCNTs	Industrial grade multi-walled carbon nanotubes

IPCC	Intergovernmental Panel on Climate Change
IEA	International Energy Agency
IPPC	Intergovernmental Panel on Climate Change
JMA	John-Mehl-Avrami
KIER	Korea Institute of Energy Teserach
MA	Mesoporous alumina
MCFs	Mesoporous cellular foams
MEA	Monoethanolamine
MDEA	Methyldiethanolamine
MOFs	Metal organic framework
NGCC	Natural gas combined cycle
PC	Pulverized coal
PEI	Polyethylenimine
PEHA	Pentaethylenehexamine
PEG	Polymeric support. Polyethylene glycol
PMMA	Polymathyl methacrylate
PSA	Pressure swing adsorption
SEM	Scanning electron microscopy
SG	Silica gel
SWCNT	Single-walled carbon nanotube
TEM	Transmission electron microscopy
TEOS	Tetraethyl orthosilicate

TEPA	Tetraethylenepentamine
TGA	Thermogravimetric analysis
TVSA	Temperature/vacuum swing adsorption
TSA	Temperature swing adsorption
UNFCCC	United Nations Framework Convention on Climate Change
VSA	Vacuum swing adsorption
WSI	Wet support impregnation

Nomenclature

A	Koble-Corrigan isotherm constant ($L^n mg^{1-n}/g$)
a	Scale parameter
a_K	Khan isotherm model exponent
B	constant related to heat of sorption of Temkin isotherm
B	Koble-Corrigan isotherm constant $(L/mg)^n$
b	Temkin isotherm constant
b	Shape parameter
b_K	Khan isotherm model exponent
D_c	Cell diameter
D_w	Window diameter
$-\Delta H$	The heat of adsorption
K_F	Empirical constant of Freundlich isotherm
k_L	Adsorption rate constant
k_n	constant for fractional-order model
K_s	Sips isotherm model constant (L/g)
k_T	Temkin isotherm equilibrium binding constant
K_T	Toth isotherm constant (mg/g)
k	Rate constant for pseudo-first order model/ pseudo-second order model
p_0	Initial partial pressure of CO_2
q_e	Equilibrium CO_2 adsorption capacity

q_{max}	Maximum monolayer coverage capacity
q_s	Theoretical isotherm saturation capacity (mg/g)
q_t	Adsorption capacity at time *t*
Q	Measure of the adsorption heat
mmol/g	(mmol of CO_2) / (g of adsorbent)
mg/g	(mg of CO_2) / (g of adsorbent)
mmol N/g	(mmol of N) / (g of adsorbent)
R_L	Langmuir separation factor
n	adsorption intensity
R	universal gas constant (8.314 J/mol/K)
R^2	Coefficient of determination
t	Toth isotherm constant
X	Fractional extent of crystallization
S_{BET}	Specific surface area
T	Absolute temperature
T_0	Reference temperature
V_{Tot}	Total pore volume
ω	Polanyi potential
α_s	Sips isotherm model constant
β_s	Sips isotherm model exponent
C_e	Equilibrium constant (mg/L)
a_T	Toth isotherm constant (L/mg)

α_{RP}	Radke-Prausnitz isotherm model constant
γ_R	Radke-Prausnitz isotherm model constant
β_R	Radke-Prausnitz isotherm model exponent
χ	an adimensional parameter
θ	The fractional coverage of the adsorbent

Chapter 1

Introduction

1.1 Background

Nowadays, global warming as a result of greenhouse gas emissions has captured worldwide attention. Many organizations such as United Nations Framework Convention on Climate Change (UNFCCC), the Intergovernmental Panel on Climate Change (IPCC) and International Energy Agency (IEA) have been attempting to solve this problem. UNFCCC [1] proposed a long term goal of controlling the increase in global average temperature below 2 °C to achieve their ultimate objective of stabilizing greenhouse gas concentrations in the atmosphere at a level that would prevent dangerous anthropogenic interference with the climate system. According to IPCC's Fifth Assessment Report: Climate Change 2013 (AR5)，there is strong evidence showing that human activities make a large contribution to the climate change [2]. Although there are other greenhouse gases including water vapor, methane, nitrous oxide, hydrofluorocarbons, perfluorocarbons and sulfur hexafluoride playing a role in global warming, the main focus is on CO_2 not only because it has the most contributing radiative warming effect, but also because it has the largest share of global greenhouse gas emissions.

1.1.1 Sources of CO_2

According to Energy Information Administration (EIA)'s released International Energy Outlook 2013 (IEO2013), the global energy consumption will grow by 56%, from 524 quadrillion British thermal units (Btu) to 820 quadrillion Btu between 2010 and 2040 [3]. Although many renewable and nuclear energies have been developed and are growing fast, 80% of global energy consumption will still be based on fossil fuels throughout 2040 [3]. Figure 1.1 shows the primary energy supply in the year 1971 and 2011[4]. It can be seen from Figure 1.1 that the global total amount of energy supply increased more than double between 1971 and 2011 resulting from the high demand of economic growth. The technology of using combustion of fossil fuels to produce energy still dominates.

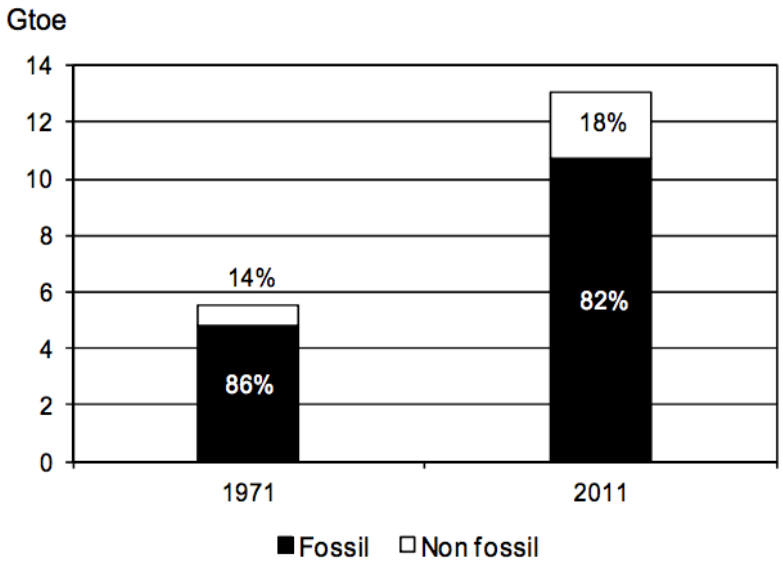

Figure 1.1 World primary energy supply [4].

According to International Energy outlook 2013 from EIA, fossil fuels including petroleum, coal and natural gas, will still supply more than three-fourths of total world energy in 2040 (see

Figure 1.2) [2]. According to IEA's world Energy Outlook 2013, around 31.6Gt of global energy-related CO_2 was emitted in 2012, which reached its historic high [5]. Table 1.1 presents the distribution of large stationary CO_2 emission sources according to the type of emission generating process [6]. As can be seen from Table 1.1, the use of energy takes up the largest source of emissions.

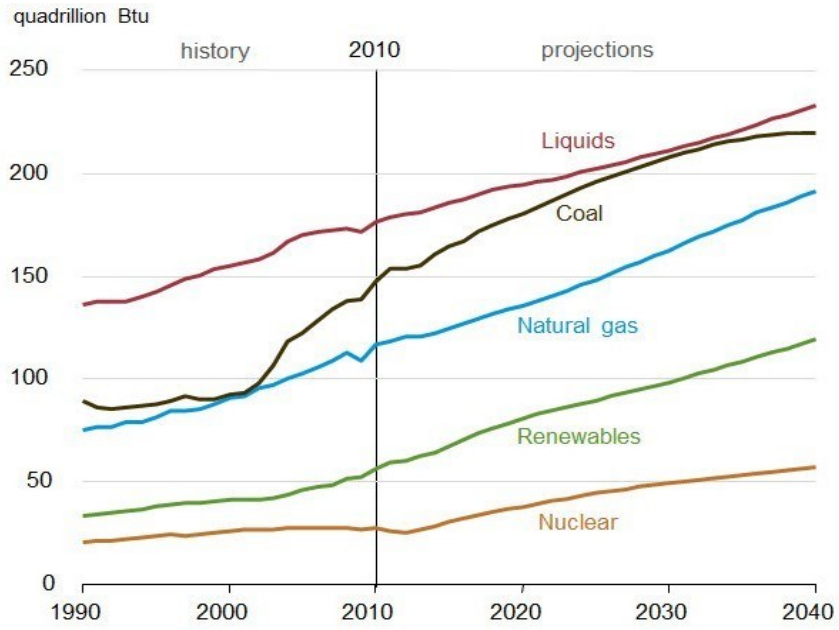

Figure 1.2 World energy consumption by fuel type between 1990 and 2040 [3].

Table 1.1 summary of large stationary CO_2 sources with emissions of more than 0.1 $MtCO_2$ per year [6].

Process	Number of sources	Emissions (Mt CO_2/year)
Fossil fuels		
Power	4,942	10,539
Cement production	1,175	932
Refineries	638	798
Iron and steel industry	269	646
Petrochemical industry	470	379
Oil and gas processing	Not available	50
Other sources	90	33
Biomass		
Bioethanol and bioenergy	303	91
Total	7,887	13,466

1.1.2 Carbon capture and storage (CCS)

For now, the technological options available for stabilization of atmospheric greenhouse gas concentration include:

1. Replace carbon intensive fuels with less carbon intensive fuels, e.g. use natural gas instead of coal;
2. Apply renewable energy sources;
3. Use nuclear power;
4. Increase energy efficiency;
5. Capture and store CO_2 chemically or physically;
6. Sequester CO_2 through enhancement of natural sinks by biological fixation.

All these mitigation options work together to control the overall atmospheric greenhouse gas concentration within a healthy level. In this work, we focus on the Carbon Capture and Storage (CCS) technology. It is considered as a potential way to cut the CO_2 concentration down to an

acceptable level. In this approach, CO_2 arising from combustion of fossil fuels or processing industries would be captured, compressed to transport and finally stored in geological formations, in the ocean, in mineral carbonates, or for industrial use.

There are typically three approaches to capture CO_2: pre-combustion capture, post-combustion capture, and oxy-fuel combustion capture. Figure 1.3 below illustrates the process of CO_2 capture using different technologies.

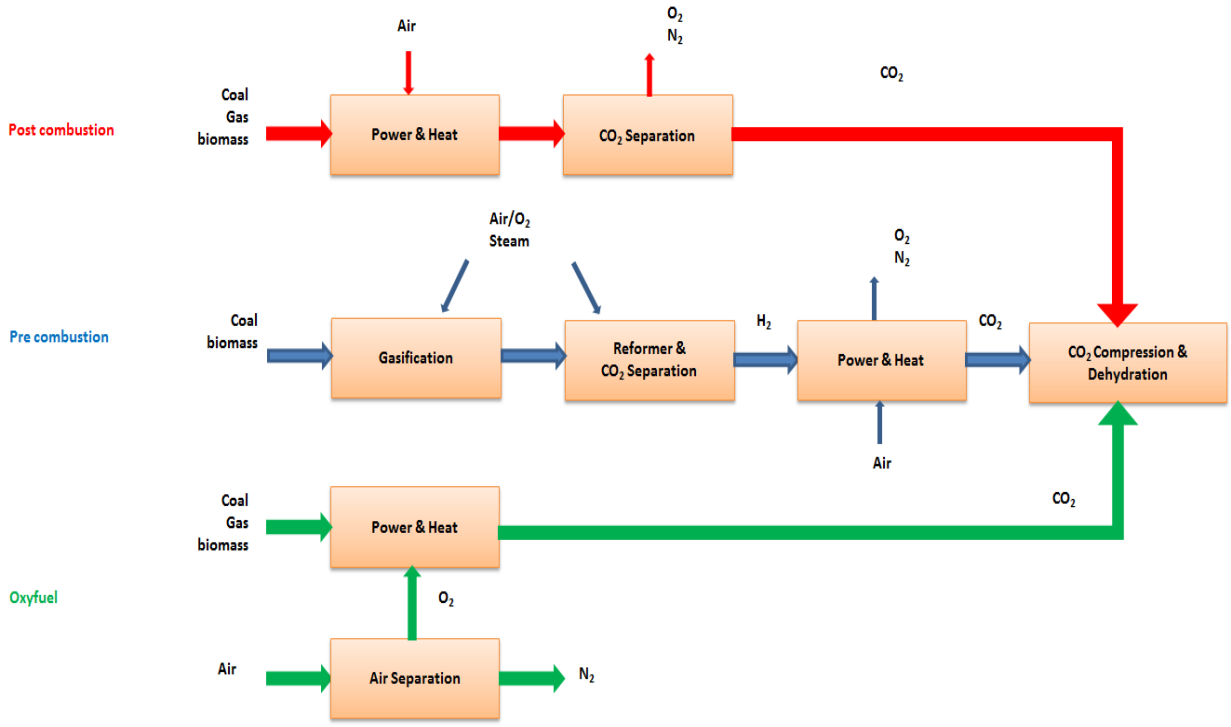

Figure 1.3 Overview of CO_2 capture approaches and processes.

For post-combustion carbon capture, CO_2 would be captured from the flue gases produced by the combustion of fossil fuels in air. In the most widely used process, CO_2 with low concentration (<15% by volume) is usually captured by a liquid solvent to form CO_2-bounded solvent. This

amine-CO_2 complex can be decomposed by heat to release high concentration of CO_2. This post-combustion capture system can be economically applied to modern pulverized coal (PC) power plants or natural gas combined cycle (NGCC) power plants. The most commonly used organic solvent for post-combustion system is 20-30 wt% monoethanolamine (MEA). Although this process is effective to capture CO_2 with high purity and recovery, additional units，such as desulphurization unit, would be necessary to remove the impurities from the flue gases before capture process in order to prevent the contamination of the solvent. For pre-combustion carbon capture, fossil fuels would be heated in steam and air or oxygen to produce a gaseous mixture of carbon monoxide and H_2 (syngas). The mixed gas will then be sent into a catalytic converter. The carbon monoxide would react with steam to produce more H_2 and CO_2. The H_2 and CO_2 can be separated. CO_2 stream can be compressed for storage. The H_2 stream is a carbon free energy, which can be combusted to produce power and heat. This process is widely applied in fertilizer manufacturing and hydrogen production. In oxy-fuel combustion, pure oxygen is applied for the combustion of fossil fuels instead of air. This resulted in a flue gas comprising mainly CO_2 and H_2O. Pure oxygen can be separated from air through cryogenic technology. This technology is currently in the demonstration phase.

The concentration and partial pressure of CO_2 in the gas stream, and the fuel type are important factors in selecting the capture system. As shown in Table 1.2, CO_2 concentration in the gas stream varies depending on the specific conditions in different industrial facilities.

Table 1.2 Typical CO_2 concentrations in various capture process [6].

Source	CO_2 concentration % vol (dry)	CO_2 partial pressure (atm)
Natural gas fired boiler	7-10	0.07-0.1
Gas turbines	3-4	0.03-0.04
Oil fired boilers	11-13	0.11-0.13
Coal fired boilers	10-14	0.1-0.14
IGCC	4.5-6	0.045-0.06

1.1.3 Technologies for post-combustion carbon capture

Post-combustion carbon capture technology can be retrofitted to existing generation facilities such as coal-fired power plants. This system is considered to be acceptable for retrofit applications, as it provides significant flexibility and low technology risk, compared with the other options. Figure 1.4 represents a schematic diagram of post-combustion CO_2 capture. This system usually contains two units: capture unit and regeneration unit.

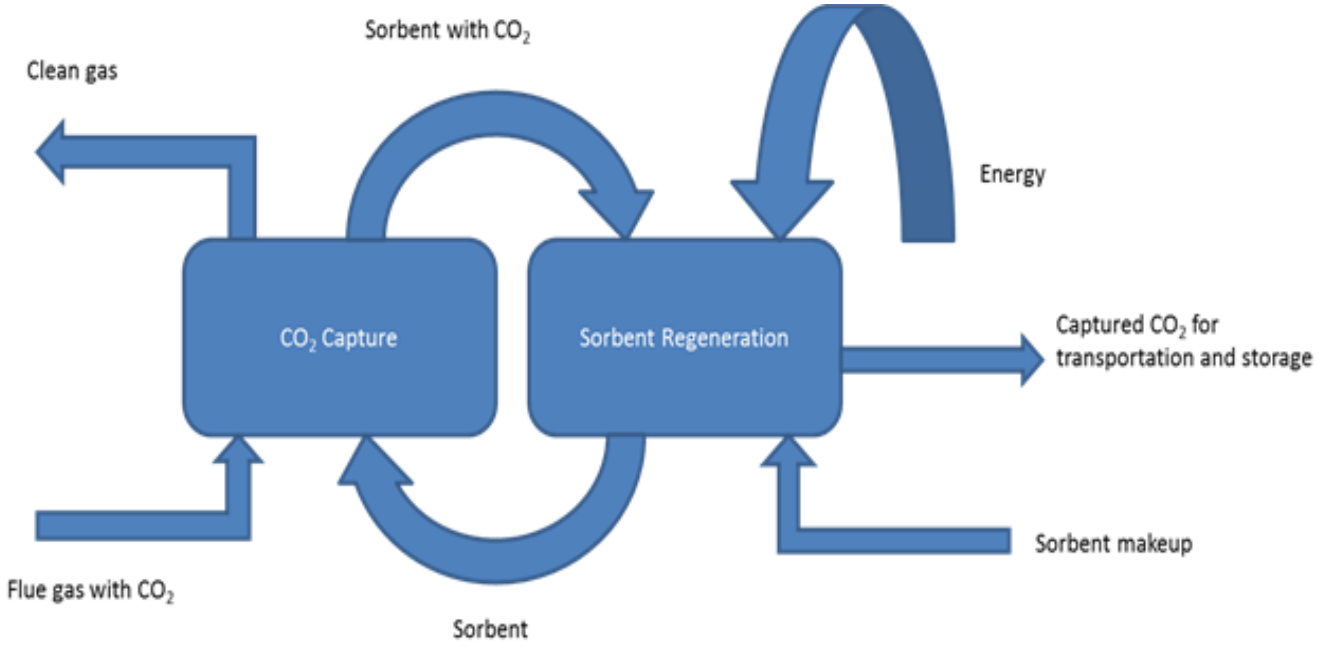

Figure 1.4 Schematic diagram of post-combustion CO_2 capture.

Amine-based absorption processes for post-combustion CO_2 capture have been widely used for decades of years. Aqueous solutions of MEA, diethanolamine (DEA), and methyldiethanolamine (MDEA) are commonly used as absorbents. Compared with other existing post-combustion capture process, amine-based absorption processes possess high CO_2 adsorption capacity, good CO_2 selectivity and fast kinetics. A representative diagram of conventional amine-based absorption processes in post-combustion CO_2 capture is presented in Figure 1.5.

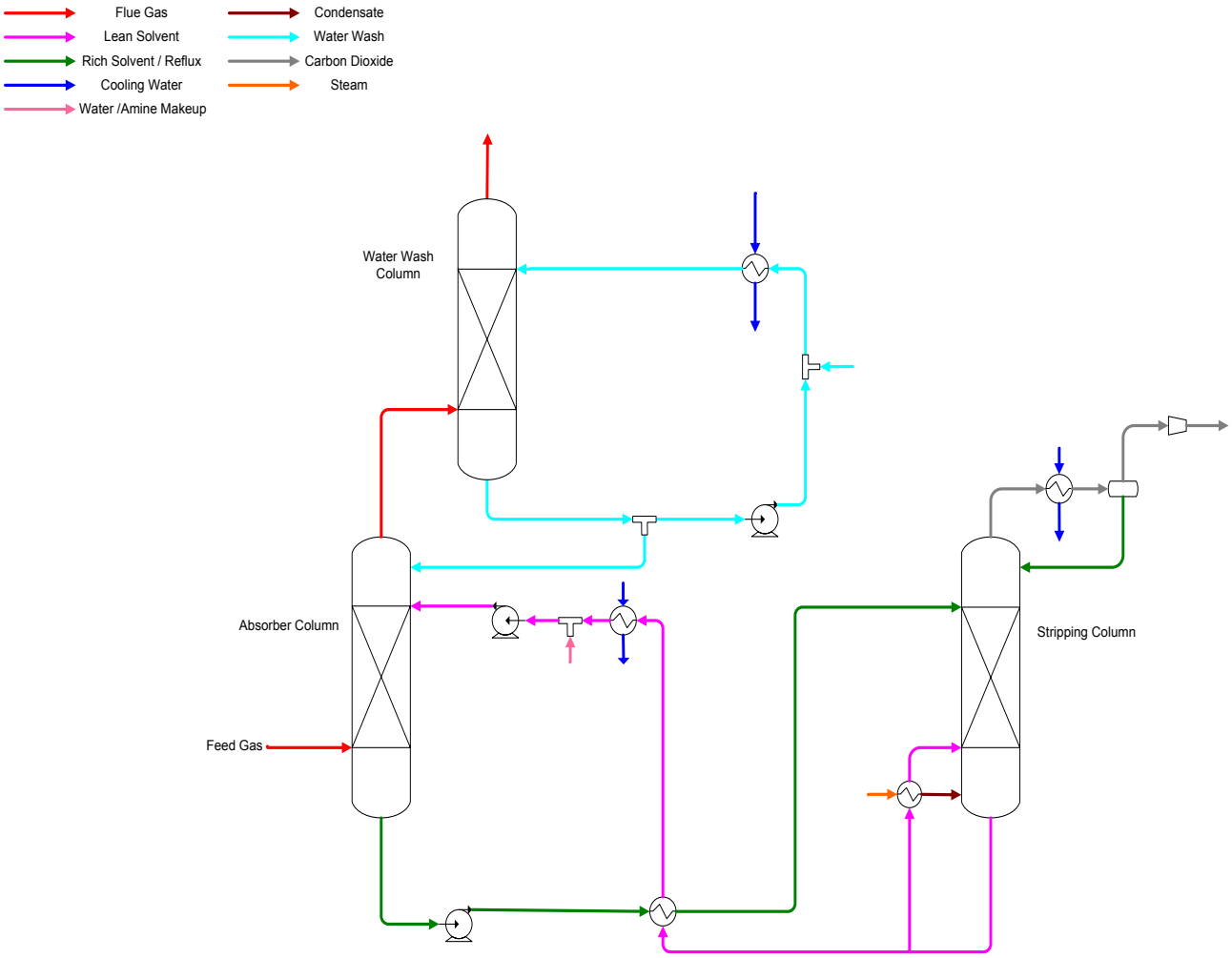

Figure 1.5 CO_2 capture using conventional amine-based absorption process.

In this conventional amine-based absorption process, the cooled near atmospheric pressure flue gases from the power plant are sent into an absorber where the CO_2 is counter-currently contacted with an aqueous amine solution. The CO_2 can be removed from the flue gases through bounding with amines. The rich solvent is then preheated by the lean solvent and then sent to the top of the stripper. The CO_2 is removed from the solvent by heating up the solution through the re-boiler, which results in an energy penalty. The lean solvent is then cooled by the heat exchanger and a cooler before going back to the top of the absorber. A condenser is used to condense the water vapor from the sour gas. Though this system is effective, it suffers from several drawbacks such as corrosion problems, high energy consumptions for solvent regeneration step, solvent degradation, and limited amine concentration in the aqueous phase due to viscosity and foaming issues. In addition, large volumes of gases that need to be handled require large scale equipment, resulting in higher capital costs. The estimated energy penalty for the solvent regeneration process is 20-30% of the total energy output of the power plant. Figure 1.6 shows the amount of CO_2 emitted from a reference coal-fired power plant without CCS process and the amount of CO_2 captured from a comparable plant with the same amount of energy output with CCS [6]. For a reference coal-fired power plant without CCS process generating 500 MW, it emits 3.0 $MtCO_2$ per year. A comparable plant with the same amount of energy output with CCS and 90% CO_2 capture emits 0.43 $MtCO_2$ per year, which is 86% less than that without capture process.

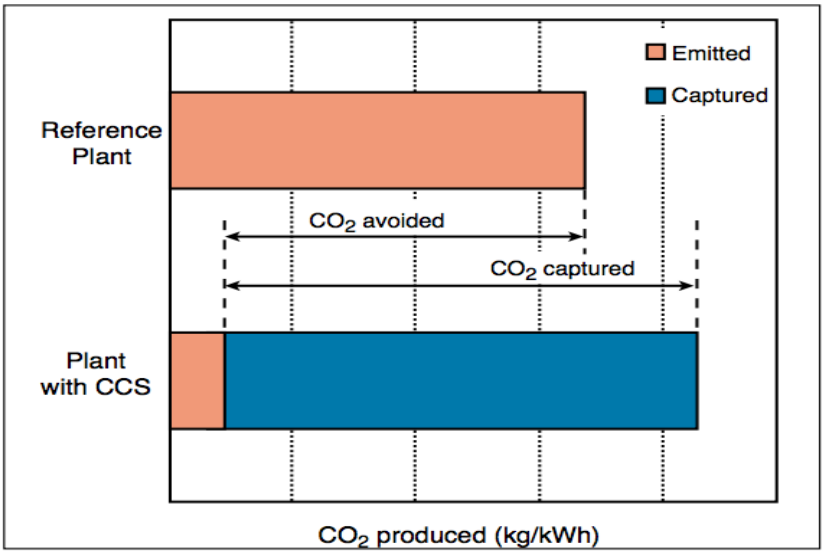

Figure 1.6 CO_2 capture and storage from power plant [6].

Recently, adsorption on porous solid sorbents through pressure and temperature swing approaches is an emerging alternative that aims at reducing the costs of regeneration step in post combustion process. Basically, there are two types of adsorption: physisorption and chemisorption. The physisorption process involves the CO_2 removal from the flue gases through van der Waals forces between the CO_2 molecule and adsorbent surfaces using the physisorbents, such as activated carbons, zeolites and metal organic frameworks (MOFs). For chemisorption process, solid adsorbents with incorporation of specific functional groups are used to improve the CO_2 adsorption capacity. It involves chemical reactions between the CO_2 molecules and adsorbents. Compared to the absorption process, adsorption process with solid adsorbents has many advantages, such as higher CO_2 adsorption capacity, less energy consumption for regeneration process and ease of handling.

1.2 Objectives

Among all the available sorbents for post-combustion CO_2 capture, amine-functionalized MCFs, as one of the solid sorbents for CO_2 capture, are outstanding and outperformed over others because of their unique structural characterization. Although some researchers have been working on PEI-impregnated MCFs, a systematic study of this type of adsorbent is still uncompleted. The main objectives of the current study i.e. synthesis and CO_2 capture performance evaluation of PEI-impregnated MCFs adsorbents are as follows:

1. To synthesize PEI impregnated MCFs and to characterize the adsorbent by nitrogen adsorption/desorption, SEM, TEM, and FTIR instruments.
2. To evaluate the CO_2 adsorption performance using PEI-impregnated MCFs in terms of PEI loading, CO_2 concentration, adsorption temperature, presence of moisture, adsorption/desorption kinetics and multi-cycle stability.
3. To describe the CO_2 adsorption behavior using various adsorption equilibrium isotherms.
4. To study the kinetics of CO_2 adsorption using different kinetic models.
5. To determine the heat of adsorption of CO_2 adsorption process using PEI-impregnated MCFs.

Chapter 2

Literature Review

2.1 Desired properties of adsorbents

For the selection of adsorbent materials for the post-combustion CO_2 capture, the following properties need to be considered.

- Adsorption capacity

Adsorption capacity is one of the most important parameters for evaluating the working performance of a solid sorbent for CO_2 capture. High adsorption capacity can reduce the total amount of adsorbents needed for the unit volumetric flow of flue gas. It also can reduce the capital cost involved in the CO_2 capture process since the size of the equipment will be reduced.

- Selectivity of CO_2

Flue gas from coal-fired power plant is mixed in compositions containing N_2, CO_2, O_2, NO_x, SO_x, moisture, particulates etc. Making sure that the solid sorbents have high CO_2 selectivity over than components in the flue gases is of great importance.

- Availability of materials

The availability of the solid adsorbent and its preparation procedures should be convenient. Complexity of material synthesis will make the capture process lengthy and less efficient.

- Energy involved for regeneration

The regeneration energy for CO_2 adsorption process should be low enough to lower the cost of capture. The heat of adsorption measures the amount of energy required for regeneration process.

For the chemisorption reaction, the heat of adsorption is in the range of 60-90 kJ/mol that for the physisorption process is in the range of 25-50 kJ/mol.

- Adsorption/desorption kinetics

The kinetics of adsorption and desorption reactions is another vital parameter to evaluate a solid adsorbent. It determines the time needed for adsorption/desorption process. Fast kinetics implies high CO_2 adsorption capacity even within first few minutes of adsorption process.

- Stability of adsorption capacity after adsorption/desorption cycles

Solid sorbents with longer working life span would be more competitive for practical and economical applications. Good re-generability and stability of a solid sorbent can maximize the utilization for each batch of adsorbents and reduce the total amount required.

- Mechanical strength

A good adsorbent should have strong and stable mechanical strength to be able to work in specified conditions, such as high operating temperatures, high pressure streams and attrition.

2.2 Physisorption adsorbents

There are many solid sorbents removing CO_2 from the flue gases through physical adsorption, such as zeolites, metal organic frameworks (MOFs), activated carbons, and silica gel. The reaction mechanism for CO_2 capture via physisorption can be presented as follows:

$$CO_2 + \text{sorbent with high porosity} \leftrightarrow CO_2 \sim \text{sorbent}$$

Basically, the adsorption occurs when the CO_2 molecules and sorbent surface attract with each other through the following possible forces:

- Van der Waals forces between the CO_2 molecules and sorbent surface

- Pole-pole interactions between the quadrupole of CO_2 and polar sites of the sorbent surface
- Pole-ion interactions between the quadrupole of CO_2 and the ion sites of the sorbent surface

2.2.1 Activated carbon based solid sorbents

Activated carbons possess some unique advantages, which make them outstanding as CO_2 adsorbents, such as low cost of raw material, wide availability and high CO_2 adsorption capacity at low temperatures, ease of regeneration. Generally speaking, there are two steps which can convert carbonaceous materials into activated carbons: carbonization and activation. The properties of the resultants depend on the various factors, such as the nature of the starting materials, the activating agent and the conditions of the carbonization and activation processes [7]. Various biomass including agricultural materials such as olive stones, corncobs, bagasse, wheat straw, sawdust, peach shells, and bark can be considered as the precursors of activated carbons. Researchers have utilized different activation methods with various activating agents to modify the surface structure of the adsorbents. For physical activation, the most commonly used activating agents are CO_2, steam or their combination. For chemical activation, the common activating agents are potassium hydroxide, phosphoric acid and zinc chloride. The surface properties of activated carbon based sorbents derived from various precursors using different activation methods are summarized in Table 2.1.

Table 2.1 Textural characteristic of various activated carbons using different activation methods.

Sorbents	Precursors	Activating agent	Activating T (°C)	S_{BET} (m^2/g)	V_{total} (cm^3/g)	Ref.
AC	Olive stones	CO_2	800	1079	0.502	[8]
AC	Spruce	Steam	792	664		[9]
AC	Orange skin	CO_2	700	1185	0.41	[10]
AC	Olive bagasse	Steam	900	1106	0.6067	[11]
AC	Anthracites	Steam	850	928	0.442	[12]
AC	Wood	Phosphoric acid		1361		[13]
AC	Peat	Steam		942		[13]
AC	Almond shell	CO_2	700	1090	0.5	[14]
AC	Palm shell	CO_2	850	1410	0.71	[15]
AC	Oil palm shell	$ZnCl_2$ & N_2	500	1118	0.51	[16]
AC	Palm shell	$ZnCl_2$ & CO_2	850	1118	0.42	[17]
AC	Palm shell	H_3PO_4 & CO_2	850	1652.89	0.89	[17]

Plaza et al. [7] applied CO_2 as the activating agent for the surface modification of carbon materials. The activation process was conducted at 800 °C to different burn-off degrees. They found that the activated samples presented a higher CO_2 adsorption capacity up to 2.11 mmol/g and 0.75 mmol/g of adsorbed CO_2 at 25 °C and 100 °C. The CO_2 adsorption capacity of four samples (AC1, AC2, charcoal and virgin bituminous coal) were compared at four constant temperatures up to 10 bar by Radosz et al. [18]. It was presented that the CO_2 adsorption capacity for four samples increased with pressures and decreased with temperatures. The sample of AC1 exhibited higher CO_2 adsorption capacity than that of others due to its high surface area and degree of activation. It was found that the selectivity of CO_2 over N_2 decreased dramatically at high pressures, indicating that the process is favored at low pressure. AC1 achieved its highest CO_2 adsorption capacity of 2.27 mmol/g at 1 bar and 5.9 mmol/g at 10 bar with the adsorption temperature of 25 °C. De Souza et al. [19] synthesized mesoporous carbons with high surface area and large pore volume for CO_2 capture using triblock copolymer F127 as the structure

directing agent and formaldehyde and either phloroglucinol or resorcinol as carbon precursors. This sorbent showed only moderate CO_2 adsorption capacity. KOH activation was used by De Souza et al. [19] for CO_2 adsorption enhancement. It was reported that the treated activated carbons showed 2-3 fold increase in the specific surface area. The CO_2 adsorption capacity was improved up to 4.4 mmol/g at ambient pressure and 25 °C, and 7 mmol/g at ambient pressure and 0 °C. Balsamo et al. [20] prepared an activated carbon (F50) using a mixture of coal tar pitch and furfural (50/50 wt%) as precursors followed by steam activation for CO_2 capture. The CO_2 adsorption/desorption tested were conducted in a fixed-bed lab-scale column with different CO_2 concentrations (1-15% by volume) and three temperatures (30, 50, 80 °C). It was found that the breakthrough curves became steeper with an increase in CO_2 concentrations under the same temperature due to the increased mass transfer rates. For each concentration of CO_2, the increase in temperature resulted in faster adsorption kinetics and lower CO_2 adsorption capacity. The CO_2 adsorption capacity of the activated carbon F50 was 0.61 mmol/g under typical flue gases with 15% CO_2 at 30 °C. It was also shown that F50 can be easily regenerated at moderate temperatures. The thermal stability of F50 was good with multi-cycle studies of adsorption/desorption. The CO_2 adsorption capacity maintained the same after 15 cycles of adsorption/desorption. Zhu et al. [21] successfully synthesized high surface area activated carbons from paulownia sawdust through carbonization and activation with KOH. The CO_2 adsorption performance was investigated focused on the effect of mass ratio between KOH and paulownia sawdust, activation temperatures, and activation time. It was found that the highest CO_2 adsorption capacity was 8.0 mmol/g at 0 °C and 1 bar, with the optimal mass ratio of KOH and paulownia sawdust equals to 4, activation temperature of 700 °C and activation time 1 hour.

Pine nut shell-derived activated carbon was synthesized by Deng et al.[22]. It was indicated that the micro-pore size of the activated carbon was highly dependent on the mass ratio of KOH/biomass and activation temperatures. The best activated carbon samples prepared at the KOH/biomass ratio of 2, activation temperature of 700 °C, could achieve the highest CO_2 adsorption capacity up to 7.7 mmol/g at 0 °C and 1 bar, and 5.0 mmol/g at 25 °C and 1 bar.

Recently, Lee et al. [23] used pitch based biomass as the precursors to synthesize activated carbons by KOH activation for CO_2 capture. The activated carbon synthesized with a KOH weight ratio of 2 showed the highest CO_2 adsorption capacity of 4.61 mmol/g at 1 bar and 25 °C due to its higher surface area (1442 m^2/g) and higher pore volume (0.504 cm^3/g).

Heidari et al. [24] prepared a series of activated carbons from *Eucalyptus camaldulensis* wood by chemical activation with H_3PO_4 and $ZnCl_2$, and carbonization followed by KOH activation. It was found that the activating agent strongly influenced the characteristics of Eucalyptus camaldulensis wood based activated carbons. The resulting surface area and porosity of activated carbons activated by different chemical agents were in the following order: KOH > H_3PO_4 > $ZnCl_2$ indicating that KOH was the most suitable activating agent producing highest surface area and porosity for CO_2 capture. The CO_2 adsorption capacity of 4.1 mmol/g was achieved at 1 bar and 30 °C, which was much higher than that for commercial activated carbons. Table 2.2 shows a summary of CO_2 adsorption capacity of various activated carbons reported in the literature under different temperatures and CO_2 partial pressures.

Table 2.2 A summary of CO_2 adsorption capacity of various activated carbons with CO_2 partial pressures at different temperatures.

Sorbents	S_{BET} (m^2/g)	V_{total} (m^3/g)	T (°C)	P_{CO2} (atm)	CO_2 capacity (mmol/g)	Ref.
AC	1150	0.62	15	1	2.86	[25]
AC	1150	0.62	30	1	2.2	[25]
AC1	809	0.45	25	1	2.27	[18]
AC2	553	0.59	25	1	1.59	[18]
Charcoal	135		25	1	1.59	[18]
Coal	>100		25	1	0.45	[18]
AC	928	0.442	30	1	1.32	[12]
AC	1300	0.6-0.8	25	1	2.6	[26]
AC			15	1	2.5	[27]
AC	954	0.48	25	0.1	0.566	[28]
AC	2829	1.55	25	1	2.92	[29]
AC	1361		30	1	1.6	[13]
AC	942		30	1	2.3	[13]
AC	1727	1.204	25	1	1.89	[30]
AC	1090	0.5	25	1	2.68	[14]
AC	831	0.37	25	0.15	1.18	[14]

AC: activated carbon

2.2.2 Carbon molecular sieves

Carbon molecular sieves (CMS), microporous with high carbon contents, are capable of separating molecules based on their size and shapes due to its high microporosity [31]. In 1997, Burchell et al. [32] developed a carbon fiber composite molecular sieves (CFCMS) based on isotropic pitch derived carbon fibers. The CO_2 isotherms for CFCMS were obtained both volumetrically and gravimetrically. A CO_2 uptake of about 2.27 mmol/g at 30 °C and atmospheric pressure was reported. It was demonstrated that the CO_2 uptake reduced at elevated temperatures. Only 0.91 mmolg/g of CO_2 uptake was achieved when the temperature increased to 100 °C. However, the increase in pressure improved the CO_2 adsorption capacity. The CO_2 uptake for CFCMS under 58 bar and 25 °C was as high as 11.14 mmol/g. Rutherford et al. [33]

conducted analysis of equilibrium and kinetics of batch adsorption of CO_2 using a carbon molecular sieve (commercially manufactured Takeda 5A). They stated that the measurements of CO_2 adsorption indicated no molecular sieving action but instead, micropore diffusion was shown to be rate limiting in the adsorption process. Microporous carbon molecular sieve monoliths from nitrated coal tar pitch were prepared by Alcañiz-Monge et al. [34]. The nitration of coal tar pitch produced the oxidation of the pitch molecules, leading to the decomposition of surface complexes. The resulting narrow microporosity was capable for fast CO_2 adsorption kinetics. Cho et al. [35] modified a carbon molecular sieves through oxy-fluorination for CO_2 capture. The CO_2 adsorption capacity of the modified CMS was improved to 2.07 mmol/g at 25 °C, compared with that of unmodified CMS with 1.60 mmol/g. Wahby et al. [36] compared a series of commercial carbon molecular sieves, prepared from different polymeric precursors in respect of their CO_2 adsorption capacity at atmospheric pressure (1 bar) and three different temperatures (0 °C, 25 °C, 50 °C). The CO_2 adsorption capacities of all the commercial molecular sieves studied by Wahby et al. [36] under 3 different temperatures and 1 bar are summarized in Table 2.3.

Table 2.3 The CO_2 adsorption capacity of different carbon molecular sieves at 1 bar and different temperatures (0, 25 and 50 °C) [36].

Sample/Temperature	Amount of CO_2 adsorbed (mmol/g)		
	0 °C	25 °C	50 °C
C-1012	5.272727	3	1.802273
C-1021	3.727273	2.431818	1.65
C-1003	4.954545	2.840909	1.904545
C-569	3.477273	2.272727	1.552273
C-S	5.045455	3.295455	2.163636
C-1016	0.170455	0.092727	0.076591
C-G60	5.090909	3.727273	2.477273
C-1000	4.022727	2.795455	1.775
C-1018	3.568182	2.659091	1.822727

2.2.3 Carbon nanotubes based solid sorbents

Zhao et al. [37] explored the adsorption behavior of various gas molecules (NO_2, O_2, NH_3, N_2, CO_2, CH_4, H_2O, H_2 and Ar) on single-walled carbon nanotubes (SWNCTs) and bundles using first principle. It was revealed that all gas molecules were weakly adsorbed on SWNTs with small charge transfer. In 2004, Bienfait et al. [38] measured the isosteric heat of adsorption of hydrogen, methane, argon, oxygen and carbon dioxide on single wall carbon nanotube bundles. It was shown that for CO_2, only one set of adsorption sites was observed, which was attributed to the grooves and the interstitial channels. For all other adsorbates, they condensed on high-energy binding sites first and then on the outer rounded surface of the bundles.

More recently, Lithoxoos and his research group [39] investigated the adsorption capacity of SWCNTs bundles experimentally and computationally with pure CH_4, N_2, CO and CO_2 at 25 °C and pressure range from 0.01 to 2.0 MPa. It was concluded that both the experimental and computational adsorption isotherms showed the same qualitative behavior of adsorption in SWCNTs. CO_2 was found to be the most favorable gas and H_2 to be the least one for adsorption.

The behavior of CO_2 and N_2 on adsorption for single walled carbon nano-tubes (CNTs) was simulated by Razavi et al. [40] with the use of Canonial Monte Carlo (CMC). Five different CNTs [(6,6), (7,7), (8,8), (9,9) and (10,10)] with diameters ranging from 0.807 to 1.35 nm were applied. Three different temperatures (27, 50, 70 °C), six pressures (0.15, 2, 4, 6, 8 and 10 MPa) and three bulk mole compositions of carbon dioxide (0.3, 0.5 and 0.7) were tested in order to investigate the effect of pore width, temperature, pressure and bulk composition on the adsorption behavior of CO_2 and N_2 on CNTs. It was stated that CNTs tended to adsorb CO_2 more preferentially than that of N_2 in a binary mixture due to the structure of the adsorbate and packing effects. It was reported by Razavi et al. [40] that the pore width of CNTs had a significant effect on the adsorption amount of CO_2, while less sensitive to the N_2 adsorption amount. In addition, the adsorption amount decreased with the increase in adsorption temperatures and pore width. Increasing in pressure and pore width had a negative effect on the selectivity of CNTs. An optimized pore size of 8.07 nm corresponding to (6,6) CNT, at 27 °C and P= 0.15 MPa at a bulk mole composition of 0.3 was found to possess highest selectivity for separation CO_2 from N_2. Skoulidas and his research group [41] applied atomically detailed simulations to investigate the adsorption and transport diffusion of CO_2 and N_2 in single-walled carbon nanotubes (CNs) at room temperature as a function of nanotube diameter. It was reported that the diffusion rate of molecules inside of CNs were very fast compared with other porous materials. Cinke et al. [42] studied the CO_2 adsorption on purified SWNTs in the temperature range of 0-200 °C. Twice the volume of CO_2 adsorbed by SWNTs compared with activated carbon was observed. The CO_2 heat of adsorption from their experimental results was 2303 J/mol in SWNTs, which was very similar to that of the binding energy obtained from their

computational results. Hsu et al. [43] studied thermodynamics and regeneration of CO_2 adsorption from gas streams using multi-walled CNTs and modified CNTs with 3-aminopropyl-triethoxysilane (APTS) solutions. It was revealed that the nature of adsorption process was exothermic due to the decrease of CO_2 adsorption capacity of CNTs and CNT (APTS) with temperatures. In addition, the low isosteric heats of adsorption demonstrated that the physical adsorption dominated. The adsorbed CO_2 on CNT (APTS) could be desorbed by thermal treatment at 120 °C for 25 min. The adsorbed CO_2 due to physical adsorption could be successfully removed by vacuum desorption at 120 °C and 0.145 atm for 30 min. A combined treatment of thermal and vacuum treatment was proposed by Hsu et al. [43] to shorten the desorption time to 5 min. A 20-cycle of adsorption/desorption was performed with CNT (APTS). It was suggested that CNT (APTS) had potential as one of the cost-effective CO_2 adsorbents in the future, as the pore structure and surface functional groups of CNT (APTS) was well preserved after 20 cycles of adsorption/desorption tests. Lu et al. [28] compared the CO_2 adsorption capacity of 3-aminopropyl- triethoxysilane (APTS) modified CNs, granular activated carbon and zeolites. Modified CNTs was found to possess highest CO_2 adsorption capacity, followed by modified zeolites and then the modified granular activated carbon. Su and his group in 2009 [44] did the similar work as Hsu [43] and Lu [28] did. They modified CNs with 3-aminopropyl-triethoxysilane (APTS) solutions and tested the CO_2 adsorption capacity at multiple temperatures (20-100 °C). It was found that CNT (APTS) was promising low-temperature adsorbents for CO_2 adsorption from flue gas, as the CO_2 adsorption capacity maximized at 20 °C. In 2013, Sun et al. [45] investigated the sorption behavior of boron carbon nanotubes (B_2CNTs) on CO_2, N_2, CH_4, and H_2. It was shown that the CO_2 molecules formed strong

interactions with B_2CNTs, indicating that B_2CNTs was a promising solid sorbent for CO_2 capture. However, N_2, CH_4, and H_2 only formed weak interactions with B_2CNTs.

2.2.4 Zeolite sorbents

Crystalline aluminosilicate zeolites with microporous structures have been widely used in gas separation and purification. The substitution of silicon with aluminum in the frameworks of zeolites induces negative charges which can be compensated with cations within the pore structures. Separations of CO_2 from flue gases using zeolites depend on various factors such as composition and framework structures of zeolites, pore size distribution and shapes, cation types, and purity. Many published papers have studied the efficiency of CO_2 adsorption over different types of zeolites [46-59]. In 1972, Ma et al. [60] used the gas chromatographic technique to measure the diffusional coefficients of CO_2, NO, NO_2 and SO_2 on zeolite 5A and 13X, natural mordenites, and synthetic Na-mordenites and H-mordenites in the temperature range of 133 to 325 °C. The isosteric heats of adsorption were also explored. The diffusional resistances for all the gases were found to decrease in the following order: natural mordenites > Na-mordenites > H-mordenites > 13X and 5A. The isosteric heats of adsorption and activation energies were also found to decrease in the same order. The sorption isotherms of methane, ethane, ethene and carbon dioxide on NaX, NaY and Na-mordenite zeolites had been studied by Choudhary et al. [61] using a gravimetric sorption technique. It was found that for all the three zeolites, the Dubinin-Polanyi equation fitted the sorption data of methane, while the Langmuir equation fitted the sorption data of CO_2. For ethane and ethene, there was no specific sorption equation which fitted the sorption data of the two gases in the three zeolites. It was also found that the isosteric

heat of adsorption as a function of surface coverage for the sorption of methane, ethane, ethene and carbon dioxide were highly dependent on the sorbate types and zeolite sorbents. Pressure swing adsorption (PSA) process, as one of the most effective way to remove CO_2 from flue gases, has been investigated both theoretically and experimentally [62]. In early 1988, Inui et al. [63] investigated the sorption behavior of various zeolites for CO_2 by PSA process. They indicated that chabazite and zeolite 13X were most suitable for the CO_2 separation from CO_2-containing gas mixtures by PSA process among many kinds of natural zeolites. Gomes et al., 2002 [62] reported that zeolite 13X can separate CO_2 from N_2/CO_2 mixtures effectively. With the help of PSA process, the purity of recovered N_2 can be increased from 30% to 90%. Ko et al. 2003 [64] utilized a pressure-swing adsorption process to recover CO_2 from a binary mixture of N_2 and CO_2 via zeolite 13X. A mathematical model of the PSA process using PDAEs was established with four steps of pressurization, adsorption, depressurization and regeneration to find optimal values of decision variables with a power constraint. It was shown from the optimization results that the feed pressure had no need to be high for zeolite 13X to obtain high purity product, while other sorbents such as zeolite 5A required high feed pressures. It was then concluded that the PSA process using zeolite 13X can be considered as a cost-effective process with high purity product and low energy cost. Díaz et al. [65] developed a new method for improving the CO_2 retention capacity of X zeolites. They treated the X zeolites with different sodium and cesium aqueous solutions. It was found that the Cs-treated X zeolites exhibited higher retention capacity and easiness of regeneration. This modified zeolite was also found to be favorable at high operating temperatures (100-200 °C). A group of 13 zeolite based adsorbents such as 5A, 13X, NaY, NaY-10, H-Y-5, H-Y-30, H-Y-80, HiSiv 1000, H-ZSM-5-30, H-ZSM-5-

50, H-ZSM-5-80, H-ZSM-5-280, and HiSiv 3000 were explored by Harlick et al., 2004 [66] for determining the heats of adsorption and Henry's Law constants for CO_2 with N_2 balance. It was pointed out that the temperature in the column and the isotherm shape can greatly affect the working capacity of the adsorbents. During the adsorption process, large quantities of heat could be produced as the nature of the reaction is exothermic. The resulting heat would increase the temperature of the local column, leading to a reduced adsorption capacity of the adsorbents. From the experimental data they obtained, the heats of adsorption of 13 zeolite based adsorbents decreased in the following order: 5A > 13X > NaY > NaY-10 > HiSiv 1000 > H-ZSM-5-30 > HiSiv 3000 > H-ZSM-5-50 = H-Y-5 > H-ZSM-5-80 > H-ZSM-5-280 > H-Y-80 > H-Y-30. Selected adsorbents, including 13X, NaY, H-Y-5, ZSM-5-30, and HiSiv 3000 were evaluated based on their CO_2 adsorption capacity. The CO_2 adsorption capacity of these adsorbents decreased in the following order: 13X > NaY > H-ZSM-5-30 > HiSiv 3000 > H-Y-5. Jiang et al. [67] investigated the effect of aging, crystallization temperature and time, and structure directing agent on the synthesis of T-type zeolite nanoparticles for the separation of CO_2/N_2 and CO_2/CH_4 by adsorption. It was shown that the selectivity of CO_2/N_2 and CO_2/CH_4 of the T-type zeolite nanoparticles was 53.71 and 19.15 under ambient pressure and 15 °C. The CO_2 adsorption capacity of T-type zeolite nanoparticles was 4.01 mmol/g, which was 30% higher than that of micro-level T-type zeolite at ambient pressure and 15 °C. Chen et al., 2014 [68] prepared highly mesoporous LTA zeolites using dimethyloctadecyl[3-(trimethoxysilyl)propyl]ammonium chloride as a mesopore- generating agent. Compared with microporous LTA zeolites, meso LTA exhibited faster CO_2 adsorption kinetics at 1 bar and higher CO_2 adsorption capacity under high pressure conditions (>10 bar). It was shown that the CO_2 adsorption capacity of meso-LTA under

1 bar and 25 °C was higher in the first 2 minutes compared with the micro-LTA. CO_2 adsorption equilibrium was reached by meso-LTA in 7 minutes. However, it took at least 30 minutes for micro-LTA to achieve equilibrium. The CO_2 adsorption capacity of meso-TLA was about 5.4 mmol/g at 30 bar and 25 °C, which was 11.8% higher than that of micro-LTA under the same conditions. Chen et al. [69] also prepared zeolite 13X from bentonite using alkaline fusion method followed by a hydrothermal treatment. It was reported that the resulting zeolite 13X exhibited higher surface area (688 m^2/g) and large micropore volume (0.3 cm^3/g). The CO_2 adsorption capacity and selectivity of the prepared zeolite 13X was 4.80 mmol/g and 37 (CO_2/N_2) at 25 °C and 1 bar.

Table 2.4 Summary of the total amount of CO_2 adsorbed by various zeolites

Sorbent	T (°C)	P (atm)	Gas composition	Capacity (mmol/g)	Experiemental procedure	Ref.
Zeolite 13X	20	1	1.5%CO_2, 98.5%N_2	1.77	Adsorption bed	[70]
TNU-9	20	1	Pure CO_2	2.6	ASAP 2020 static volumetric apparatus	[71]
IM-5	20	1	Pure CO_2	2.42	ASAP 2020 static volumetric apparatus	[71]
Ferrierite	20	1	Pure CO_2	2.03	ASAP 2020 static volumetric apparatus	[71]
ZSM-5	20	1	Pure CO_2	2.3	ASAP 2020 static volumetric apparatus	[71]
ZSM-11	20	1	Pure CO_2	2.18	ASAP 2020 static volumetric apparatus	[71]
SSZ-74	20	1	Pure CO_2	1.92	ASAP 2020 static volumetric apparatus	[71]

Li-ZSM-5	30	3	20%CO_2, 80%N_2	0.89	Gas chromatography (HITACHI 163)	[72]
Na-ZSM-5	30	2	20%CO_2, 80%N_2	1.03	Gas chromatography (HITACHI 163)	[72]
K-ZSM-5	30	2	20%CO_2, 80%N_2	0.67	Gas chromatography (HITACHI 163)	[72]
Rb-ZSM-5	30	5	20%CO_2, 80%N_2	0.67	Gas chromatography (HITACHI 163)	[72]
Cs-ZSM-5	30	1.2	20%CO_2, 80%N_2	0.4	Gas chromatography (HITACHI 163)	[72]
Zeolite 13X	25	10	Pure CO_2	6.5	Magnetic suspension microbalance	[73]
Zeolite 13X	35	10	Pure CO_2	5.80	Magnetic suspension microbalance	[73]
Zeolite 13X	50	10	Pure CO_2	4.82	Magnetic suspension microbalance	[73]
Zeolite 13X	25	1	Pure CO_2	2.27	Magnetic suspension microbalance	[74]
Erionite (ZAPS)	17	0.26	Pure CO_2	3.0	High-vacuum volumetric system	[75]
Mordenite (ZNT)	17	0.26	Pure CO_2	1.9	High-vacuum volumetric system	[75]
Clinoptiloli te (ZN-19)	17	0.26	Pure CO_2	1.8	High-vacuum volumetric system	[75]
Zeolite 5A	30	1.2	Pure CO_2	3.07	Volumetric apparatus	[76]
Zeolite 5A	30	10	Pure CO_2	3.55	Volumetric apparatus	[76]
Zeolite 5A	100	1.2	Pure CO_2	2.12	Volumetric apparatus	[76]
Zeolite 5A	300	1.2	Pure CO_2	0.24	Volumetric apparatus	[76]
Zeolite 1	25	20	15%CO_2, 82%N_2,	3	Fixed-bed reactor	[77]

			$3\%O_2$			
Zeolite 2	25	20	$15\%CO_2$, $82\%N_2$, $3\%O_2$	1.4	Fixed-bed reactor	[77]
Zeolite 3	25	20	$15\%CO_2$, $82\%N_2$, $3\%O_2$	0.8	Fixed-bed reactor	[77]
13X	120	19	$15\%CO_2$, $82\%N_2$, $3\%O_2$	0.70	Fixed-bed reactor	[78]
5A	120	19	$15\%CO_2$, $82\%N_2$, $3\%O_2$	0.38	Fixed-bed reactor	[78]
4A	120	19	$15\%CO_2$, $82\%N_2$, $3\%O_2$	0.50	Fixed-bed reactor	[78]
WE-G-592	120	19	$15\%CO_2$, $82\%N_2$, $3\%O_2$	0.60	Fixed-bed reactor	[78]
APG-II	120	19	$15\%CO_2$, $82\%N_2$, $3\%O_2$	0.38	Fixed-bed reactor	[78]
LiCHA	0	1	Pure CO_2	0.123	Volumetric apparatus	[79]
NaCHA	0	1	Pure CO_2	0.118	Volumetric apparatus	[79]
KCHA	0	1	Pure CO_2	0.1	Volumetric apparatus	[79]
MgCHA	0	1	Pure CO_2	0.095	Volumetric apparatus	[79]
CaCHA	0	1	Pure CO_2	0.102	Volumetric apparatus	[79]
BaCHA	0	1	Pure CO_2	0.08	Volumetric apparatus	[79]
NaX	0	1	Pure CO_2	1.14	Volumetric apparatus	[79]

2.2.5 Metal organic frameworks (MOFs)

Metal organic frameworks (MOFs) have received much attention for CO_2 capture from flue gases due to its high potential applications in separation process. They are synthesized using organic linker molecules and metal joints. After self-assemble, crystalline materials with well-defined porous structures, high surface area, and desired chemical functionalities are formed, making them attractive as promising candidates for CO_2 capture [80]. Saha et al. [81] studied different MOFs and hybrid materials containing MOFs for CO_2 capture. Several ways to enhance the CO_2 adsorption capacity, such as synthesizing fluorinated metal organic frameworks (FMOFs) using perfluorinated polycarboxylate ligands, amino functionalization of MOFs, application of light main group metals such as Mg^{2+} and Al^{3+} to form MOFs, were compared and discussed. They pointed out that although the CO_2 loadings were not high; the most important aspect of these MOFs was that they can physisorb CO_2 at room temperature and pressure. In 2008, Banerjee et al. [82] described a series of eight zeolitic imidazole framework (ZIFs), which was one of the class of MOFs with metal atoms such as Zn linked through N atoms by ditopic imidazolate ($C_3N_2H_3^-$). The results of selectivity of eight different ZIFs of CO_2 over N_2 or CH_4 are shown in Table 2.5. In 2009, Yazaydın and his research group [83] reported an interesting discovery that the CO_2 adsorption capacity and its selectivity over N_2 and CH_4 of MOF Cu-BTC was improved dramatically by the presence of water molecules coordinated to open-metal sites in the framework. The reason for the increased CO_2 uptake was probably due to the interaction between the quadrupole moment of CO_2 and the electric field of the water molecule. Yazaydın et al. [84] explored further on the MOFs for CO_2 adsorption and screened a collection of 14 MOFs for CO_2 capture from flue gases at 0.1 bar under 293-298 K. The results were shown in Fig. 2.1

below. Liu et al. [85] explored the adsorption equilibria of CO_2, H_2O and their mixtures for two kinds of MOFs: HKUST-1 and Ni/DOBDC. The highest CO_2 adsorption capacity of 0.55 and 3.28 mmol/g was reached at 25 °C and CO_2 partial pressure of 0.1 bar for HKUST-1 and Ni/DOBDC, respectively.

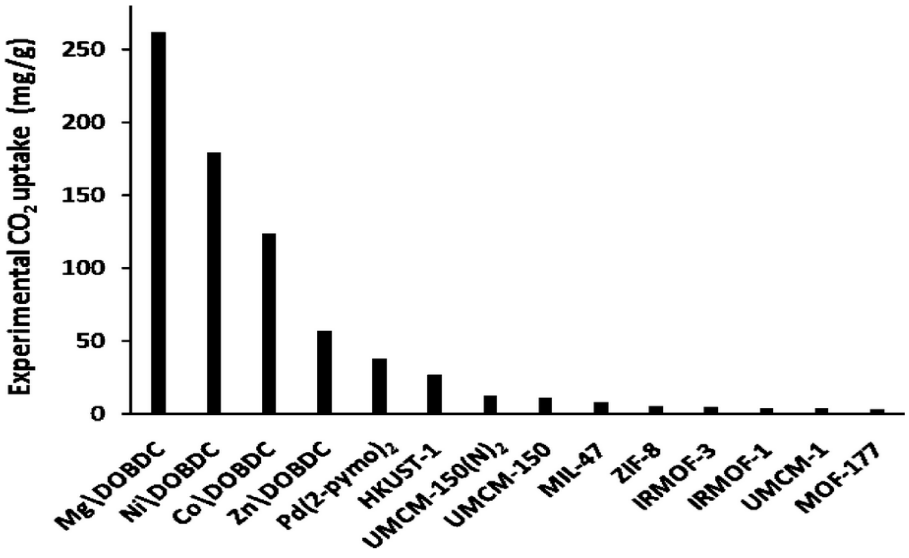

Figure 2.1 Experimental CO_2 uptake in screened 14 MOFs at 0.1 bar with a temperature range of 20-25 °C [84].

More recently, Yang and his research group [86] proposed a new Zr-based MOFs with two carboxylic functions grafted on the organic linkers. They concluded that this new adsorbent exhibited excellent CO_2/N_2 selectivity, high CO_2 adsorption capacity, mild conditions for regeneration, no kinetic limitations, good water stability and high-scale production. In 2014, Zhao et al. [87] developed a copper-based MOFs and graphene oxide composite (HKUST-1/GO) as adsorbent for the separation of CO_2 from flue gas. It was demonstrated that the CO_2 adsorption capacity was improved by a 38% increase compared to that of MOF HKUST-1 at 32 °C and 5 atm.

Table 2.5 Calculated selectivity of CO_2/CH_4 and CO_2/N_2 at 1atm and 25 °C [82].

MOF	Mixture	Selectivity
Zn(bIm)(nIm)[ZIF-68]	CO_2 & N_2	19.5
Zn(bIm)(nIm)[ZIF-68]	CO_2& CH_4	5.5
Zn(cblm)(nIm)[ZIF-69]	CO_2 & N_2	20
Zn(cblm)(nIm)[ZIF-69]	CO_2& CH_4	5.6
Zn(lm)(nIm)[ZIF-70]	CO_2 & N_2	18
Zn(lm)(nIm)[ZIF-70]	CO_2& CH_4	5.6
Zn(nblm)(nIm)[ZIF-78]	CO_2 & N_2	50
Zn(nblm)(nIm)[ZIF-78]	CO_2& CH_4	10.5
Zn(mblm)(nIm)[ZIF-79]	CO_2 & N_2	22.5
Zn(mblm)(nIm)[ZIF-79]	CO_2& CH_4	6
Zn(bblm)(nIm)[ZIF-81]	CO_2 & N_2	23
Zn(bblm)(nIm)[ZIF-81]	CO_2& CH_4	6.3
Zn(cnlm)(nIm)[ZIF-82]	CO_2 & N_2	35.5
Zn(cnlm)(nIm)[ZIF-82]	CO_2& CH_4	9.8

2.3 Chemisorption adsorbents

In order to improve the CO_2 adsorption capacity, various solid sorbents were functionalized with amino group, which can facilitate the CO_2 capture process. Typically, there are three ways to load amino groups in porous materials:

- Physically loading amine species into the pores and onto the surface of the porous materials through impregnation method.
- Covalently tether amine-containing silane to the porous materials
- Hybrid of the above two methods

2.3.1 Alkali metal carbonates based sorbents

Alkali metal carbonates (M_2CO_3; M = Li, Na, K), as one of the potential candidates for CO_2 capture, are suitable for the flue gases with temperature below 200 °C. The CO_2 capture process

using alkali metal carbonate sorbents consists of two reactions: carbonation and de-carbonation. The detailed reaction equations are as follows:

Carbonation: $M_2CO_3 + CO_2 + H_2O \rightarrow 2MHCO_3$ (2.1)

$\Delta H = -31.69$ kcal/mol when M = Na

$\Delta H = -33.74$ kcal/mol when M = K

Decarbonation: $2MHCO_3 \rightarrow M_2CO_3 + CO_2 + H_2O$ (2.2)

In 1998, Hayashi et al. [88] stated that the presence of moisture can badly affect the CO_2 adsorption capacity of conventional adsorbents such as zeolites. However, this drawback can be avoided by using alkali metal carbonates, as moisture is necessary since it participated in the reactions. For regeneration, the steam was introduced into the system to decompose hydrogen carbonate. The resulting off-gas can be cooled to obtain high-purity CO_2. It was also stated that K_2C0_3 on activated carbon was outperformed other alkaline-earth carbonates (Li_2C0_3, Na_2C0_3).

The kinetics of CO_2 adsorption with K_2CO_3/ Al_2O_3 in a gradient less adsorber at ambient temperature was explored by Sharonov et al. [89]. It was found that the order of sorption rate with respect to CO_2 concentration was 1.04 ± 0.07. The maximum CO_2 adsorption capacity was found to be 1.89 mmol/g. Okunev et al. [90] pointed out the similar concerns as Hayashi et al. [88] did that the CO_2 adsorption capacity of conventional sorbents wouldn't maintain with the presence of moisture. They conducted experiments on investigating the CO_2 sorption behavior of K_2CO_3/ Al_2O_3 composite sorbents in the presence of water vapor. They found that the high dynamic capacity of the sorbents was attributed to the crystallization of water in the sample in form of $K_2CO_3 \cdot 1.5H_2O$. This was supported by the results of IR spectroscopy revealing the

formation of intermediate compounds during the CO_2 adsorption process. The reaction mechanism of sorption was presented as below:

$$K_2CO_3 \cdot 1.5H_2O + CO_2 \rightarrow HCO_3^- + H^+ + K_2CO_3 + 0.5H_2O \quad (2.3)$$

$$HCO_3^- + H^+ + K_2CO_3 \rightarrow 2KHCO_3 \quad (2.4)$$

However, if there is no sufficient amount of crystallization water, which is the process-limiting step, the reaction scheme is replaced as follows.

$$K_2CO_3 + xH_2O \rightarrow K_2CO_3 \cdot xH_2O \quad (2.5)$$

The capacity of the composite sorbents after first 10 cycles was found to decrease due to the formation of an inactive phase of K_2CO_3/Al_2O_3 by Okunev et al. [90]. The effect of water on the CO_2 adsorption capacity of alkali-metal based sorbents was explored by Lee et al. [91]. The potassium based sorbents supported on the AC was found to be better with higher CO_2 adsorption capacity compared with other sorbents. An activation process was conducted before CO_2 adsorption with humid nitrogen containing 1.3-52 vol% H_2O for 2 hours at 60 °C or 90 °C. It was reported that a new active species ($K_2CO_3 \cdot 1.5H_2O$) was formed during activation process, which played a positive role in improving CO_2 adsorption. Zhao and his research group conducted a lot of work on investigation of CO_2 sorption using dry potassium-based sorbents [92-98]. Dry potassium-based sorbents with various supports such as coconut activated charcoal (AC#1), coal active carbon (AC#2), activated alumina (Al_2O_3) and silica gel (SG) were prepared by Zhao and his research group [95] in 2009 for CO_2 adsorption in a bubbling fluidized-bed reactor. Zhao et al., 2010 [94] conducted further work on the CO_2 capture performance of dry potassium-based sorbents with various supports using a bubbling fluidized-bed reactor. They impregnated K_2C0_3 on supports such as coconut activated charcoal (AC#1), coal activated

carbon (AC#2), activated alumina (Al_2O_3), SG and diatomite. It was found that K_2CO_3/ AC#1, K_2CO_3/ AC#2 and K_2CO_3/ Al_2O_3 possessed high CO_2 adsorption capacity, high conversion rates and fast regeneration rate. However, K_2CO_3/ AC sorbents could not be used in fluidized bed, as its anti-attrition character was poor. For K_2CO_3/ diatomite and K_2CO_3/ SG, the CO_2 adsorption capacity was very low. This was probably due to the non-porous structure, the low conversion rate and the impossibility of loading K_2CO_3 on diatomite and silica gel supports. They concluded that K_2CO_3/ Al_2O_3 could be a promising candidate for CO_2 capture process in fluidized-bed reactor. Zhao et al., 2010 [96] explored the effect of different reaction conditions on the carbonation characteristics of K_2CO_3 calcined from $KHCO_3$ with a pressurized thermogravimetric apparatus. It was shown that the conversion rate decreased as the reaction temperature and pressure increased. The concentration of CO_2 and H_2O affected the conversion rate. The reaction rate increased as the temperature and H_2O concentration increased and the pressure decreased. The optimum reaction condition for CO_2 capture was found to be 60 °C, 18% CO_2, 18% H_2O and 1 atm. Zhao et al., 2014 [97] prepared a series of potassium-based sorbents using various supports such as activated carbon, Al_2O_3, zeolite 5A, zeolite 13X, and silica gel. The CO_2 adsorption capacity of various sorbents at ambient temperature and CO_2 concentration of 5000 ppm were 0.87, 1.18, 0.34, 0.53, and 0.15 mmol/g for K_2CO_3/AC, K_2CO_3/ Al_2O_3, K_2CO_3/5A, K_2CO_3/13X, and K_2CO_3/SG. It was shown that the sorbents of K_2CO_3/AC and K_2CO_3/SG can be completely desorbed in the range of 100-200 °C. However, for the other sorbents, they might need higher temperatures for desorption. In 2011, Lee et al. [99] prepared and characterized six potassium-based dry regenerable sorbents containing 35 wt% K_2CO_3 by spray-drying techniques. It was noted that Sorb KT-5, KT-7 and KZ-5 with high surface area and

high CO_2 adsorption capacity over 1.36 mmol/g, satisfied almost all the requirements for a commercial fluidized-bed process in the initial lab-scale tests. Park et al. [100] reported that Korea Institute of Energy Research (KIER) and Korea Electric Power Research Institute (KEPRI) developed a CO_2 capture system consisting of two processes: carbonation and decarbonation using potassium-based dry solid sorbents prepared by spray-drying method for CO_2 adsorption in the real flue gas from 2MW coal-fired circulating fluidized bed combustor power plant. The sorbents supplied by KEPRI was tested under continuous circulating mode with the residence time of 3 second in carbonation reactor and 15 minutes in regeneration reactor. The average CO_2 removal was above 70% during 2 hours. The temperature in the carbonation reactor was found to be of great importance for CO_2 removal. Lower temperature in the carbonation reactor can effectively improve the CO_2 adsorption capacity of the sorbents. Therefore, in-bed heat transfer unit was applied in the carbonation reactor to control the reactor temperature under 80 °C. The average CO_2 removal during 50 hours continuous operation was reported to be above 85% using 2 Nm^3/hr of gas treatment facility with simulated flue gas. Lee et al. [101] prepared potassium-based sorbents using ZrO_2 and TiO_2 as supports and investigated the CO_2 sorption and desorption characteristics of the two sorbents in the fixed-bed in a temperature range of 60-150 °C. It was found that potassium-based sorbents using ZrO_2 exhibited the CO_2 adsorption capacity of 1.89-2.11 mmol/g regardless of the calcination temperature in N_2 or air atmosphere.

Table 2.6 Summary of the CO_2 adsorption capacity of alkali metal carbonate based sorbents.

Active phase	Support	T_{ads} (^oC)	T_{des} (°C)	Gas composition	Capacity (mmol/g)	Ref.
K_2CO_3	AC	50-60	130-150	1% CO_2, 0-11% H_2O, N_2 balance	1.96-2.09	[102]
K_2CO_3	TiO_2	50-60	130-150	1% CO_2, 0-11% H_2O, N_2 balance	1.89-1.98	[102]
K_2CO_3	ZrO_2	50-60	130-150	1% CO_2, 0-11% H_2O, N_2 balance	1.73-1.89	[102]
K_2CO_3	Al_2O_3	50-60	290-350	1% CO_2, 0-11% H_2O, N_2 balance	1.89-2.02	[102]
K_2CO_3	MgO	50	350-400	1% CO_2, 0-11% H_2O, N_2 balance	4.06	[102]
K_2CO_3	CaO	50-60	550-650	1% CO_2, 0-11% H_2O, N_2 balance	1.11	[102]
K_2CO_3	ZrO_2	50-100	130-200	1% CO_2, 9% H_2O, N_2 balance	2.08	[103]
Na_2CO_3	Sorb N2A	50-70	120	14.4% CO_2, 5.4 O_2, 10% H_2O, N_2 balance	1.25	[104]
Na_2CO_3	Sorb N2B	50-70	120	14.4% CO_2, 5.4 O_2, 10% H_2O, N_2 balance	0.9	[104]
Na_2CO_3	Sorb N2C	50-70	120	14.4% CO_2, 5.4 O_2, 10% H_2O, N_2 balance	0.23	[104]
Na_2CO_3	Sorb NX	50-70	120	14.4% CO_2, 5.4 O_2, 10% H_2O, N_2 balance	1.93	[104]
$NaHCO_3$	Sorb NH	50-70	120	14.4% CO_2, 5.4 O_2, 10% H_2O, N_2 balance	3.18	[104]
Na_2CO_3	Sorb NX30	50-70	120	14.4% CO_2, 5.4 O_2, 10% H_2O, N_2 balance	2.27	[104]
K_2CO_3	CaO	50-100	450		0.087-0.083	[105]
K_2CO_3	CaO	50	450		0.044	[105]
K_2CO_3	AC	60	130-400	1% CO_2, 9% H_2O, N_2 balance	1.95	[106]
K_2CO_3	Al_2O_3	60	130-400	1% CO_2, 9% H_2O, N_2 balance	1.93	[106]
K_2CO_3	USY	60	130-400	1% CO_2, 9% H_2O, N_2 balance	0.43	[106]
K_2CO_3	CsNaX	60	130-400	1% CO_2, 9% H_2O, N_2 balance	1.35	[106]
K_2CO_3	SiO_2	60	130-400	1% CO_2, 9% H_2O, N_2 balance	0.234	[106]
K_2CO_3	MgO	60	130-400	1% CO_2, 9% H_2O, N_2	2.7	[106]

				balance		
K_2CO_3	CaO	60	130-400	1% CO_2, 9% H_2O, N_2 balance	1.11	[106]
K_2CO_3	TiO_2	60	130-400	1% CO_2, 9% H_2O, N_2 balance	1.89	[106]
Na_2CO_3	Sorb NH	50-100	80-160	14.4% CO_2, 5.4 O_2, 10% H_2O, N_2 balance	1.59-3.18	[107]
Na_2CO_3	Sorb NX30	50-100	80-160	14.4% CO_2, 5.4 O_2, 10% H_2O, N_2 balance	1.81-2.73	[107]
Na_2CO_3	Sorb KX35	50-100	80-160	14.4% CO_2, 5.4 O_2, 10% H_2O, N_2 balance	0.9-2.05	[107]
Na_2CO_3	Al_2O_3	45	150	10% CO_2, 5-12.5% H_2O, Ar balance	2.70	[108]

2.3.2 Reaction scheme of CO_2 with amines

Eqs. (2.6)-(2.8) showed the reactions of CO_2 with amines in dry conditions:

$$2\mathrm{RN}H_2 + CO_2 \rightarrow RNH_3^+ + RNHCOO^- \quad (2.6)$$

$$2R_2NH + CO_2 \rightarrow R_2NH_2^+ + R_2NCOO^- \quad (2.7)$$

$$R_3N + CO_2 + R'NH_2 \rightarrow R_3NH^+ + R'NHCOO^- \quad (2.8)$$

Eqs (2.6)-(2.7) & Eqs (2.9)-(2.12) showed the reactions of CO_2 with amines in humid conditions:

$$2\mathrm{RNH_2} + \mathrm{CO_2} \rightarrow \mathrm{RNH_3^+} + \mathrm{RNHCOO^-} \quad (2.6)$$

$$\mathrm{RNHCOO^-} + \mathrm{H_2O} \rightarrow \mathrm{RNH_2} + \mathrm{HC0_3^-} \quad (2.9)$$

$$2\mathrm{R_2NH} + \mathrm{CO_2} \rightarrow \mathrm{R_2NH_2^+} + \mathrm{R_2NCOO^-} \quad (2.8)$$

$$\mathrm{R_2NCOO^-} + \mathrm{H_2O} \rightarrow \mathrm{R_2NH} + \mathrm{HC0_3^-} \quad (2.10)$$

$$\mathrm{R_3N} + \mathrm{H_2O} \rightarrow \mathrm{R_3NH^+} + \mathrm{OH^-} \quad (2.11)$$

$$\mathrm{CO_2} + \mathrm{OH^-} \rightarrow \mathrm{HC0_3^-} \quad (2.12)$$

Through all the equations above, it can be concluded that in dry conditions, two moles of amine functional groups interact with one mole of CO_2 to form carbamate, while in humid conditions,

one mole of amine functional group interact with one mole of CO_2 to form bicarbonate. In this case, amines with high nitrogen content such as PEI and TEPA would be more competitive as contributors of amine functional groups to incorporate with substrates.

2.3.3 Amine functionalized carbon supported sorbents

The adsorption capacity of a solid sorbent is determined by its porous structure and surface chemistry. It was found that the CO_2 adsorption capacity of the activated carbons, which is physical adsorption, can be improved by introducing nitrogen functional groups into their structure [8, 12, 109-112]. It has been demonstrated that the presence of nitrogen functionalities into the carbon structure can enhance the adsorption of acid gases [8, 112]. There are mainly two approaches for the introduction of nitrogen functionalities: introducing nitrogen into the carbon structure and impregnating the surface with appropriate chemicals.

It was reported by many researchers that nitrogen can be introduced into the carbon matrix by reaction with gaseous ammonia at high temperature [109, 113-116]. It can be explained by the fact that ammonia decomposes at high temperatures with the formation of various radicals such as $NH^{\bullet}_2$, $NH^{\bullet}$ and $H^{\bullet}$. Those radicals may react with the carbon surface to form functional groups, such as $–NH_2$, -CN, pyridinic, pyrrolic, and quaternary nitrogen [8, 109]. Plaza et al. [7] treated the carbon materials with gaseous ammonia (amination and ammoxidation). For the amination treatment, they brought the char directly into contact with gaseous ammonia at 800 °C. For the ammoxidation treatment, the char was brought into contact with the gas mixture of ammonia and air at ratio of 1:2 with the operating temperature of 300 °C. It was found that the aminated samples presented higher CO_2 adsorption capacity than that for the starting char due to

the fact that basic nitrogen functionalities has a positive effect on CO_2 adsorption. However, the ammoxidised sample did not show any improvement on the CO_2 adsorption capacity despite of its higher nitrogen content. They explained this by the probability of introduction of different nitrogen functionalities by the two treatments. They demonstrated that the functionalities introduced by ammoxidation method probably more tended to be amide groups which were more acidic than the pyridinic and pyrrolic nitrogen presented in the aminated samples. Pevida et al. [117] treated the activated carbon with ammonia with various temperatures and found the nitrogen content was increased up to 8 wt% at 700 °C. They found that the nitrogen content reaches maximum at 700 °C and decreases at higher temperature. This is probably due to partial gasification of the carbon with ammonia at higher temperatures. They also found that for the carbon modified at 600 °C a decrease CO_2 adsorption capacity was obtained compared to that for the untreated carbon. Although the nitrogen content in the modified carbon (treated at 600 °C) is higher than that for the untreated carbon, the CO_2 adsorption capacity did not improve. They concluded that the temperature of ammonia used for the treatment determines the type of nitrogen functionalities incorporated [8, 109]: in the case of the sample treated above 600 °C, nitrogen is incorporated onto the layer system of the carbon as thermally stable pyrrol and pyridinic-type functionalities, while in the case of samples obtained below 600 °C, nitrogen might be forming amide-like functionalities. Mercedes et al. [12] prepared a high surface area activated anthracites by steam activation and then treated it in ammonia gas at high temperatures. It was found that the CO_2 adsorption capacity of the untreated activated anthracites was slightly higher than that for the treated samples at 30 °C. However, at higher temperature (e.g. 75 °C), the CO_2 adsorption capacity of the treated samples was higher than that for the untreated samples.

Tang at al. [118] modified the surface of the activated anthracites with gaseous amination treatment and HNO_3 treatment to improve the CO_2 adsorption capacity and came up with similar results. They showed that the amination treatment and HNO_3 treatment can improve the CO_2 adsorption of the anthracite, particularly at higher temperatures. Through the amination and HNO_3 treatments, the pore structure of the activated anthracites was changed. It was reported that amination treatment introduced nitrogen groups on the surface of the activated anthracites, while HNO_3 treatment introduced both oxygen and nitrogen functional groups. Plaza et al. [8] showed that the heat treatment with gaseous ammonia can be an alternative way to produce efficient CO_2 adsorbents. The CO_2 adsorption capacity of up to 8.6 wt% at 25 °C and 2.6 wt% at 100° C in pure CO_2 were obtained for the aminated samples. A series of activated carbon samples were treated with gaseous ammonia at elevated temperatures ranging from 200 to 1000 °C by Przepiórski et al. [112]. It was demonstrated that all the carbons treated with ammonia showed enhanced ability in adsorbing CO_2. The increase in CO_2 adsorption capacity depended on the treated temperatures. The impregnation with PEI can increase the basicity and nitrogen content of the carbon. This resulted in the dramatic decrease in the surface area of the activated anthracites due to the pore blockage and surface coverage by PEI. Gray et al. [119] dissolved the fly ash carbon concentrate into the 3-chloropropylamine- hydrochloride (CPAHCL) solution at 25 °C. It was reported that the best sample had the CO_2 adsorption capacity of 0.175 mmol/g, which was only 9% of the CO_2 adsorption capacity of the commercially available sorbents with surface area of 1000-1700 m^2/g. This is probably due to its low surface area which was only 27 m^2/g. Further treatment is required before incorporating the amines onto the fly ash. Mercedes et al. [12] found that the PEI impregnation can increase the CO_2 adsorption capacity at higher

temperatures due to the introduction of alkaline nitrogen group on the surface. Mercedes et al. 2008, [111] conducted further work on the CO_2 adsorption performance of impregnated activated fly ashes. They claimed that the CO_2 adsorption performance of the high carbon fly ashes without activation prior to the impregnation was very low due to their low surface area. Therefore, they activated the samples with steam at 850 °C, resulting in a significant increase of the surface area up to 1075 m^2/g. Different amine compounds (e.g. MEA, MDEA, DEA) were used to impregnate the activated samples. They presented that the CO_2 adsorption capacity of the activated fly ash carbons with MEA was 1.56 mmol/g at 25 °C, which is much higher than that for carbon molecular sieves with alcohol amines with the CO_2 adsorption capacity of 0.57 mmol/g reported by Zinnen at al. [120]. Zhang et al. [121] made some modifications on the preparation steps of the activated carbon fly ash. They not only used the conventional acid digestion method to remove the ash from the samples and concentrate the unburned carbon but also further treated the samples with boiling HNO_3, resulting in a high surface area and microporosity of the samples. They found that the CO_2 adsorption capacity of the PEI impregnated sample was 2.13 mmol/g at 75 °C. Plaza et al., 2007 [110] impregnated a series of activated carbon samples with different amine compounds: diethylentriamine (DETA), pentaethylenehexamine (PEHA), and polyethylenimine (PEI). It was found that the CO_2 adsorption capacity for the raw activated carbon decreased dramatically with temperatures. However, the impregnated carbons presented a softer slope with temperature than that for raw carbon due to the strong interactions between the CO_2 and the amine groups. It was also found that the raw carbon presented the highest CO_2 adsorption capacity at room temperature compared to others. It was probably due to the fact that amine impregnation decreased the pore volume of

the treated samples, which is mainly responsible for the CO_2 physisorption. Tang et al. [118] impregnated PEI onto the surface of the activated anthracites and found that the PEI impregnation can increase the CO_2 adsorption capacity of the activated anthracites. Arenillas et al. [122] studied the CO_2 adsorption performance of fly ash derived carbon materials by impregnating it with different kinds of amines. It was found that different CO_2 adsorption capacities were achieved by using different type of amines. They also explored the CO_2 adsorption by adding PEG onto the PEI-loaded adsorbents. It was shown that the mixture of the two amines impregnated onto the surface of the substrate not only improved the CO_2 adsorption capacity but also decreased the time taken for the sample to reach saturation. Lu et al. 2008 [28] impregnated the CNTs, granular activated carbon and zeolites with 30% monoethanolamine (MEA), 30% NH_3 (aq) and 10% APTS (90 ml of 99.8% purity toluene + 10 ml of 97% purity APTS), and compared their CO_2 adsorption capacity with 10% CO_2 at 25 °C. Fig. 2.2 summarizes the results of the four adsorbents. The PEI impregnated SWNT with different PEI molecular weights were prepared and characterized by Dillon et al. [123] for CO_2 adsorption. It was demonstrated that the CO_2 adsorption capacity was dependent on the molecular weight of PEI. The CO_2 adsorption efficiency (the mass of CO_2 per mass of PEI) was investigated as a function of molecular weight of PEI for PEI-SWNT. It was concluded that the CO_2 adsorption capacity was improved as the PEI molecular weight increased from 600 Da to 25000 Da. A good stability and moderate speed of PEI-SWNT to adsorption/desorption cycles was achieved. A CO_2 adsorption capacity of 2.1 mmol/g was reported at 27 °C with pure CO_2.

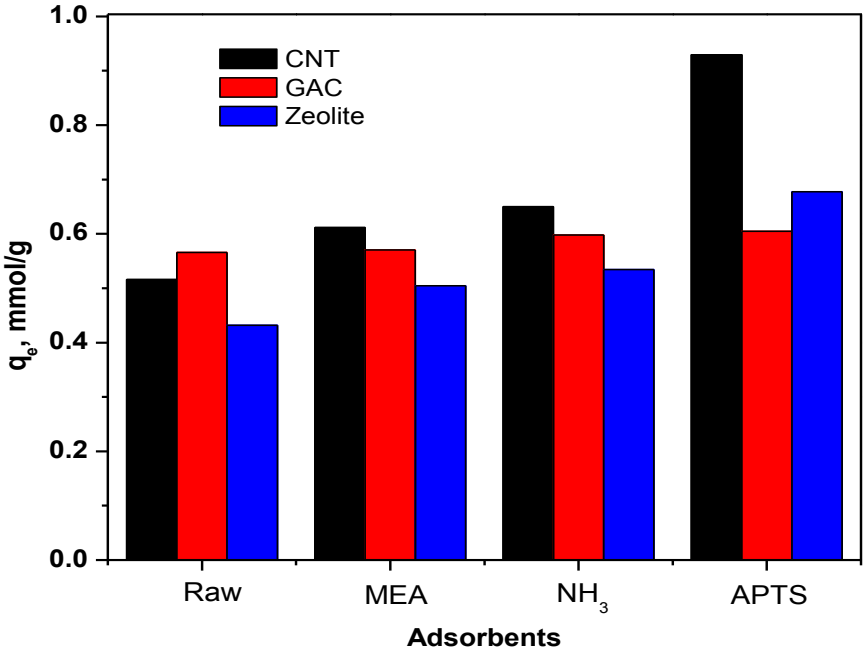

Figure 2.2 Equilibrium amount of CO_2 adsorbed on various raw and modified adsorbents with a CO_2 concentration of 10% [28].

Table 2.7 Summary of CO_2 adsorbed by activated carbon using different activation methods.

Sorbent	Treatment method	T (°C)	CO_2 pressure (atm)	Adsorption Capacity (mmol/g)	Testing equipment	Ref.
AC	Amination	30	1	2.2	Volumetric TriStar 3000	[124]
AC	Impregnation with MEA			1.11	CO_2 gas monitor	[125]
AC	Impregnation with AMP	25	0.15	0.77	CO_2 gas monitor	[125]
AC	Amination	25	1	3.75	Rubotherm	[29]
AC	Amination	30	1	2.3	Volumetric TriStar 3000	[13]
AC	Impregnation with MEA	25	1	1.02	Rubotherm	[30]
AC	Amination	25	1	2.16	TGA	[14]
AC	Amination	25	0.15	1.1	TGA	[14]

More recently, Gui et al. [126] modified the multi-walled carbon naotubes (MWCNTs) with 3-aminopropyltriethoxysilane (APTES) solution for CO_2 capture. The highest CO_2 adsorption capacity of the APTES-functionalized MWCNTs was 1.71 mmol/g. Badu et al. [127] reported the gas adsorption of CO_2 and N_2 over a wide range of pressure using highly aligned dense double-walled carbon nanotube arrays with high surface area. High pressures were required for high CO_2 adsorption capacity. The highly aligned CNTs were then modified with the treatment of oxygen plasma. At low pressures, oxygen plasma grafting was found to be an effective way to enhance the CO_2 adsorption capacity. While for high pressure, the structural modification by decreasing the diameter of the tubes was found to be more effective in increasing the adsorption capacity [127]. Liu et al. [128] applied industrial grade multi-walled carbon nanotubes (IG-MWCNTs) as the support for the impregnation with TEPA. The maximum CO_2 adsorption capacity of TEPA impregnated IG-MWCNTs was achieved as high as 3.088 mmol/g with 50% TEPA loading at 70 °C. Su et al. [129] studied the cyclic CO_2 adsorption of 3-aminopropyltriethoxysilane loaded CNs using a dual-column temperature/vacuum swing adsorption (TVSA) process. The CO_2 adsorption capacity and physiochemical properties of the sorbents were preserved after 100 TVSA cycles under dry and wet conditions, indicating a high thermal stability of the sorbents. The CO_2 adsorption capacity of the sorbent was improved with the presence of moisture (~1.6 mmol/g), compared with that under dry conditions (~0.91 mmo/g). Zhang et al. [130] developed a novel method termed as “wet support impregnation (WSI)” for impregnation of PEI on the fly ash. It was shown that the PEI-FA sorbents were more suitable at lower temperatures for CO_2 capture. The CO_2 adsorption capacity of the sorbents was 3.30 mmol/g at 90 °C with 10%CO_2/90%N_2. Such high resulting CO_2 adsorption capacity was

probably attributed to the fact that WSI allowed more amine to be loaded onto the support than the conventional wet impregnation method.

2.3.4 Amine functionalized zeolite supported sorbents

Zeolites as an alternative candidate for CO_2 capture from flue gases have been investigated by researchers for a long time. However, zeolite based sorbents suffer from drawbacks limiting their practical applications in industry, such as sensitive to high temperatures and inhibits CO_2 adsorption capacity in humid conditions. Therefore, some researchers modified them with different amines.

Jadhav et al. 2007, [131] modified zeolite 13X with monoethanol amine (MEA). MEA was loaded using the impregnation method with different MEA loadings ranging from 0.5-25 wt%. The CO_2 adsorption capacity of MEA modified zeolite 13X was improved by a factor of ca. 1.6 at 30 °C, while the efficiency was improved by a factor of ca. 3.5 at 120 °C. Fisher II et al. [132] impregnated TEPA on three different supports, including beta zeolite, SiO_2, and Al_2O_3. The TEPA modified beta zeolite showed highest CO_2 adsorption capacity of 2.08 mmol/g at 30 °C with 10% CO_2 and 90% Ar, compared with the other two sorbents. Su et al. [133] applied the Y-type zeolite with Si/Al molar ratio of 60 (abbreviated as Y60) was the support for the TEPA impregnation. The CO_2 adsorption capacity of the sorbent was significantly increased after modification. With the presence of moisture, the CO_2 adsorption capacity was further facilitated up to 4.27 mmol/g at 7% water vapor. The sorbent can be fully desorbed at 75 °C for 4 hours. The thermal stability of the sorbent was excellent. The physiochemical properties and CO_2 adsorption capacity of the sorbent were preserved after 20 cycles of adsorption/desorption. Kim

et al., 2013 [134] investigated the adsorption and diffusion behaviors of CO_2/N_2 mixtures using pure silicate structures of zeolites TON as the support. They modified the surface of zeolite TON with amino functional group and evaluated the effect of surface modifications on the adsorption and diffusion compared with the normal TON surface. It was shown that the CO_2 adsorption capacity of the sorbents was enhanced after amine modification. However, the CO_2 adsorption capacity at high pressures was lower than that of normal zeolite TON due to the reduction of pore volumes after modification. For the adsorption isotherms, the selectivity of CO_2 over N_2 was higher. In addition, the modified sorbents had a lower diffusivity compared with the normal zeolite TON. This was probably due to the additional attractive interactions between the amino functional groups and the support. In 2014, Aruldoss et al. [135] synthesized and characterized a template-free ZSM-5 with molar ratio SiO_2/Al_2O_3 of 50. Different amine species such as TEA, DEA, DETA, and TETA were used for the modification of the ZSM-5 support. It was found that the CO_2 adsorption capacity of the sorbents with different amine-grafted decreased in the following order: TETA/ZSM-5 > DETA/ZSM-5 > DEA/ZSM-5 > TEA/ZSM-5.

2.3.5 Amine functionalized polymer and resin supported sorbents

Satyapal et al., 2001 [136] reported that HSC^+, a regenerable solid sorbent developed by Hamilton Sunstrand Space Systems International (HSSSI), consisted of PEI bonded to a high surface area, solid polymethyl methacrylate (PMMA) polymeric support. Polyethylene glycol (PEG) was also coated on the HSC^+ support to enhance CO_2 adsorption and desorption rates. The CO_2 adsorption capacity of this sorbent was around 0.91 mmol/g at ambient pressure and 40 °C. The thermal stability of the sorbent was tested by hundreds of cycles with adsorption followed

by equal time of vacuum desorption. No loss of amines was found even after hundreds of cycles, indicating the excellent thermal stability of the sorbent with amine strongly bonded to the support. Li et al., 2008 [137] developed a novel fibrous sorbents for CO_2 adsorption. The PEI was coated on a glass fiber matrix with epoxy resin (EP) as cross-linking agent. The cross-linked fibrous sorbents had an excellent thermal stability of about 280 °C. The CO_2 adsorption capacity maximized with a PEI/EP ratio of 10:1. The maximum CO_2 adsorption capacity of 6.29 mmol/g of PEI was obtained at 1 atm, 30 °C under flue gases with a relatively humidity of 80%. With the presence of moisture, the CO_2 adsorption capacity of the fibrous sorbents was 19 times higher than that in the dry conditions. In addition, this novel sorbent can be completely regenerated at 120 °C. In the same year, Li et al. [138] synthesized another fibrous sorbent for CO_2 capture by coating PEI on a glass fiber matrix with epichlorohydrin (ECH) as crosslinking agent. The CO_2 adsorption capacity of this sorbent was about 4.12 mmol/g with a PEI/ECH ratio of 20:1 at ambient pressure 30 °C with flue gases with a relative humidity of 80%. This sorbent can also be completely regenerated at 120 °C. Pevida et al. [139] synthesized and characterized a novel adsorbent by incorporating nitrogen into the melamine-formaldehyde resin derived polymer matrix, using silica as template material, and carbonization at different temperatures. The thermal stability of the sorbent was greatly improved by introducing nitrogen functionalities. The CO_2 adsorption capacity of melamine-formaldehyde resin derived sorbents was up to 2.25 mmol/g at 25 °C. In 2014, Jo and his group [140] explored the effect of TEPA structure on the CO_2 adsorption by impregnating TEPA and modified TEPA in a poly methyl methacrylate (PMMA) support. TEPA was transformed from primary amine to secondary amine via Michael addition reaction between TEPA and acrylonitrile (AN). Table 2.8 shows the molar ratio of primary,

secondary and tertiary amines before and after TEPA modification. With the process of Michael addition reaction, pH was reduced, while the viscosity and thermal stability of the modified TEPA was enhanced. Therefore, the durability of the sorbent was improved with amine modification, as the thermal stability of the amine was improved, resulting in a less amine loss during desorption process. In addition, the TEPA modified sorbents of ST1AN and ST2AN showed a high CO_2 adsorption capacity above 3 mmol/g, and a lower desorption energy. The amine efficiency was improved during transformation, with ST2AN possessing the highest amine efficiency of 0.495. However, further transformation from secondary amine to tertiary resulted in a decreased in adsorption capacity and amine efficiency in dry conditions.

Table 2.8 Molar ratios for TEPA modification and expected amine type ratio of Primary: Secondary: Tertiary amine [140].

Product	Amine type (P:S:T)	TEPA (mol)	AN (mol)
TEPA	2:3:0	1	N/A
T1AN	1:4:0	1	1
T2AN	0:5:0	1	2
T3AN	0:4:1	1	3

2.3.6 Amine functionalized silica supported sorbents

Xu and his research group did a series of work on the CO_2 adsorption performance by PEI-impregnated MCM-41 with different operating conditions. Various influencing factors, such as adsorption temperatures, gas flow rates, moisture effects, loading percent, and multi-cycle studies, were explored. Xu et al., 2002 [141] were the first to propose concept of “molecular basket” for CO_2 adsorption using nanoporous solid adsorbents. This was explained by using mesoporous adsorbent with large pore channels as a basket, filled with a substance with numerous CO_2-affinity sites to increase the CO_2 adsorption selectivity and CO_2 adsorption

capacity. In their case, PEI-impregnated MCM-41 was prepared and tested as CO_2 adsorbent. It was reported that the mosoporous solid adsorbent had a synergetic effect for the adsorption of CO_2 by PEI modification when the PEI loading was higher than 30 wt%. A highest CO_2 adsorption capacity of around 2.44 mmol/g was obtained with MCM-41 with 50 wt% PEI at 75 ^oC. The CO_2 adsorption capacity increased with the increase of CO_2 concentration in the gas mixtures. The multi-cyclic adsorption/desorption studies were also explored. It was reported that the CO_2 adsorption performance of the PEI modified MCM-41 was very stable. In 2003, Xu et al. [142] conducted further experiments on the effect of PEI loadings and preparation methods on the CO_2 adsorption capacity. It was reported that the CO_2 adsorption capacity initially held identical when the PEI loading of the MCM-41 was very less (e.g. 5 wt%). Further, increases in PEI loadings onto the MCM-41 improved the CO_2 adsorption capacity effectively. The highest CO_2 adsorption capacity of 3.022 mmol/g was obtained when the PEI loading was 75 wt%. It was also found that the adsorbent prepared by a one-step impregnation method had a higher CO_2 adsorption capacity than that prepared by a two-step impregnation method. A simulated flue gas with 14.9% CO_2, 4.25% O_2 and 80.85% N_2 was used to test the CO_2 adsorption capacity of the modified MCM-41 at 75 ^oC [143]. The adsorbent showed a separation selectivity of >1000 for CO_2/N_2 and 180 for CO_2/O_2. Xu. et al. [144] found that the presence of minor gas compositions (e.g. NO_x, SO_x) in the flue gas mixtures influenced the CO_2 adsorption by MCM-41with the PEI loading of 50 wt%. NO_X adsorption was even stronger than that of CO_2 under certain conditions. This indicates need of pre-removal of NO_x and SO_x from the flue gases for the CO_2 separation process using MCM-41with the PEI loading of 50 wt%. They also discovered a promoting effect of moisture from the gas mixtures on the CO_2 adsorption [143, 145]. It was demonstrated that

when the moisture concentration is higher than that of the CO_2, the CO_2 adsorption capacity by PEI impregnated MCM-41 increases dramatically with the moisture concentration. However, when the moisture concentration is lower than that of the CO_2 concentration, the CO_2 adsorption capacity is barely influenced by the moisture concentration in the flue gas mixtures. It was discovered that the maximum promoting effect of moisture on CO_2 adsorption from simulated flue gases appeared at the moisture concentration approaching that of CO_2 in the flue gas [145]. Xu et al. [146] prepared modified MCM-41 using linear and branched PEI and compared the CO_2 adsorption capacity of the adsorbents with different PEI structures. It was found that the adsorbent with linear PEI showed a higher CO_2 adsorption capacity as well as faster CO_2 adsorption/desorption rate than that of adsorbent with branched PEI.

A new generation of molecular basket sorbent, SBA-15 with 50 wt% PEI was developed by Ma [147] for CO_2/H_2S capture. The adsorbent showed a high adsorption capacity of at 75 °C under 15% CO_2 partial pressure. This reported data was 50% higher than that of their previously prepared PEI impregnated MCM-41. A two-stage process for removing CO_2 and H_2S from gas streams was also proposed. This adsorbent and process was demonstrated to have many advantages, such as capable of removing H_2S to less than 60 ppbv, higher adsorption/desorption rate, good regenerability and stability in multi-cycles, and promoting effect of moisture in the gas mixtures on CO_2 adsorption. In 2008, Son et al. [148] synthesized a series of mesoporous materials, namely MCM-41, MCM-48, SBA-15, SBA-16, and KIT-6, and impregnated with 50 wt% PEI to evaluate and compare the CO_2 adsorption performance at 75 °C. All the adsorbents exhibited reversible CO_2 adsorption/desorption behavior with >99% recovery. They all had higher CO_2 adsorption capacity and faster adsorption kinetics than that of pure PEI. The CO_2

adsorption capacity was found in the order as: KIT-6> SBA-16≈ SBA-15> MCM-48> MCM-41. This was explained by the influence of their different pore sizes on the CO_2 adsorption performance. It was discovered that the KIT-6 with the largest pores showed the highest CO_2 adsorption capacity of around 3.07 mmol/g in the fastest response time. The stability of KIT-6 with 60 wt% PEI loading was maintained after three consecutive test cycles without deterioration. Based on the work conducted by Son et al. [148], Chen et al. [149] prepared a monolithic silica exhibiting a hierarchical pore structure as a support for PEI impregnation. It was demonstrated that this sorbent showed higher CO_2 adsorption capacity compared with those prepared by Son et al. [148]. It was reported that the CO_2 adsorption capacity of the monolith with 65 wt% PEI loading achieved around 3.75 mmol/g using 5% CO_2 under 75 °C, which was still higher than that obtained using PEI/KIT-6 with high purity CO_2. It was also presented that the CO_2 adsorption capacity in humid conditions was 24% higher than that under dry conditions. Yue et al. [150] impregnated TEPA onto the as-prepared mesoporous silica SBA-15. The modified sorbent exhibited a high CO_2 adsorption capacity as high as 3.93 mmol/g. It was also reported that the hydroxyl groups of the P123 template modified the interactions between CO_2 and amine, enhanced the CO_2 adsorption capacity of the sorbent. More recently, Yue at al. [151] modified the as-sythesized mesoporous silica SBA-15 with mixed amines of TEPA and DEA. They found that the modified SBA-15 had high CO_2 adsorption capacity at low CO_2 concentration. They explained that the existence of hydroxyl groups in DEA promoted the CO_2 adsorption capacity in the amine-containing SBA-15. Without the presence of hydroxyl groups, two molars of amine groups interacted with only one molar of CO_2 to form carbamate. In the presence of hydroxyl groups, one molar of amine group can capture two molars of CO_2. It was

reported that the CO_2 adsorption capacity of the mixed-amine modified SBA-15 (30 wt% TEPA and 20 wt% DEA) achieved 3.7 mmol/g. Yue et al. [152] developed an as-synthesized MCM-41 with TEPA impregnation as the CO_2 capturer. The highest CO_2 adsorption capacity of around 5.39 mmol/g was reported with 60 wt% TEPA loading. Different amount and type of surfactants were also explored to investigate the influence of micelles on the CO_2 adsorption. They concluded that amount, type, and distribution of the surfactant occluded in the channel of the support had strong influences on the final CO_2 adsorption capacity of the resulting composites. It was proven that the spoke-like structure of the micelles in the channel of support was the most competitive candidate as CO_2 capturer. It was presented that the as-synthesized MCM-41, with the optimal TEPA loading of 50 wt%, exhibited CO_2 adsorption capacity of around 4.16 mmol/g in 5% CO_2. Goeppert et al. [153] used different organo-amines to impregnate nanostructured precipitated and fumed silica and compared their CO_2 adsorption capacities. They concluded precipitated and fumed silica as excellent supports for impregnation of amines without showing any difference in adsorption performance. It was found that precipitated silica with 67 wt% PEI loading achieved the CO_2 adsorption capacity of 4.55 mmol/g. For desorption process, fumed silica had slightly better desorption capacity because of its higher surface area. Goeppert et al. [153] indicated that the size of the silica particles and the meso and macropores of the support were more important than the surface area. It was also reported that low-molecular weight PEI had better CO_2 adsorption capacity than high-molecular weight PEI, but suffered from leaching problem. They pointed out that although shorter chain oligomers of ethyleneimine, tetraethylenepentamine (TEPA) and pentaethylenehexamine (PEHA) had higher CO_2 adsorption capacities than linear PEI, they had serious leaching problems and were more difficult for

desorption. Gargiulo and his research group [154] prepared and characterized PEI-impregnated mesoporous silicas using MCM-48 and SBA-15 as supports. Two kinds of adsorbents were compared for CO_2 adsorption performance. It was demonstrated that the surface area and pore size of the adsorbents were reduced as the PEI loading increased. This was proved by XRD and N_2 analysis results that PEI gradually filled the channels of the mesoporous adsorbents as the PEI loading increased. It was stated that the CO_2 adsorption capacity of 50 wt% PEI-MCM-48 and 40 wt% PEI-SBA-15 was over 1.36 mmo/g at 75 ^oC. Franchi et al. [155] developed a novel adsorbent for CO_2 capture namely, DEA loaded PE-MCM-41 silica. The CO_2 adsorption capacity of this novel adsorbent was examined and the CO_2 uptake rate was monitored using TGA. It was demonstrated that this novel adsorbent not only had high CO_2 adsorption capacity compared with other sorbents such as activated carbon, silica gel and standard MCM-41 silica, but also was tolerant to moisture. They explained that the high capacity for CO_2 was due to the high pore volume of the adsorbent which allowed for higher loading of DEA. It was found that the CO_2 adsorption capacity and the CO_2 uptake rate of DEA-impregnated PE-MCM-41 reached maximum when the DEA loading slightly exceeded pore saturation. They also discovered that the CO_2/DEA ratio failed to reach the stoichiometric ratio of the reaction (i.e. 0.5) under dry conditions. This was probably due to the malfunctions of a portion of DEA through interactions with the support surface. Franchi et al. [155] compared their novel adsorbent with zeolite 13X. Although, the adsorption kinetics of the two kinds of adsorbents were similar at a CO_2 partial pressure of 0.15 atm, DEA-impregnated PE-MCM-41 had overwhelmingly high CO_2 adsorption capacity. Another advantage of DEA-impregnated PE-MCM-41 over zeolite 13X, according to Franchi et al. [155], was its tolerance to moisture. It was indicated that with the presence of

moisture, the CO_2 adsorption of zeolite 13 X was hindered. However, the CO_2 adsorption capacity of DEA-impregnated PE-MCM-41, although not improved with the presence of moisture, was not inhibited as much as that of zeolite 13X. Multi-cyclic tests for CO_2 adsorption/desorption of DEA-impregnated PE-MCM-41 and zeolite 13X were conducted and compared. A better stability was maintained by DEA-impregnated PE-MCM-41 than zeolite 13X under same regeneration conditions. A highly efficient adsorbent for CO_2 capture was synthesized and prepared by Qi et al. [156] using PEI or TEPA functionalized mesoporous silica. This novel adsorbent showed extremely high CO_2 adsorption capacity up to 7.9 mmol/g under simulated flue gas conditions (10% CO_2) with the presence of moisture at 75 °C. The kinetics of the adsorbent for the CO_2 adsorption was found to be very fast, reaching 90% of the saturation level within first few minutes. Qi et al. [156] also explored the influencing factors such as particle size as shell thickness on the CO_2 adsorption capacity. It was found that larger particle size, higher pore volume and thinner shell thickness of the adsorbent promoted the CO_2 adsorption performance of the adsorbent. In addition, a good stability of PEI and TEPA functionalized mesoporous silica during multi-cyclic adsorption/desorption tests was shown. A series of different amines were immobilized on a silica support using grafting and impregnation methods by Pirngruber et al. [157] for investigating CO_2 adsorption in a VSA or TSA process using simulated flue gases. They concluded that neither conventional TSA nor conventional VSA operation seem to be viable options. Drage et al. [158] studied the thermal stability of PEI based adsorbents for CO_2 adsorption and two approaches using thermal swing strategy (use of nitrogen or CO_2 as stripping gas for desorption process). It was reported that using thermal swing desorption in the CO_2 atmosphere for a PEI based adsorbent resulted in successive loss of

adsorption capacity after multi-cycles of adsorption/desorption process. It was probably due to the bonding of CO_2 into the PEI polymers, leading to the formation of a urea type linkage above 135 °C. The formation of urea linkage resulted in an irreversible degradation of adsorbent. It was concluded that thermal swing desorption for PEI based adsorbents at high temperatures (e.g. 140 °C) was not practical due to the degradation of the adsorbents, although the kinetics for desorption was very fast. It was stated that pure nitrogen for stripping, although was used in this paper to overcome the problems stated above, would not be used in real application of the technology. Wang et al., 2013 [159] studied the SBA-15 with different PEI loadings for CO_2 capture using a model flue gas containing 15% CO_2, 4.5% O_2 and 80.5% N_2. It was noted that the structure of SBA-15 was preserved after PEI loading, while the surface area and pore volume were decreased dramatically. PEI was dispersed inside the pore channels of SBA-15 when the PEI loading was less than 50 wt%. Higher PEI loading resulted in the extra PEI coated on the external surface of the SBA-15 particles, leading to agglomeration of the sorbent particles. The CO_2 adsorption capacity and adsorption/desorption rate decreased. The optimal PEI loading was at 60 wt% with the highest CO_2 adsorption capacity of 3.5 mmol/g at 75 °C. However, the SBA-15 with 30 wt% PEI loading showed the highest ratio of CO_2 uptake to the potential amine sites. This was probably due to the better PEI dispersion inside the pores with lower diffusional barrier. Pérez et al. [160] prepared SBA-15 functionalized by amino groups to test for CO_2 capture under a simulated flue gas. The SBA-15 material was functionalized by grafting with aminopropyl-trimethoxysilane and diethylene-triamine-trimethoxy- silane, and by impregnation with polyethyleneimine (PEI) and tetraethylene- pentamine (TEPA). It was indicated that the grafted sorbents and impregnated sorbents with amine loading higher than 50 wt% were not sensitive to

the concentration of CO_2 in the feed gas for CO_2 capture. The adsorption capacity was maintained after 10 cycles of adsorption/desorption for grafted sorbents and PEI-impregnated sorbents. However, for TEPA-impregnated sorbents, the CO_2 adsorption capacity decreased. For all amine-functionalized SBA-15, the CO_2 adsorption capacity decreased significantly with the presence of 1000 ppm SO_2 for 5 cycles, indicating an interaction with the nitrogen content of the sorbents. In addition, the CO_2 adsorption capacity of the grafted samples was not affected by the presence of moisture. However, the humid conditions improved the CO_2 adsorption capacity of impregnated samples up to 3.7 mmol/g for 50 wt% TEPA-SBA-15 with 15% CO_2 and 5% moisture at 45 °C and 1bar.

2.3.7 Amine functionalized alumina supported sorbents

Chen et al., 2011 [161] synthesized and prepared a mesoporous alumina (MA) with a high surface area and large pore volume using a sol-gel process. It was reported that the CO_2 adsorption capacity of MA was about 1.18 mmol/g at 1 bar, which was higher than that of a commercial alumina or 3-aminopropyl-trimethoxy-silane-grafted MCM-41. The CO_2 adsorption capacity at high pressures (0-30 bar) was found in the sequence of MA > 13X > SBA-15 > commercial alumina. The PEI impregnated MA was also prepared by Chen et al. [161]. The CO_2 adsorption capacity of PEI-impregnated MA was 2.73 mmol/g, which was comparable to the sorption capacity of PEI-impregnated mesoporous materials. Cai et al., 2014 [162] successfully synthesized a novel amino-functionalized MA with enhanced affinity towards Cr (VI) and CO_2. The TEPA was impregnated in the MA support. The CO_2 adsorption capacity of the modified sorbent was 0.7 mmol/g at room temperature.

Chapter 3

Materials and methods

3.1 Material synthesis

3.1.1 Chemicals

Non-ionic tri-block copolymer surfactant Pluronic P123, (poly (ethylene oxide)-block-poly (propylene oxide)-block-poly (ethylene oxide), EO20-PO70-EO20, M_w=5800) purchased from Sigma–Aldrich was used as the organic structure directing agent. Hydrochloric acid (HCl) with purity of 36.8%-38% purchased from Capital Scientific was used as a pH controlling agent. Tetraethyl orthosilicate (TEOS 98%) purchased from Sigma–Aldrich was used as a silica source. 1,3,5-trimethylbenzene (TMB 99%) purchased from Sigma–Aldrich was used as organic swelling agent. Ammonium fluoride (NH_4F 98%) purchased from Sigma–Aldrich was used as window size expander. Methanol (≥99.9%) purchased from Sigma–Aldrich was used as solvent in impregnation step. Branched polyethylenimine (PEI) with average molecular weight about 800 g/mol was purchased from Sigma–Aldrich. Deionized water was obtained from a Milli-Q integral pure and ultrapure water purification system. Pure CO_2 (99.99%) and pure N_2 (99.999%) gases were ordered from Praxair for the CO_2 adsorption/desorption measurements.

3.1.2 Preparation of MCFs substrate

The mesoporous cellular foams (MCFs) support used in this work was synthesized based on the method reported by Schmidt-Winkel et al. [163]. In a typical synthesis, the following steps are followed:

1. 4.0 g of Pluronic P123 was dissolved in 150 ml of 1.6 M HCl aqueous solution at ambient temperature. A homogeneous mixture was obtained after stirring for long enough time.
2. 4.0 g of TMB and 46 mg of NH_4F were then added to the above solution
3. The mixture was heated to 37-40 °C and stirred for long enough time
4. 8.8 g of TEOS was added drop wise and stirred at 37-40 °C for 24 hours
5. The slurry was transferred into an autoclave and aged at 100 °C for 24 hours
6. The mixture was then filtered, washed with DI water and ethanol and then dried at 60 °C overnight
7. The as-synthesized sample was calcined at 500 °C for 8 hours

A detailed scheme of calcined MCFs substrate is shown in Figure 3.1.

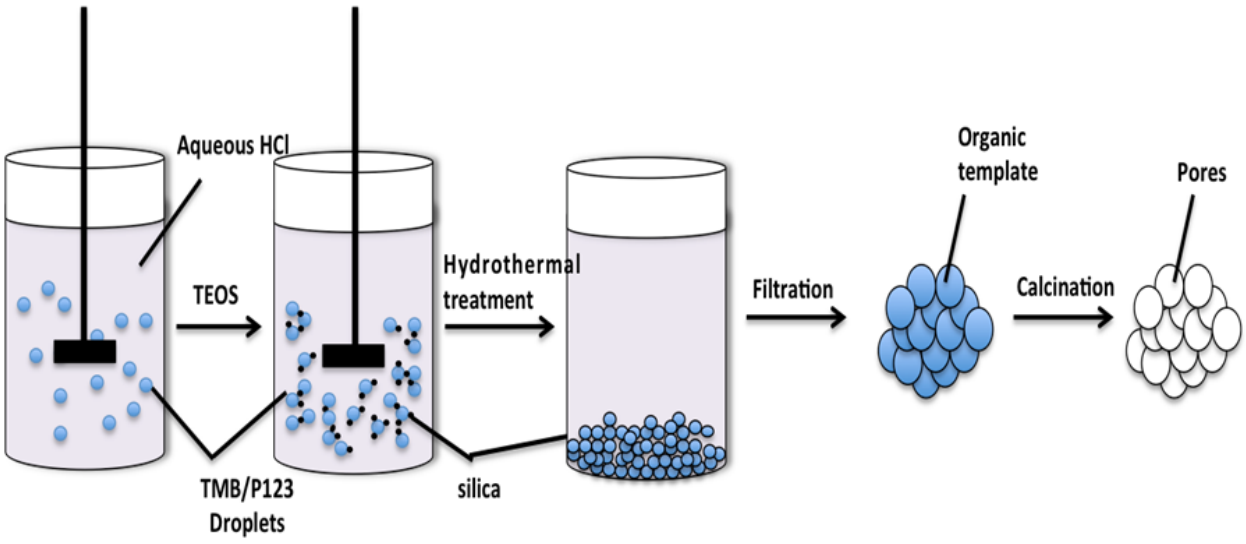

Figure 3.1 Scheme of calcined MCFs substrate preparation.

3.1.3 PEI impregnation onto MCFs

The PEI-modified MCFs sorbents were prepared by wet impregnation method [141, 164]. In a typical preparation process, a desired amount of PEI was dissolved in 4 g of methanol under stirring for 15 min. Then 1 g of calcined MCFs support was added to the solution mixture and stirred for another 30 min. The resulting slurry was transferred in an aluminum pan and dried in a vacuum dryer at 70 °C for 6 hours.

3.2 Characterization of adsorbents

Various characterization methods, including Nitrogen adsorption/desorption, Scanning Electron Microscopy (SEM), Transmission Electron Microscopy (TEM), Thermo-gravimetric analysis (TGA), and Fourier Transform Infrared Spectroscopy (FTIR), were used for the characterization of as-synthezied MCFs, calcined MCFs and PEI-impregnated MCFs.

3.2.1 Nitrogen sorption analysis

3.2.1.1 Brunauer-Emmett-Teller (BET) theory and multi-point measurements

The specific surface area of the porous materials can be determined by the amount of adsorbate on a monomolecular layer of the sorbent surface caused by the van der Waals forces between the adsorbate gas molecules and the adsorbent surface. The determination is carried out using liquid nitrogen. The BET adsorption isotherm equation [165] is used to calculate the surface area of the sorbents using multi-point measurement.

$$\frac{1}{V_a\left(\frac{P_0}{P}-1\right)} = \frac{C-1}{V_m C} \cdot \frac{P}{P_0} + \frac{1}{V_m C} \tag{3.1}$$

Where,

P = partial vapour pressure of adsorbate gas in equilibrium with the surface at -196.15 °C, in Pa.

P_0 = saturated pressure of adsorbate gas, in Pa.

V_a = volume of gas adsorbed at standard temperature and pressure (STP), in mL.

V_m = volume of gas (STP) adsorbed to produce an apparent monolayer on the sample surface, in mL.

C = constant that is related to the enthalpy of adsorption of the adsorbate.

The BET value $\frac{1}{V_a(\frac{P_0}{P}-1)}$, is plotted against $\frac{P}{P_0}$ based on equation 1. Linearity is obtained between the pressure ranges from 0.05 to 0.3, with the correlation coefficient of the linear regression not less than 0.997.

3.2.1.2 Experimental

Nitrogen adsorption/desorption isotherms were collected under the relative pressure (P/P_0) range of 0-0.997 at -196.15 °C using Autosorb iQ. Prior to nitrogen adsorption measurement, the calcined MCFs and PEI-impregnated MCFs were degassed to remove all the gases and vapors previously adsorbed after manufacture, or during handling or storage. Different degassing conditions were applied for calcined MCFs and PEI-impregnated MCFs to avoid affecting the nature of the surface of the sorbents during outgassing process. For the calcined MCFs, it was degassed at 150 °C for 4 h. For PEI-impregnated MCFs, the modified samples were degassed at 70 °C for only 30 min to avoid any amine loss during the degassing. The surface area was calculated based on the Multi-point BET measurements at a range of relative pressure points between 0.05 and 0.30. The Barrett-Joyner-Halenda (BJH) pore analysis method was used to

determine the cell diameter (D_c) from the adsorption branch of N_2 sorption isotherms and window diameter (D_w) from desorption branch of N_2 sorption isotherms. The total pore volume (V_t) was determined by the volume of liquid nitrogen adsorbed at a relative pressure (p/p_0) of 0.997. Table 3.1 shows the detailed degassing conditions of sorbents for N_2 adsorption analysis.

Table 3.1 Summary of degassing conditions of sorbents for N_2 adsorption analysis.

Sample	Degassing temperature (°C)	Degassing time (h)	Ramping rate (°C/min)
Calcined MCF	150	4	2
50 wt% PEI-MCF	70	0.5	2
60 wt% PEI-MCF	70	0.5	2
70 wt% PEI-MCF	70	0.5	2
80 wt% PEI-MCF	70	0.5	2

3.2.2 Scanning electron microscope (SEM)

The SEM analysis was carried out to study the morphology of the samples using a Hitachi S-2700 scanning electron microscope. Samples were placed on a sample holder with a carbon tape/coating and then coated with gold for SEM analysis.

3.2.3 Transmission electron microscope (TEM)

The TEM images of the samples were performed on a JEOL 2010 TEM. This high resolution TEM was equipped with LaB6 electron gun. The samples were prepared in the methanol solution and then deposited on a copper grid.

3.2.4 Fourier transform infrared spectroscopy (FTIR)

An iS50 FTIR spectrometer equipped with Smart iTR diamond ATR was used to obtain FTIR spectra of samples. Each sample was scanned 100 times over the frequency range 500 – 4000 cm^{-1}. The resolution in use was 4 cm^{-1}.

3.2.5 Thermal behaviours of pre-calcined MCFs and PEI-impregnated MCFs

The pre-calcined MCFs were subjected to thermogravimetric analysis (TA Instruments Q500 STARe System, Mettler Toledo). The thermal stability of pre-calcined MCFs was determined and the components of pre-calcined MCFs were obtained. The pre-calcined MCFs were first properly grinded into uniform particle sizes. Around 5 mg of pre-calcined MCFs were loaded. They were heated up to 105 °C at a heating rate of 10 °C /min under pure N_2 with a flow rate of 100 cm^3/min to remove all the moisture and adsorbed CO_2. After being isothermal for 30 minutes, the temperature was then continuously heated up to 600 °C at a heating rate of 10 °C /min under pure N_2 with a flow rate of 100 cm^3/min and kept isothermal for 30 minutes. For samples of PEI-impregnated MCFs, around 5mg of the sample was loaded each time. They were heated from room temperature to 600 °C with a heating rate of 10 °C/min under pure N_2 with a flow rate of 100 cm^3/min and kept isothermal at 600 °C for 30 min.

3.3 CO_2 adsorption/ desorption measurements

The CO_2 adsorption capacity as a function of time was monitored using thermo-gravimetric Analysis (TGA) apparatus (TA Instruments Q500 STARe System, Mettler Toledo). 95% CO_2/5% N_2 gas mixture or simulated flue gas (10% CO_2/90% N_2) in dry or humid conditions under

atmospheric pressure was used for CO_2 adsorption measurements. Pure N_2 was used as the purge gas for CO_2 desorption measurements. The sample was first properly grinded into uniform particle sizes. Around 5 mg of PEI impregnated MCF was loaded for each run. The sorbent was heated up to 105 °C at a heating rate of 10 °C/min under pure N_2 with a flow rate of 100 cm^3/min to remove all the moisture and adsorbed CO_2. After being isothermal for 30 minutes, the temperature was then cooled down to the desired adsorption temperature (e. g. 25 °C, 40 °C, 60 °C, 75 °C, , 90 °C). Once the temperature was equilibrated with the desired temperature, the gas was switched from pure N_2 to 95% CO_2/5% N_2 or simulated flue gas (10% CO_2/90% N_2) with the flow rate of 100 cm^3/min. The adsorption process started and was kept isothermal at desired adsorption temperature for 60 min. Then the temperature was increased from desired temperature to 105 °C with a ramping rate of 2 °C/min. The gas was switched back to the N_2 as the purge gas to desorb all the adsorbed CO_2 from the sorbents. The temperature was held at 105 °C for 60 min for desorption process.

The effect of moisture on the CO_2 adsorption capacity was also studied by exposing the sorbent to a humid stream of 10% CO_2/ 90% N_2 gas mixture. 10% CO_2/90% N_2 gas mixture was passed via a water saturator maintained at room temperature to obtain humid CO_2/N_2 gas stream.

50 multi-cycle adsorption/desorption tests were conducted to explore the durability performance of PEI-impregnated MCFs using simulated flue gas under 10% CO_2 and 90% N_2 in humid conditions at various adsorption temperatures. Each cycle was comprised of 10 min of CO_2 adsorption at desired adsorption temperature, followed by 10 min of desorption at 105 °C.

Chapter 4

Sorbent Characterization and Performance Evaluation

4.1 Material characterization

The calcined MCFs and PEI-impregnated MCFs were characterized using nitrogen adsorption/desorption, SEM, TEM, and FTIR. The characterization results are discussed in this section.

4.1.1 Nitrogen adsorption/desorption

Figure 4.1 shows the typical N_2 adsorption/desorption isotherms and pore size distributions of the calcined MCFs substrate. It can be seen from this figure that the calcined MCFs substrate has typical Type IV isotherm with hysteresis loop, which is the characteristic feature of the mesoporous materials. The pore size distribution for adsorption of calcined MCFs exhibit a sharp and narrow peak, which represents the pore diameter of the silica substrate centered at around 33 nm. The pore size distribution for desorption of calcined MCFs exhibited a sharper peak, which represents the window diameter of the substrate centered at around 16 nm. The high and narrow peaks of the pore size distribution curves indicate that the calcined MCFs have a good uniformity of pore structures.

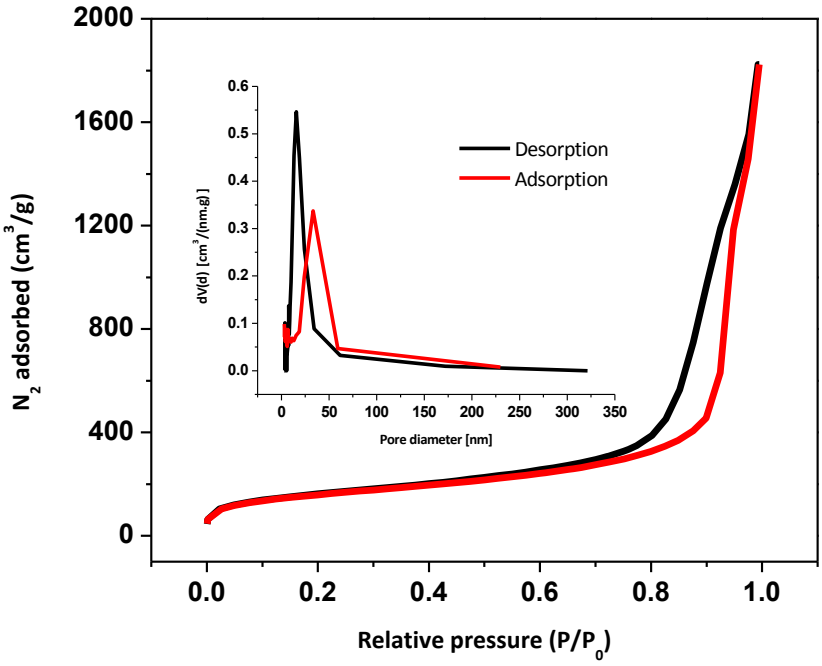

Figure 4.1 Nitrogen adsorption/desorption isotherm at -196.15 °C and BJH pore size distribution of calcined MCFs silica support.

Figure 4.2 shows the N_2 adsorption/desorption isotherms of calcined MCFs and the functionalized MCFs with different PEI loadings for comparison. It can be observed that the shape of all the nitrogen adsorption/desorption isotherms is typical Type IV isotherm and no change of hysteresis was observed with different loadings of PEI impregnation. It indicates that the order of the pores was not altered by the PEI impregnation. However, a huge decrease in specific surface area and total pore volume occurred as PEI was impregnated into the substrate. As PEI loading increases, the specific surface area and total pore volume decrease. The detailed specific surface area and total pore volume of calcined MCF before and after impregnation are summarized in Table 4.1. As can be seen in Table 4.1, calcined MCFs exhibits the largest BET

surface area, highest pore volume and pore diameters. Its large surface area and large pore volume allow more amines to be impregnated onto it. The CO_2 adsorption capacity would therefore increase due to increased amount of amines. After impregnation step, a significant decrease in the surface areas and total pore volumes of the functionalized MCFs was observed. The shrinking of the specific area and total pore volume of the modified MCFs is due to the pore filling by PEI molecules. The schematic diagram of MCFs before and after calcination is shown in Figure 4.3.

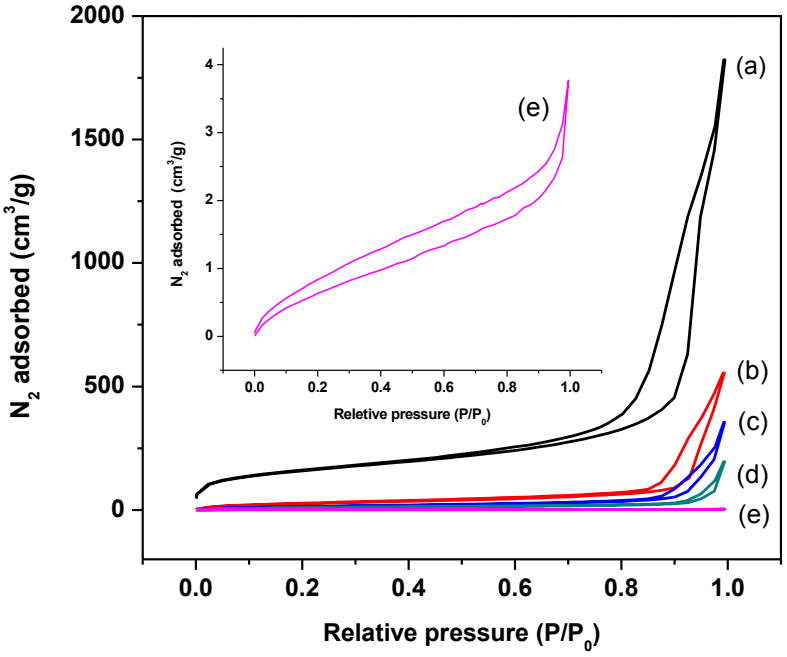

Figure 4.2 N_2 adsorption/desorption isotherms of calcined MCFs before and after impregnation. ((a) Calcined MCFs, (b) 50 wt % PEI-MCFs, (c) 60 wt% PEI-MCFs, (d) 70 wt% PEI-MCFs, (e) 80 wt% PEI-MCFs.)

The pore size distribution of calcined MCFs with/without PEI impregnation according to the BJH method is illustrated in Figure 4.4. For all the samples, cell and window size distributions

tend to stay within a range. This result suggested that MCFs supports were uniformly coated with PEI molecules. A slightly increase in cell and window diameters was observed after PEI loading was 50 wt% and 60 wt%. It is probably due to the loss of small pores becoming significant after complete filling with PEI molecules. It can be seen that Figure 4.4 that almost no porosity was observed after PEI loading exceeded 70 wt%. This indicates that all the pores are completely filled with PEI molecules.

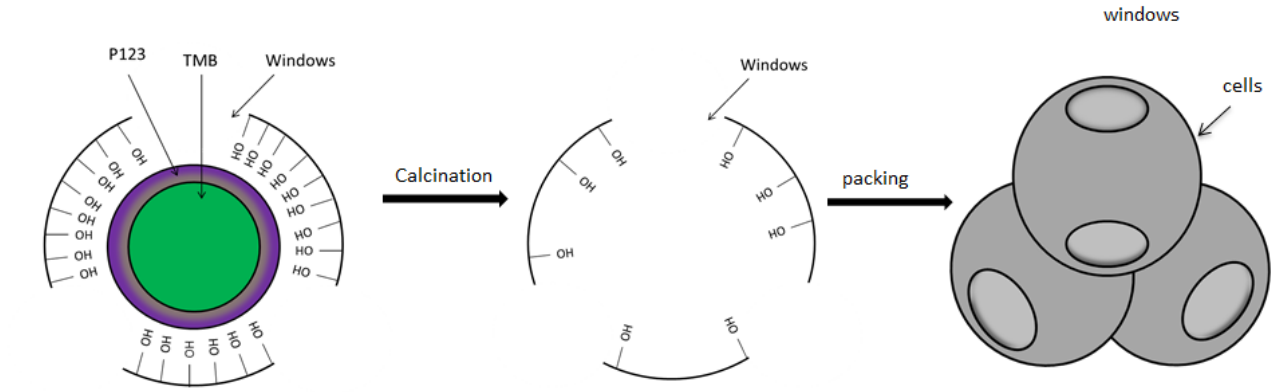

Figure 4.3 Schematic diagram of template removal from as-synthesized MCFs.

Table 4.1 Properties of calcined MCFs and PEI-impregnated MCFs.

Sample	S_{BET} [m^2/g]	V_{Tot} [cm^3/g]	D_c [nm]	D_w [nm]
Calcined MCFs	557.87	2.82	33.23	15.57
MCF-50PEI	98.87	0.857	34.19	18.81
MCF-60PEI	52.12	0.55	33.4	18.93
MCF-70PEI	31.02	0.302	6.138	3.301
MCF-80PEI	3.035	0.00583	4.186	3.49

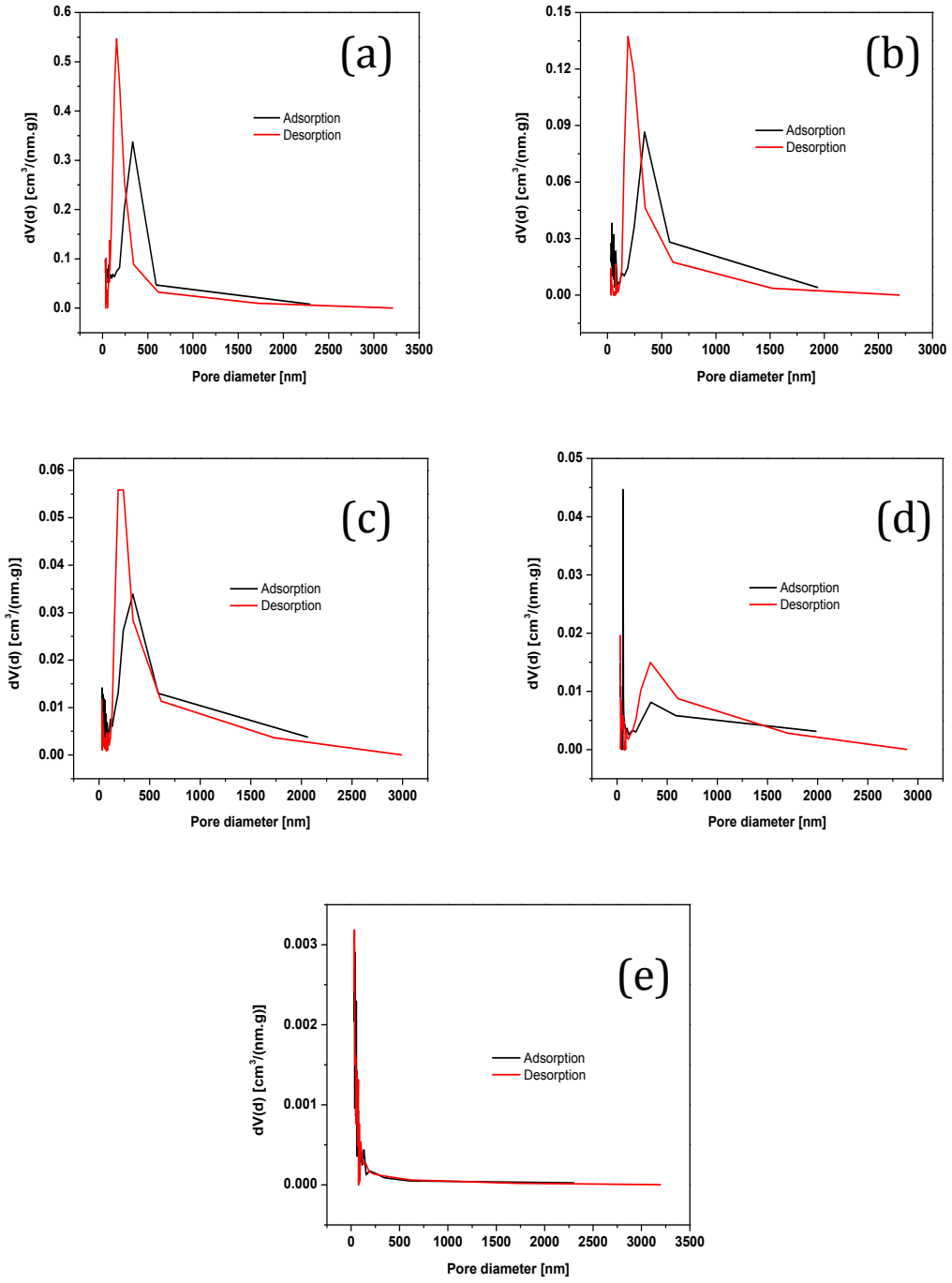

Figure 4.4 Pore size distributions of calcined MCFs and PEI-impregnated MCFs ((a) Calcined MCFs, (b) 50 wt % PEI-MCFs, (c) 60 wt% PEI-MCFs, (d) 70 wt% PEI-MCFs, (e) 80 wt% PEI-MCFs).

4.1.2 SEM and TEM

Figure 4.5 (a) presents the SEM image of calcined MCFs without PEI impregnation. From these images, it can be seen that the surface of the MCFs is very porous. Figure 4.5 (b)-(e) show the TEM images of calcined MCFs and PEI impregnated MCFs with different PEI loadings. It can be observed that calcined MCFs consist of large spherical cavities interconnected by apertures with the diameter of apertures smaller than that of spheres. TEM images of calcined MCFs before and after impregnation are very similar, indicating that PEI impregnation does not change the morphology of the MCFs.

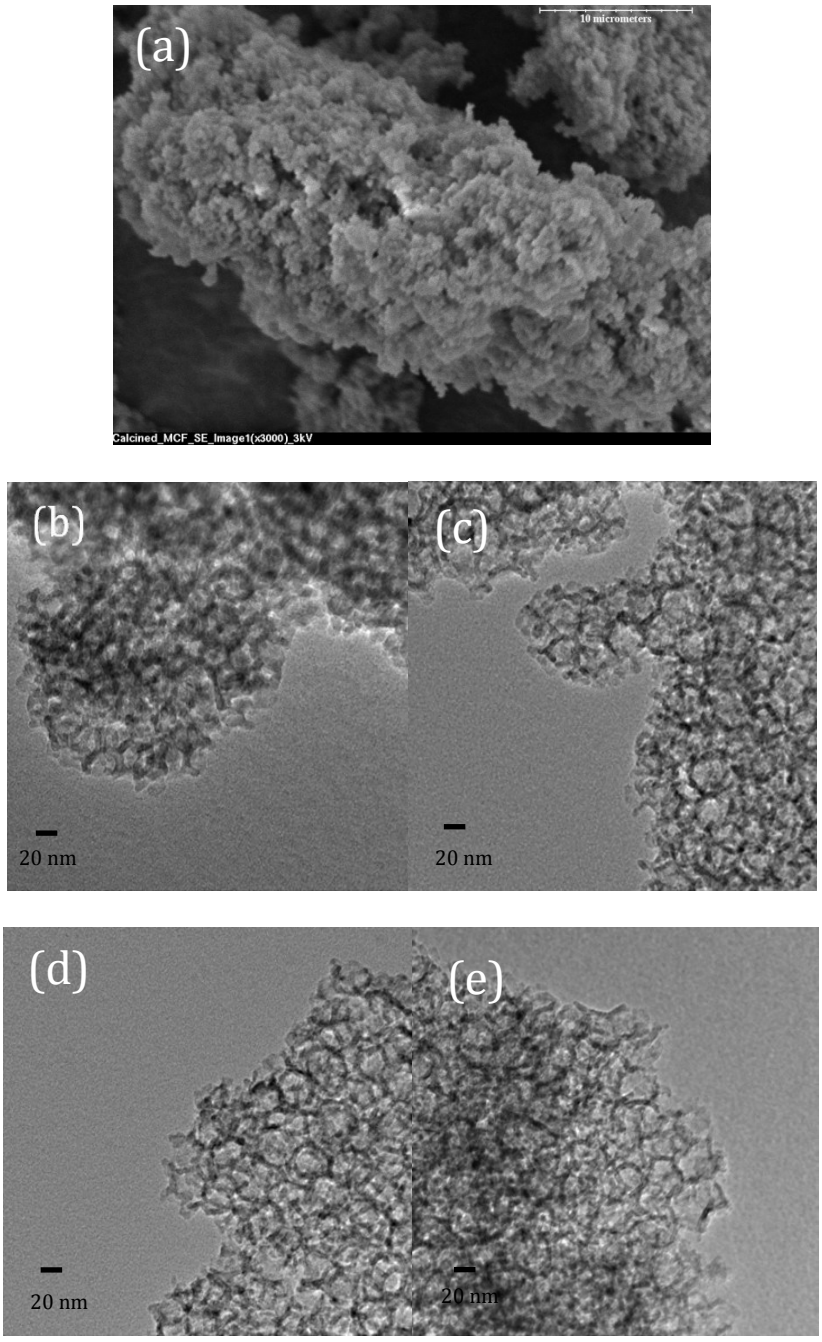

Figure 4.5 (a) SEM image for the calcined MCFs substrate, (b)-(e) TEM images for 50wt% PEI-MCFs, 60wt% PEI –MCFs, 70wt% PEI-MCFs, respectively.

4.1.3 FTIR analysis

In order to determine the functional groups on the surface of the substrate, the FTIR was used. Its spectrum is shown in Figure 4.6. From this figure, it can be seen that in the spectrum of impregnated MCFs, there is a peak in the region 3500-3300 cm^{-1} due to amine N-H stretching. Another two peaks due to C-H asymmetric stretching and symmetric stretching appear in the region 2950-2850 cm^{-1}, respectively. N-H bending vibration produced a peak in the region 1650-1580 cm^{-1}. A peak in the region 1250-1020 cm^{-1} was assigned to C-N stretching of amines. For both calcined MCFs and amine-functionalized MCFs, there is a sharp and intense peak in the region 1200-1000 cm^{-1} due to the Si-O-Si asymmetric stretching. All these peaks resulting from strong interactions between amine groups and the silica surface indicate that the PEI was successfully impregnated.

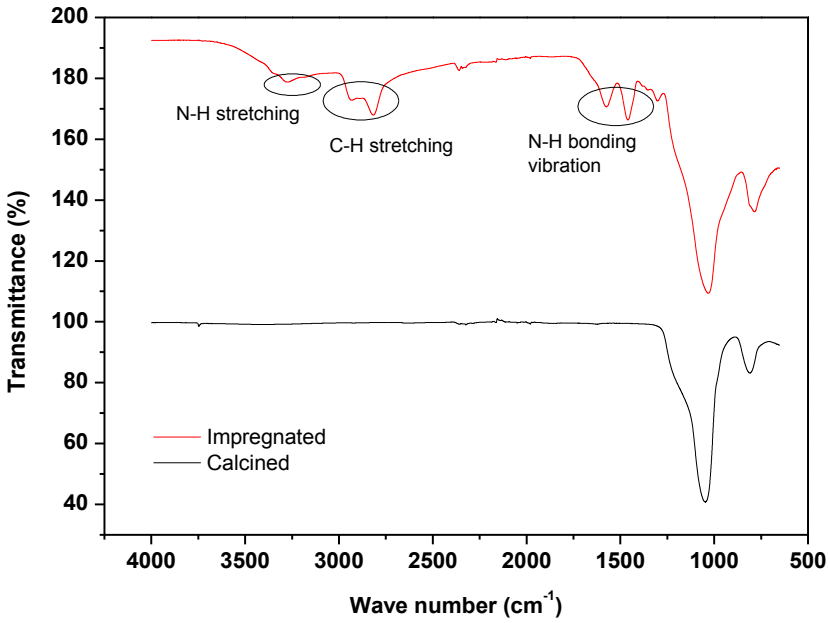

Figure 4.6 Infrared spectra of MCFs before and after PEI modification.

4.1.4 Thermal behaviours of pre-calcined MCFs and PEI-impregnated MCFs

In order to investigate the thermal behavior of pre-calcined MCFs and to determine its composition, the MCFs before calcination were exposed at high temperatures in pure N_2 with the application of TGA instrument to monitor the mass change during the process. The temperature rose from room temperature to 600 °C with a ramping rate of 10 °C /min. Figure 4.7 presents the thermal stability of the pre-calcined MCFs. It can be seen that the total weight loss of the pre-calcined MCFs was around 70%. A 31% weight loss happened as the temperature increased from room temperature to 105°C due to desorption of water and adsorbed CO_2. Another 40% weight loss occurred as temperature further increased up to 600 °C due to the decomposition of P123 and other organics. Four samples of PEI-impregnated MCFs with different amine loadings were prepared and measured using the same TGA method in dry N_2 in order to determine the thermal behavior of PEI-impregnated MCF. Figure 4.8 shows the thermal stability of PEI-impregnated MCFs with different amine loadings. It can be seen from this figure that for all the four samples a first weight loss occurred as the temperature increased from room temperature to 105°C due to the desorption of water and CO_2. As temperature continues increasing, a steep weight loss happened at the temperature of 250 °C to 400 °C due to the desorption and decomposition of amines. As the temperature goes beyond 400 °C, the weight change for the four samples diminishes indicating all the amine loaded has been fully removed from the substrate. Through all the data from TGA, it can be calculated that the real amounts of PEI impregnated onto the MCFs were 50.02wt%, 59.59wt%, 70.67wt% and 81.37wt%.

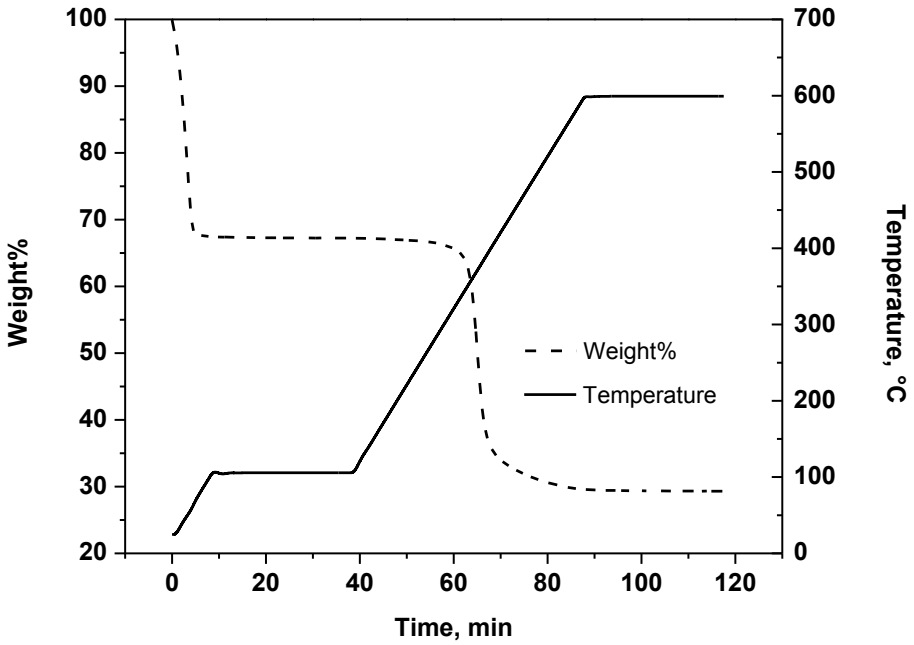

Figure 4.7 Thermal behavior of pre-calcined MCFs using TGA.

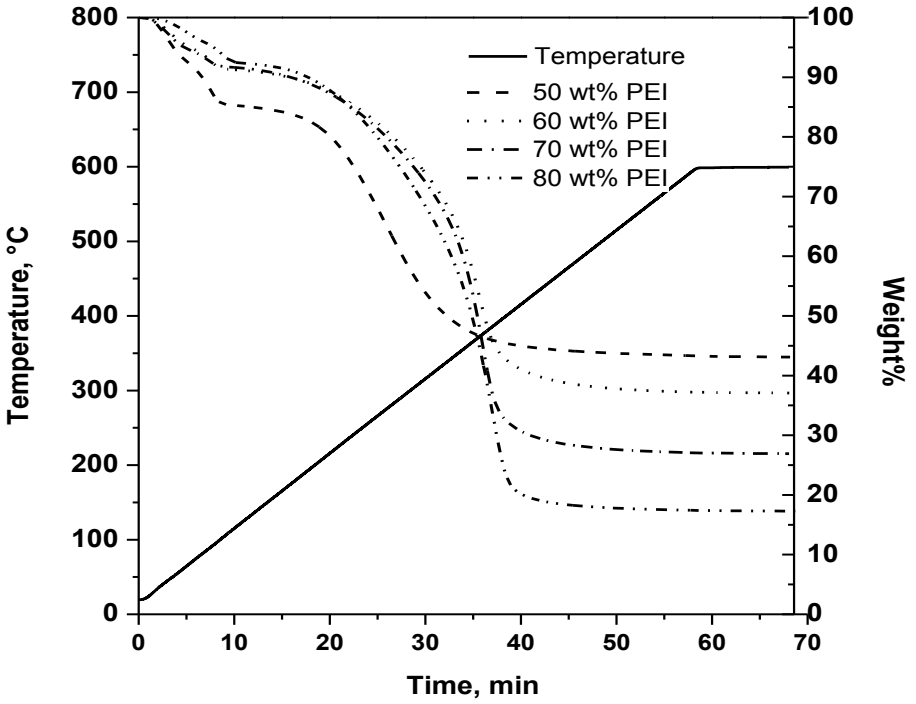

Figure 4.8 Thermal stability of PEI-impregnated MCFs using TGA.

4.1.5 Effect of synthesis conditions on textural properties of calcined MCFs

The effect of amount of TMB, presence of NH_4F, synthesis temperature and stirring time were investigated for the preparation of calcined MCFs substrate.

4.1.5.1 Effect of amount of TMB

The amount of TMB added plays an important role in determining the pore size of the mesoporous silicas. It has been reported that the addition of TMB into the solution resulted in the phase transformation from highly ordered p6mm mesostructure of SBA-15 type mesoporous silica to disordered MCFs [163]. With TMB/P123 mass ratio less than 0.2, SBA-15 type mesoporous silicas were obtained; with TMB/P123 mass ratio between 0.2-0.3, mixed silicas of SBA-15 and MCFs were found; with TMB/P123 mass ratio beyond 0.3, MCFs wereformed. The added TMB can solubilize with hydrophobic parts of P123 and therefore expands the pore size of calcined MCFs, which is shown in Figure 4.9.

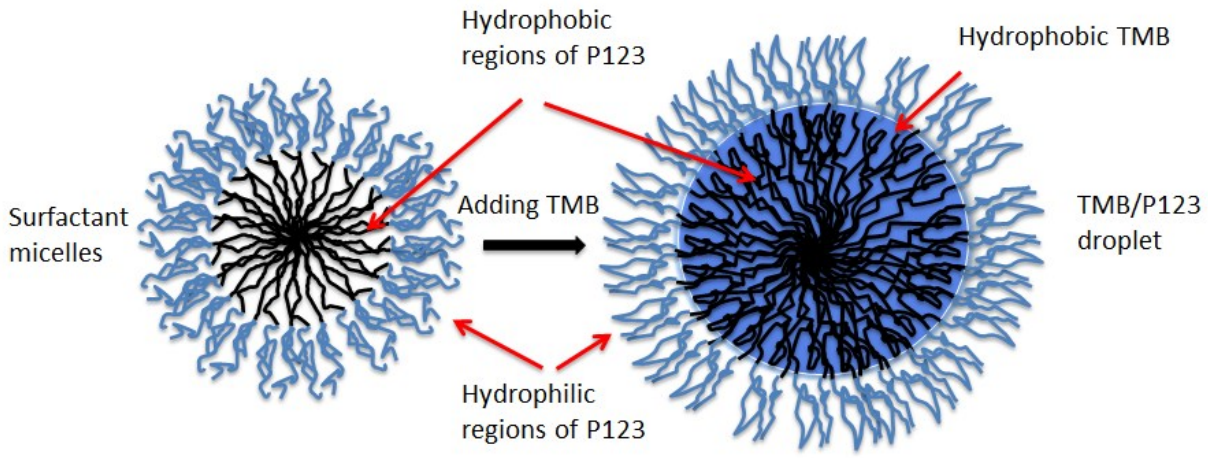

Figure 4.9 Schematic diagram of TMB effect on pore expansion.

In this case, MCFs with different TMB/P123 mass ratio were synthesized. A fixed amount of P123 (4g) was used with a mass ratio of TMB/P123 varied from 1 to 2. The resulting textural properties of MCFs with different TMB/P123 mass ratio are shown in Table 4.2. It can be observed that the cell diameter (D_c) increases with the increase in mass ratio of TMB/P123.

Table 4.2 Comparison of calcined MCFs properties with different TMB/P123 mass ratio.

TMB/P123 mass ratio	S_{BET} [m^2/g]	V_{Tot} [cm^3/g]	D_c [nm]	D_w [nm]
1	948.51	3.52	23.86	13.16
2	998.96	3.88	33.7	15.5

4.1.5.2 Effect of NH_4F

In order to investigate the effect of NH_4F on the structure of MCFs, two batches of calcined MCFs were prepared with and without the presence of NH_4F and the resulting textural properties of MCFs are shown in Table 4.3. It can be observed that the window diameter was effectively enlarged with the presence of NH_4F. Figure 4.10 compares the schematic diagrams of calcined MCFs with and without NH_4F addition.

Table 4.3 Comparison of calcined MCFs properties with and without the presence of NH_4F.

Presence of NH_4F	S_{BET} [m^2/g]	V_{Tot} [cm^3/g]	D_c [nm]	D_w [nm]
Without NH_4F	879.16	2.10	23.45	7.89
With NH_4F	711.64	2.65	23.86	15.5

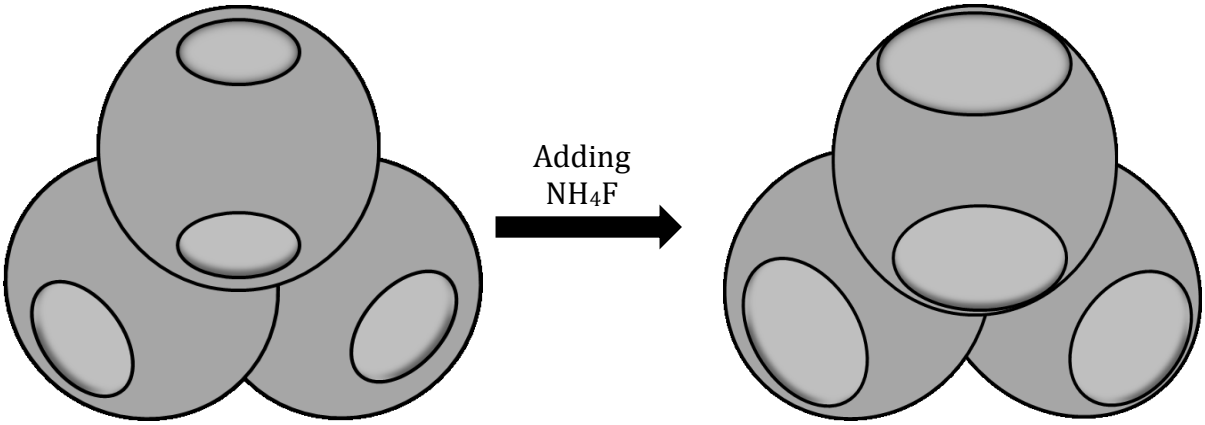

Figure 4.10 Schematic diagram of MCFs with effect of NH_4F.

4.1.5.3 Effect of synthesis temperature

Different synthesis temperatures ranging from 30-40 °C were applied for the preparation of calcined MCFs. The properties of obtained calcined MCFs are summarized in Table 4.4. It can be observed that the specific surface area, total pore volume, cell and window diameters of calcined MCFs increased considerably with increase in synthesis temperature, indicating that the optimal temperature for synthesis is at 40 °C. Lower synthesis temperature results in the negative effect on MCFs preparation.

Table 4.4 Comparison of calcined MCFs properties with different synthesis temperatures.

Synthesis T (°C)	S_{BET} [m^2/g]	V_{Tot} [cm^3/g]	D_c [nm]	D_w [nm]
30	436.62	1.15	6.14	7.65
35	674.13	2.13	18.56	11.41
40	752.8	3.24	33.78	15.48

4.1.5.4 Effect of stirring time

The stirring time after adding TMB and NH_4F into the homogeneous solution has significant influence on the total pore volume and pore diameters of the MCFs. From Table 4.5, it can be

observed that with the increase in the stirring time, the cell diameter increases considerably. As we know that the amount of TMB added into the solution plays an important role in controlling the pore size and pore volume of the structure of mesoporous silicas. However, it takes time for TMB to penetrate and solubilize into the hydrophobic parts of P123. Stirring for a longer time after addition of TMB allows it to fully swelling into the inner-core of P123 micelles, expanding the pores of silica substrate.

Table 4.5 Comparison of calcined MCFs properties with different stirring time.

Stirring time (h)	S_{BET} [m^2/g]	V_{Tot} [cm^3/g]	D_c [nm]	D_w [nm]
0.5	617.29	2.48	3.28	8.47
4	711.64	2.65	23.78	15.5
8	752.8	3.24	33.78	15.48

4.2 CO_2 adsorption performance

4.2.1 Effect of amine loading on CO_2 adsorption capacity

Mesoporous silica supports with different PEI loadings were prepared to determine the effect of amine loadings on CO_2 uptake performance. Figure 4.11 shows the CO_2 adsorption capacities of PEI impregnated MCFs with different amine loadings in 10% CO_2/90% N_2 and 95% CO_2/5% N_2 at 75 °C and atmospheric pressure. It can be observed from the figure that MCFs with 70wt% PEI obtained the highest CO_2 uptakes for both two different gas mixtures. For both 10% CO_2/ 90% N_2 and 95% CO_2/ 5% N_2 gas mixtures, the CO_2 adsorption capacity increases as the amine loadings increases from 50 wt% to 70 wt%. The amine loading at 70 wt% exhibits the maximum value of CO_2 adsorption capacity of 5.16 mmol/g of the dry adsorbent in 95% CO_2/5% N_2 at 75 °C and under atmospheric pressure and 3.95 mmol/g of the dry adsorbent in 10% CO_2/90%N_2 and 95% CO_2/5%N_2 at 75 °C and under atmospheric pressure. As the amine loading continues

increasing from 70 wt% to 80 wt%, the CO_2 adsorption capacity decreases sharply. The reason leading to the reduction of CO_2 uptake over 70 wt% amine loading is probably due to the increased diffusional resistances.

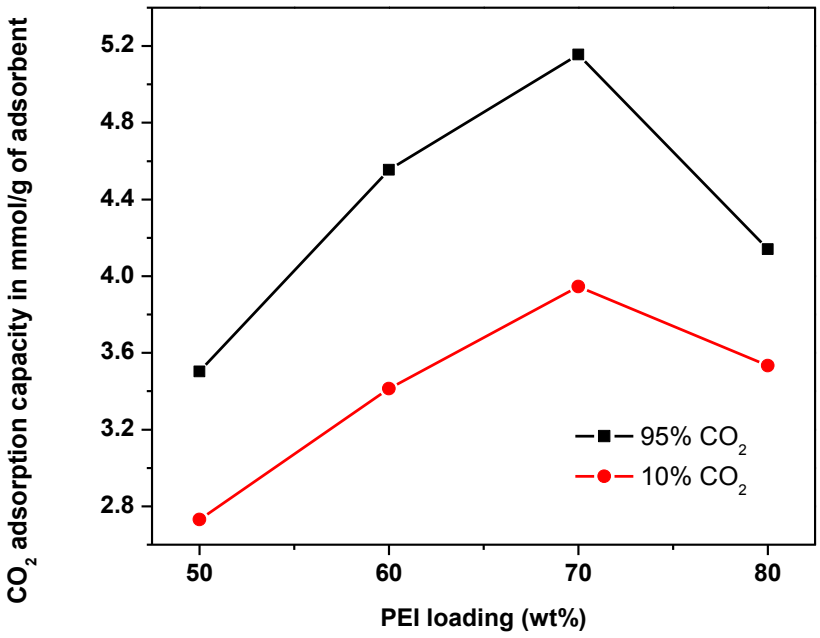

Figure 4.11 CO_2 adsorption capacities of amine-modified MCFs as a function of PEI loadings in 10% CO_2/ 90% N_2 and 95% CO_2/5% N_2 at 75 °C and atmospheric pressure.

In order to use amine efficiently, the amine efficiency (mmol CO_2/ mmol of N) was also evaluated. Figure 4.12 presents the amine efficiency for CO_2 uptake in 10% CO_2/ 90% N_2 and 95% CO_2/5% N_2 gas mixtures at 75 °C and atmospheric pressure. For the gas mixture of 95% CO_2/5% N_2 at 75 °C under atmospheric pressure, the amine efficiency was 0.322 mmol CO_2/ mmol of N with 60 wt% PEI, and 0.312 mmol CO_2/ mmol of N with 70 wt% PEI. For the gas mixture of 10% CO_2/90% N_2 at 75 ^{o}C under atmospheric pressure, the amine efficiency was

0.241 mmol CO_2/ mmol of N with 60 wt% PEI, and 0.239 mmol CO_2/ mmol of N with 70 wt%PEI which indicates that the amine efficiency for both samples are extremely close.

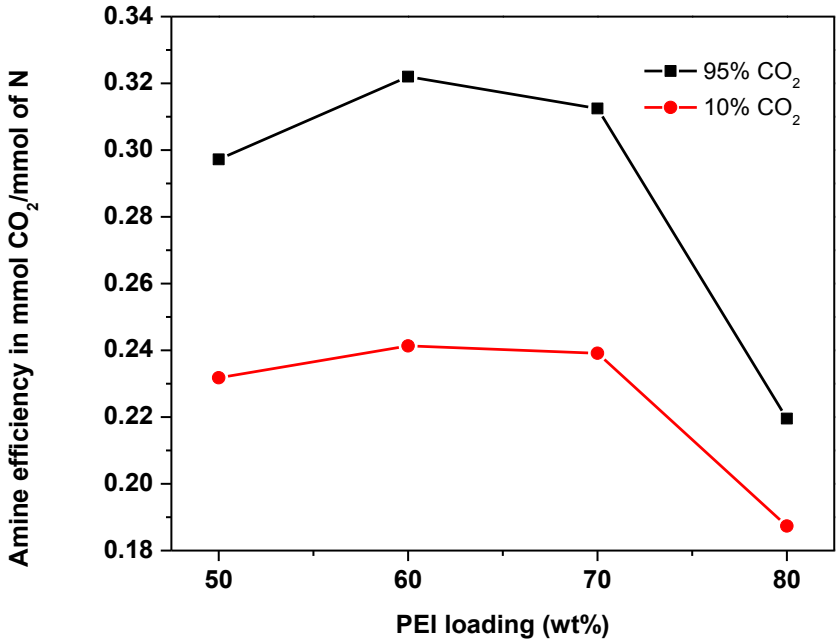

Figure 4.12 Amine Efficiencies of PEI-impregnated MCFs as a function of PEI loadings in 10% CO_2/ 90%N_2 and 95% CO_2/5%N_2 at 75 °C and atmospheric pressure.

Table 4.6 shows the summary of the CO_2 adsorption capacity and amine efficiency of MCFs support with different PEI loadings. It can be observed that for the gas mixture of 10% CO_2/ 90%N_2 at 75 °C and atmospheric pressure, 70 wt% is the optimal PEI loading with the highest CO_2 adsorption capacity and relatively high amine efficiency.

Table 4.6 The amine efficiency and CO_2 adsorption capacity of MCFs with different PEI loadings in 10% CO_2/ 90%N_2 at 75 °C and atmospheric pressure.

PEI loading	Amine loading (wt%)	Adsorption capacity (mmol/g)	N content (mmol N/g)	Amine efficiency (mmol CO_2/mmol N)
50wt%	50.02	2.732	11.63	0.232
60wt%	59.59	3.413	13.95	0.241
70wt%	70.67	3.945	16.28	0.239
80wt%	81.37	3.533	18.6	0.187

4.2.2 Effect of CO_2 adsorption temperature

Figure 4.13 shows the CO_2 adsorption performance of 70 wt% PEI with MCFs under 10% CO_2/90% N_2 and 95% CO_2/5% N_2 at different temperatures. For both gas mixtures, the CO_2 adsorption capacity reached the maximum value at 75 °C, which indicates that 75 °C is the optimal adsorption temperature for CO_2 adsorption. For 10% $C0_2$/90% N_2 gas mixture, the CO_2 adsorption capacity of the sample increased from 2.49 mmol/g at 25 °C to 3.95 mmol/g at 75 °C. While the CO_2 adsorption capacity decreased to 2.55 mmol/g at 90 °C after the temperature was over 75 °C. For 95% $C0_2$/5% N_2 gas mixture, the CO_2 adsorption capacity of the sample increased from 2.68 mmol/g at 25 °C to 5.16 mmol/g at 75 °C. While the CO_2 adsorption capacity decreased to 5.12 mmol/g at 90 °C after the temperature was over 75 °C. It can be observed from this figure that the CO_2 adsorption capacity increased with temperature up to 75 °C and after that decreased with temperature for both gas mixtures. The CO_2 adsorption capacities of the sample in the 95% $C0_2$/5% N_2 gas mixture were higher than that in the 10% $C0_2$/90% N_2 gas mixture. It may be due to the higher concentrations of CO_2 in the 95% $C0_2$/5% N_2 gas mixture resulting in higher CO_2 adsorption capacity. The CO_2 adsorption uptake of the sample was lower at low temperatures (e.g. 25 °C). It is probably because of the slow diffusion

of CO_2 into the multilayers of the amine impregnated onto the support. The low temperature resulted in a higher kinetic barrier for diffusion. The low CO_2 adsorption capacity of the sample at high temperatures (e.g. 90 °C) is due to the exothermic nature of the reaction. The optimal adsorption temperature in the consideration of kinetics and thermodynamics is 75 °C.

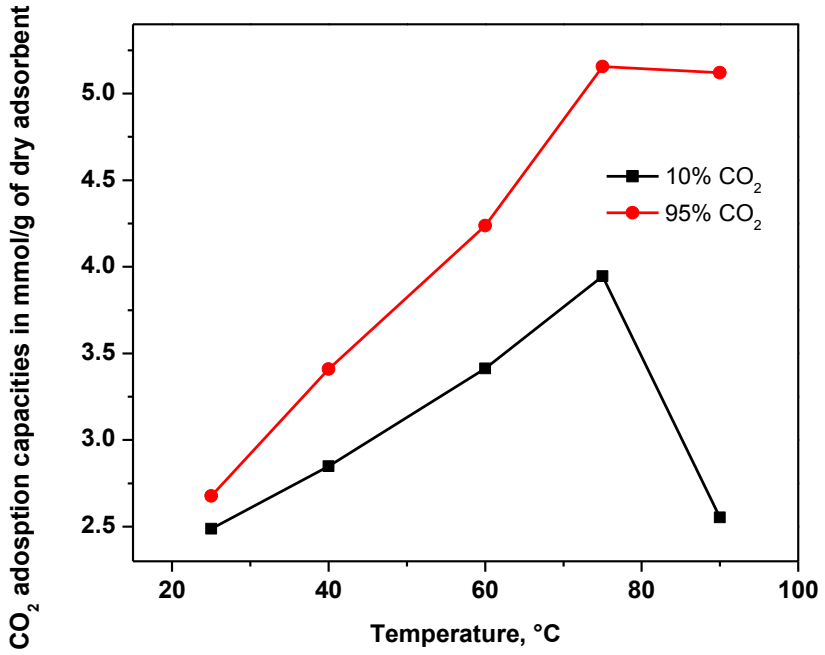

Figure 4.13 CO_2 adsorption capacities of 70 wt% PEI with MCFs in 10% CO_2/ 90% N_2 and 95% CO_2/5% N_2 at different temperatures.

4.2.3 Effect of CO_2 partial pressure

Figure 4.14 shows the effect of CO_2 adsorption capacity of 70 wt% PEI-MCFs as a function of CO_2 partial pressure at 75 °C and atmospheric pressure. It can be seen from the figure that the CO_2 adsorption capacity increased as the CO_2 partial pressure of the gas increased from 10% to 95%. The CO_2 adsorption capacity increased fast at the lower partial pressures of CO_2 and then increased slowly as the partial pressure of CO_2 continued to increase.

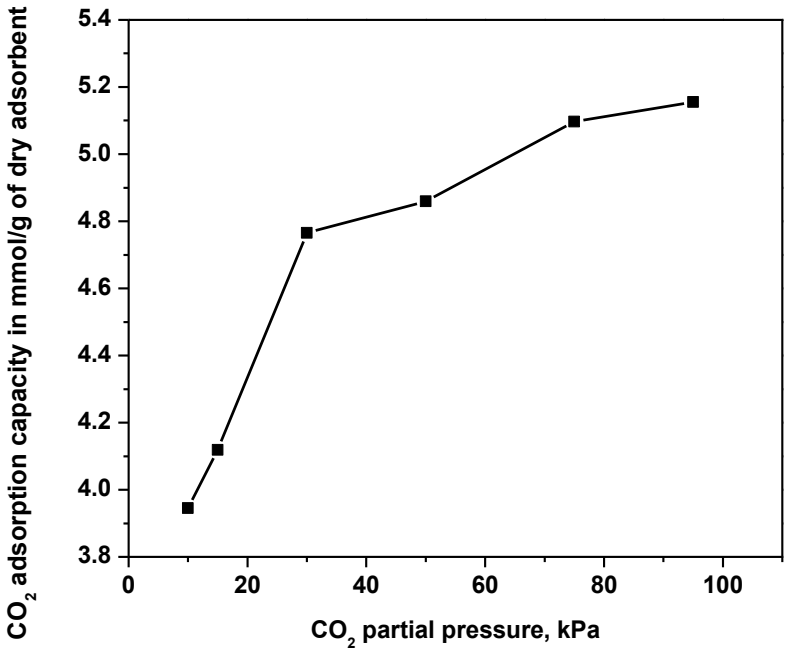

Figure 4.14 The CO_2 adsorption capacity of 70 wt% PEI-MCFs as a function of CO_2 partial pressure at 75 °C and atmospheric pressure.

4.2.4 Kinetics analysis

The kinetics of the reaction needs to be fast enough to obtain high efficiency for CO_2 capturing. In order to evaluate the kinetics of the samples for CO_2 adsorption performance, a series of TGA experiments were conducted under specified conditions. Figure 4.15 illustrates the CO_2 adsorption capacity of MCFs support with different amine loadings as a function of time in the mixed gas of 10% CO_2/ 90% N_2 at 75 °C and atmospheric pressure. The CO_2 adsorption capacity was calculated according to the weight gain per initial weight of the dry adsorbent during the reaction process of adsorption. It can be observed from the figure that the CO_2 adsorption capacity for the samples of MCFs with 60 wt% PEI and 70 wt% PEI increased sharply at the beginning with CO_2 exposure time indicating that the kinetics for the CO_2 capturing with these

two samples are very fast, followed by the samples with 50wt% and 80 wt% PEI. For the adsorbents with 50 wt% PEI, 60 wt% PEI and 70 wt% PEI, they reached pseudo-equilibrium status within 2 minutes. For the adsorbents with 80 wt% PEI, it takes longer time for the saturation status.

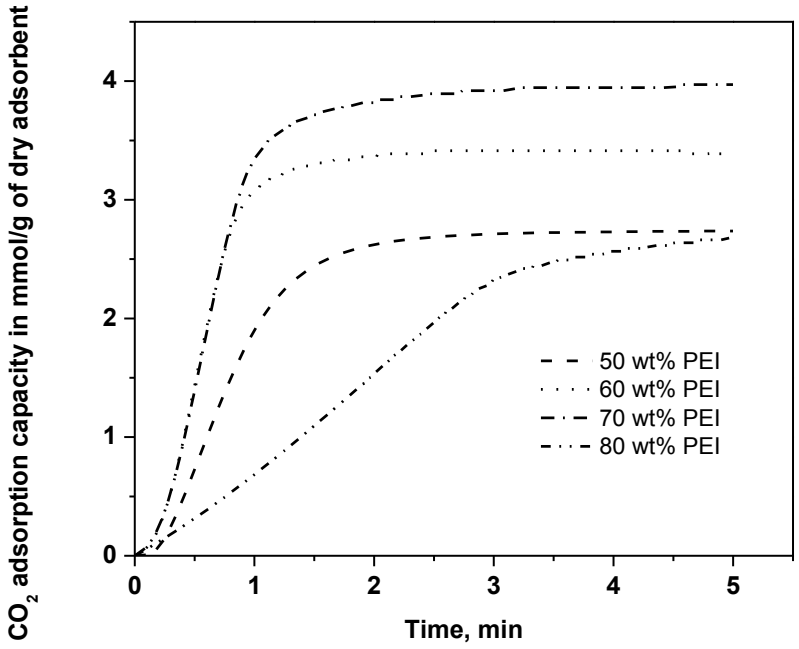

Figure 4.15 CO_2 adsorption capacity of MCFs support with different amine loadings as a function of time in the mixed gas of 10% CO_2/ 90% N_2 at 75 °C and atmospheric pressure.

Table 4.7 shows the comparison of the CO_2 adsorption capacity for the samples of MCFs with different PEI loadings exposed for the adsorption period of 5 minutes and 1 hour. It was found that for the MCFs with 50 wt% PEI, 60 wt% PEI and 70 wt% PEI, the kinetics of the reaction was very fast. Though we extend the adsorption time from 5 minutes to 1 hour, the CO_2 adsorption capacity still maintain the same which means that the reaction achieved the pseudo-equilibrium status within 5 minutes. However, for the sample with 80 wt% PEI, there is still

some room to improve the CO_2 adsorption capacity if the time of reaction was prolonged. It can be seen from the table, the CO_2 adsorption capacity within 5 minutes was only 76.2% of that for 1 hour. It indicates that for the sample with 80 wt% PEI, it requires longer time to reach equilibrium capacity for CO_2 adsorption under the same conditions.

Table 4.7 The summary of CO_2 adsorption capacity of MCFs with different PEI loadings for the adsorption time of 5 minutes and 1 hour in the gas mixture with the 10% CO_2/90%N_2.

CO_2 adsorption capacity	50 wt% PEI (mmol/g)	60 wt% PEI (mmol/g)	70 wt% PEI (mmol/g)	80 wt% PEI (mmol/g)
5 min	2.74	3.39	3.97	2.69
1 hour	2.73	3.41	3.97	3.53
%	100	99.4	100	76.2

Figure 4.16 presents the CO_2 adsorption capacity variation of MCFs with 70 wt% PEI in different concentrations of CO_2/N_2 gas mixtures within 2 minutes. It can be seen that the kinetics for CO_2 uptake increased with the increase in the CO_2 concentrations in the CO_2/N_2 gas mixture. MCFs with 70 wt% PEI present an extremely fast CO_2 capture in the 95% CO_2/5% N_2. The kinetics for CO_2 capture in different CO_2 concentrations of gas mixture was found in the following order: 95% CO_2/5% N_2 > 75% CO_2/25% N_2 > 50% CO_2/50% N_2 > 30% CO_2/70% N_2 > 15% CO_2/85% N_2 > 10% CO_2/90% N_2.

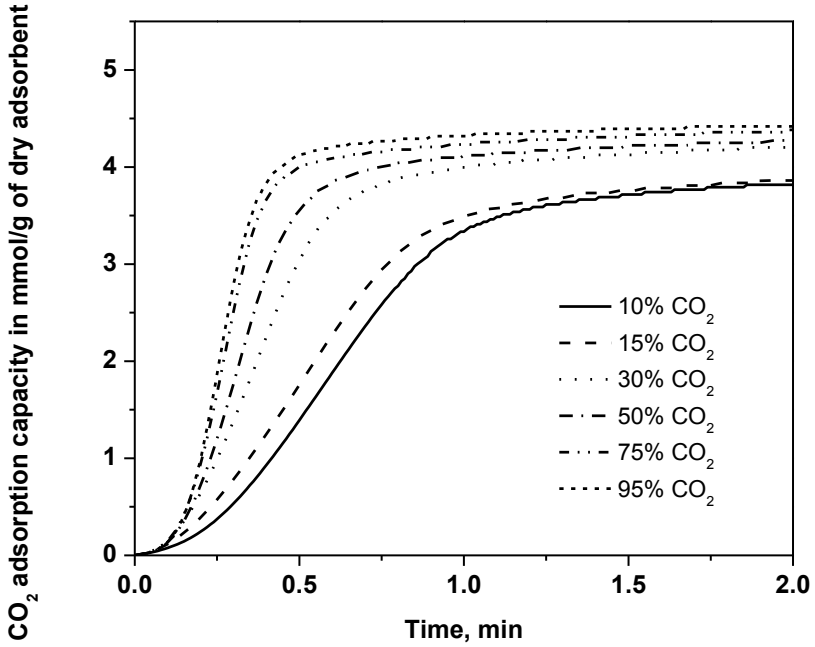

Figure 4.16 CO_2 adsorption capacity variation of MCFs with 70 wt% PEI in different concentrations of CO_2/N_2 gas mixtures within 2 min.

Table 4.8 presents the comparison of the CO_2 adsorption capacity of 70 wt% PEI in the gas mixture with different CO_2 concentration for the adsorption time of 2 minutes and 1 hour. Generally speaking, the kinetics for MCFs with 70 wt% PEI under 75 °C is fast for all the CO_2 concentrations. It can achieve high CO_2 adsorption capacity within 2 minutes. It was found that for higher CO_2 concentrations, it has shorter induction periods. However, for the gas mixtures with low CO_2 concentrations, it takes shorter time to achieve equilibrium status even though the kinetics for the reaction is not as fast as those with higher CO_2 concentrations since their CO_2 adsorption capacity is relatively low. For the gas mixture with high CO_2 concentrations, the CO_2 adsorption capacity within 2 minutes was as high as 91% of that for the adsorption time of 1 hour. While for the low concentrations, the CO_2 adsorption capacity within 2 minutes can reach

almost 100% indicating that for higher concentrations of CO_2, it requires longer time to reach saturation.

Table 4.8 Table for the CO_2 adsorption capacity of the sample with 70 wt% PEI under the gas mixture with different CO_2 concentrations for the adsorption time of 2 minutes and 1 hour.

CO_2 adsorption capacity	10% CO_2 (mmol/g)	15% CO_2 (mmol/g)	30% CO_2 (mmol/g)	50% CO_2 (mmol/g)	75% CO_2 (mmol/g)	95% CO_2 (mmol/g)
2 min	3.97	4.09	4.53	4.55	4.69	4.67
1 hour	3.95	4.12	4.77	4.86	5.10	5.16
%	100	99	95	94	92	91

Figure 4.17 shows the CO_2 adsorption capacity of MCF with 70 wt% PEI as a function of time in 10% CO_2/90% N_2 gas mixture with different adsorption temperatures. The kinetics of the sample for different adsorption temperatures was found in the following order: MCFs-70wt% PEI@75 °C > MCFs-70wt% PEI@60 °C > MCFs-70wt% PEI@90 °C > MCFs-70wt% PEI@40 °C > MCFs-70wt% PEI@25 °C.

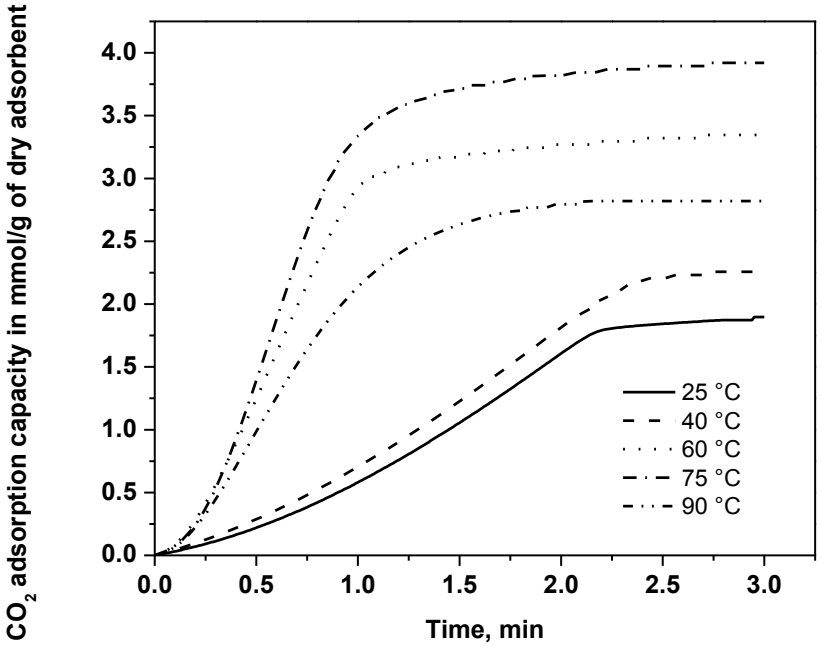

Figure 4.17 CO_2 adsorption capacity of MCFs with 70 wt% PEI as a function of time in 10% CO_2/90% N_2 gas mixture with different adsorption temperatures.

Table 4.9 shows the comparison of the CO_2 adsorption capacity for the sample of MCF with 70 wt% PEI under different adsorption temperatures in 10% CO_2/90% N_2 for the adsorption time of 3 minutes and 1 hour. It was shown that for the adsorption temperatures below 75°C, the ratio of the CO_2 adsorption capacity for 3 minutes over that for 1 hour was found in the following order: MCFs-70wt% PEI@75 °C > MCFs-70wt% PEI@60 °C > MCFs-70wt% PEI@40 °C > MCFs-70wt% PEI@25 °C, which is in accordance with the trend we found from Figure 4.17, indicating that the kinetics can be improved with the increase in temperature. However, as the temperature goes beyond 75 °C, the desorption starts to occur. Therefore, the ratio of the CO_2 adsorption capacity for 3 minutes over that for 1 hour to be over 100% can be explained by the desorption of CO_2 from the surface of the mesoporous support under the temperature of 90 °C.

Table 4.9 The comparison of CO_2 adsorption capacity of MCFs with 70 wt% PEI under different adsorption temperatures in the 10% CO_2/ 90% N_2 gas mixture for the adsorption time of 3 minutes and 1 hour.

CO_2 adsorption capacity	25°C (mmol/g)	40°C (mmol/g)	60°C (mmol/g)	75°C (mmol/g)	90°C (mmol/g)
3 min	1.90	2.28	3.35	3.92	2.82
1 hour	2.49	2.85	3.96	3.95	2.55
%	76.3	80	85	99.2	111

The rate of CO_2 uptake as a function of time and temperature is illustrated in Figure 4.18 Generally speaking, for all the adsorption temperatures, the CO_2 uptake rate increases to a maximum value and then decreases as the adsorbent approaches saturation. From Figure 4.18, it can be seen that for the sample with 70 wt% PEI using 10% CO_2/90% N_2, the peak height of the derivative adsorption capacity with time for different adsorption temperatures is found in the following order: MCFs-70wt% PEI@75 °C > MCFs-70wt% PEI@60 °C > MCFs-70wt% PEI@90 °C.

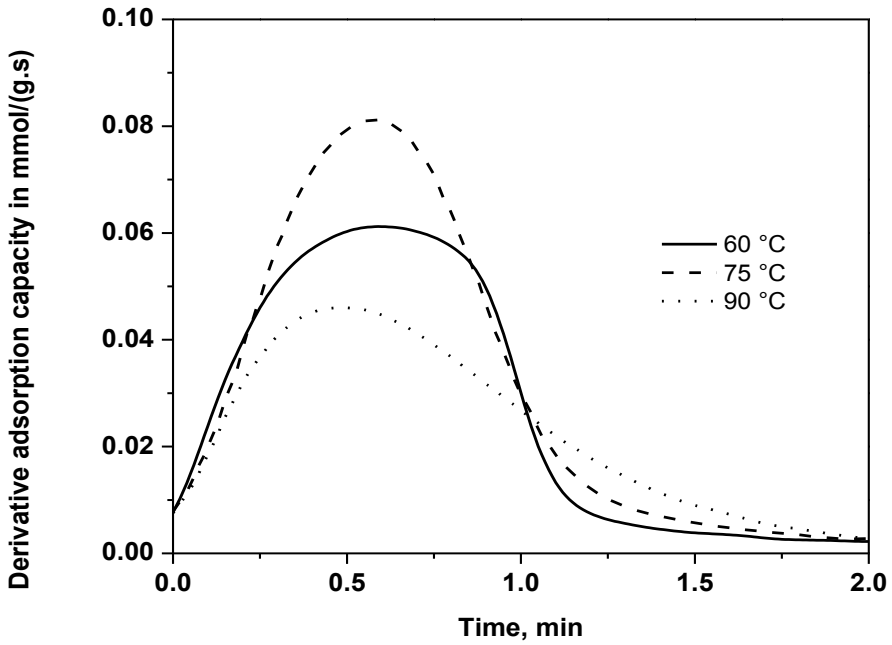

Figure 4.18 Rate of adsorption using MCFs with 70 wt% PEI as a function of time and temperature in 10% CO_2/90% N_2 at 75 °C.

Figure 4.19 provides the adsorption and desorption kinetics for CO_2 capture using 70 wt% PEI-MCFs in 10% CO_2/90% N_2. The CO_2 was adsorbed for 5 min at 75 °C and 1 atm and was then desorbed for 5 min in pure N_2 at 105 °C and 1 atm. It can be found that the kinetics for both adsorption and desorption is very fast. Around 90% of maximum CO_2 adsorption capacity was achieved within first two minutes of adsorption time. Almost 90% of adsorbed CO_2 was desorbed at first 2.5 minutes of desorption time.

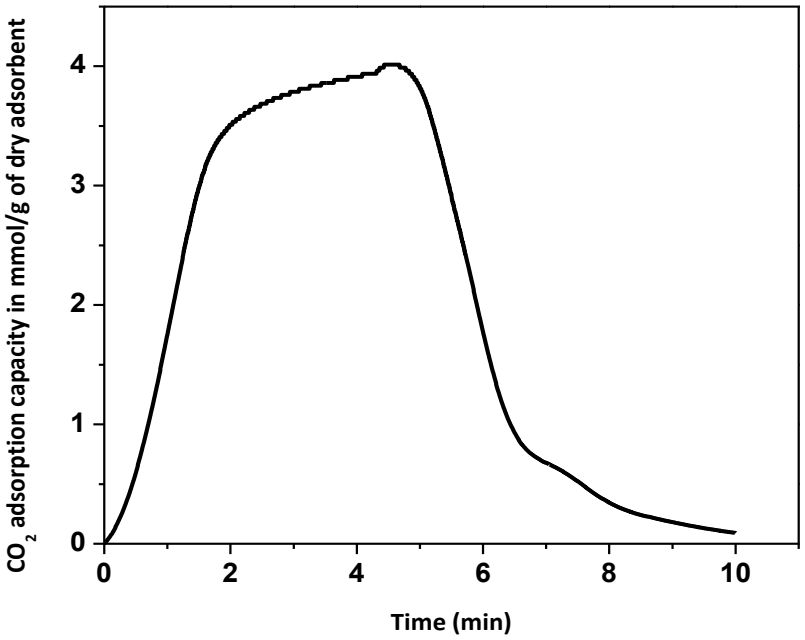

Figure 4.19 Kinetics of adsorption in 10% CO_2/90% N_2 at 75 °C and desorption in pure N_2 at 105 °C using 70 wt% PEI-MCFs.

4.2.5 Heat of adsorption

The determination of heat of adsorption is of great importance in evaluating the energy required for desorption process. In our study, the heat of adsorption was measured using differential scanning calorimetry (DSC STARe system) under the adsorption time of 10 min. Figure 4.20 presents the heat of adsorption of 70 wt% PEI-MCFs at various adsorption temperatures under dry 10% CO_2/90% N_2 and 95% CO_2/5% N_2 gas mixtures. It can be observed that all the heat of adsorption values at various adsorption temperatures for both gas mixtures are higher than 60 kJ/mol of CO_2 (1.36 kJ/g of CO_2), which indicates that CO_2 is captured through chemisorption using PEI-impregnated MCFs. The heat of adsorption values obtained from 95% CO_2/5% N_2 gas mixtures are slightly higher than those obtained from 10% CO_2/90% N_2 gas mixtures at the same

temperatures. The heat of adsorption values for both gas mixtures increase with temperatures first and then decreases with temperatures. In 10% CO_2/90% N_2, the heat of adsorption increases from 2.64 kJ/g at 25 °C to 2.7 kJ/g at 40 °C. Then it decreases from 2.7 kJ/g to 2.4 kJ/g at 90 °C. In 95% CO_2/ 5% N_2 gas mixture, the heat of adsorption increases from 2.66 kJ/g at 25 °C to 2.72 kJ/g at 40 °C. Then it decreases from 2.7 kJ/g to 2.57 kJ/g at 90 °C.

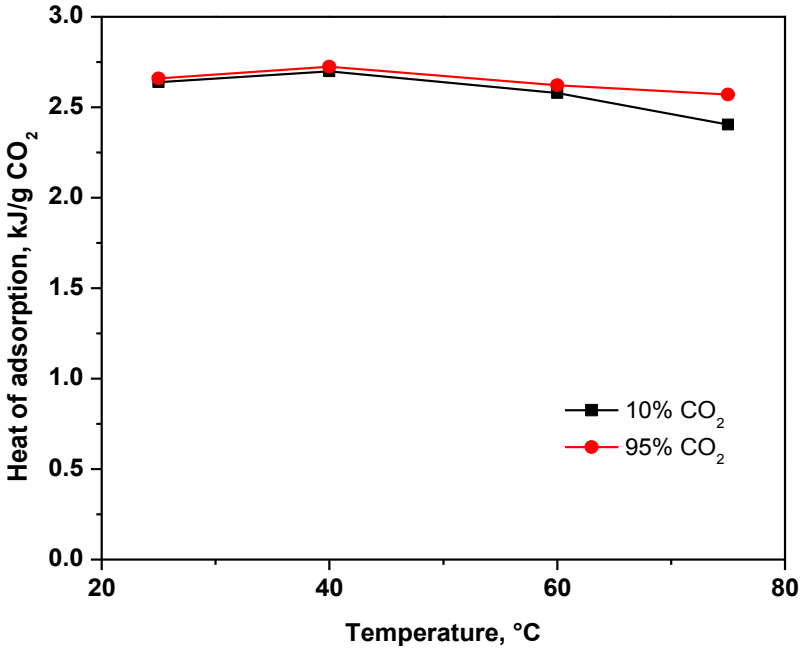

Figure 4.20 Heat of adsorption using 70 wt% PEI-MCFs at different adsorption temperatures in 10% CO_2/90% N_2 and 95% CO_2/5% N_2 gas mixtures.

In order to investigate the effect of moisture on the heat of adsorption, the 10% CO_2/90% N_2 gas mixture was sent into a moisture saturator at room temperature for humidification. Figure 4.21 shows the heat of adsorption with 10% CO_2/90% N_2 gas mixture using 70 wt% PEI-impregnated MCFs under both dry and humid conditions. It can be observed that in dry condition, the heat of adsorption values decreases with adsorption temperatures; while in humid condition, the values

of heat of adsorption slightly increase with different adsorption temperatures. Since both moisture and CO_2 adsorption contribute to the heat of adsorption in the humid condition, the heat of adsorption in humid condition refers to the heat evolved in kJ/g of (H_2O + CO_2) adsorbed. As can be seen from Figure 4.21, the heat of adsorption in the humid condition is less than that in the dry condition. This is probably because that in the humid condition, the heat of adsorption value comes from two parts: moisture adsorbed and CO_2 captured. The moisture adsorbed only contributes a small part to the heat of adsorption values.

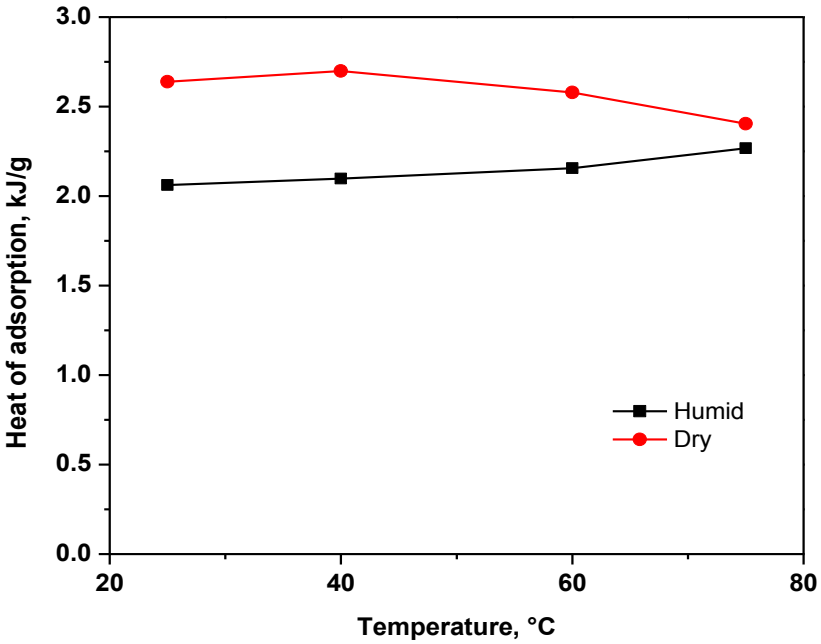

Figure 4.21 Heat of adsorption using 70 wt% PEI-MCFs with 10% CO_2/90% N_2 gas mixture in both dry and humid conditions.

4.2.6 Effect of moisture on CO_2 adsorption capacity

Since flue gas from the coal-fired power plant usually contains 10-15% moisture, it is of great importance to make sure that PEI-impregnated MCFs are highly tolerable to moisture to be

applicable as adsorbents for CO_2 capture. In order to investigate the moisture effect on the CO_2 adsorption capacity, 70 wt% PEI-MCFs was used in humid 10% CO_2/90% N_2 gas mixture. The moisture was introduced into the system by sending 10% CO_2/90% N_2 gas mixture through a water saturator at room temperature. The sample was first heated from room temperature to 105 °C for 30 minutes in pure N_2 gas (100 mL/min) to remove all the moisture and previously adsorbed gas prior to the adsorption process. After that, the temperature was adjusted to the desired adsorption temperature. The sample was wetted for adsorption process by flowing humid 10% CO_2/90% N_2 gas mixture through the sample at desired adsorption temperature. Figure 4.22 presents the comparison of adsorption capacity of 70 wt% PEI-MCFs in humid and dry 10% CO_2/90% N_2 gas mixtures at various adsorption temperatures for adsorption of 1 hour and 10 min. It can be observed that in the humid condition, the adsorption capacities are higher than those in the dry condition at adsorption temperatures below 75 °C. The adsorption capacity improves considerably, especially at lower adsorption temperatures. It also can be observed that the adsorption capacity increases dramatically with the decrease in adsorption temperature under humid conditions, while in dry conditions, the CO_2 adsorption performance is enhanced as adsorption temperature increases. The opposite trends in CO_2 adsorption capacity as a function of adsorption temperature in dry and humid conditions indicates that the presence of moisture in CO_2 adsorption process using PEI-MCFs altered the reactions involved and affected the CO_2 adsorption performance to a large extent. Since moisture adsorption contributes to the total adsorption capacity in the humid condition, it is hard to determine if the improved adsorption capacity is mainly due to the adsorption of moisture or the enhancement of CO_2 adsorption in humid conditions from data presented in Figure 4.22. In order to obtain the real CO_2 adsorption

capacity in the humid condition, it is vital to understand how much moisture is adsorbed at each adsorption temperature. The moisture was introduced into the system by using pure N_2 as the purge gas. Since N_2 is barely adsorbed, moisture adsorption capacity can be calculated through the weight change of the samples during adsorption process by passing humid pure N_2 gas through samples.

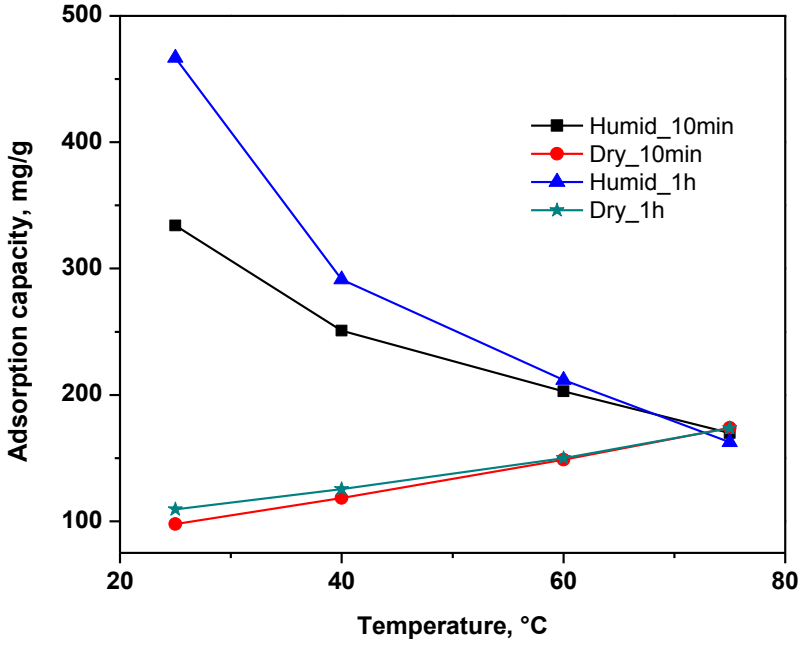

Figure 4.22 Adsorption capacity of 70 wt% PEI-MCFs in humid and dry conditions at various adsorption temperatures in 10% CO_2/90% N_2 gas mixture.

Figure 4.23 illustrates the CO_2 adsorption capacity of 70 wt% PEI-MCFs in dry 10% CO_2/90% N_2 gas mixture at various adsorption temperatures along with the total adsorption capacity and moisture adsorption capacity of 70 wt% PEI-MCFs in humid conditions. It can be seen that the total adsorption capacity of 70 wt% PEI-MCFs in humid conditions is comprised of two parts: CO_2 adsorption capacity and moisture adsorption capacity. By comparison of the CO_2

adsorption capacity in dry conditions and that in humid conditions, it can be observed that the CO_2 adsorption performance is enhanced with the presence of moisture at adsorption temperatures no higher than 60 °C. A minor decrease in CO_2 adsorption capacity happened at adsorption temperature at 75 °C. The CO_2 adsorption capacity in humid conditions maximized at 60 °C i.e. around 184.2 mg/g (4.19 mmol/g), which is 124% of that in dry 10% CO_2/90% N_2 gas mixture. The enhancing effect of moisture content on the CO_2 adsorption performance using PEI-impregnated MCFs can be attributed to the changes on chemical interactions between CO_2 and amino groups. In the dry condition without any moisture participating into the reactions, the involved interactions between CO_2 and amino groups are shown as follows [166]:

$$CO_2 + 2RNH_2 \leftrightarrow RNHCOO^- + RNH_3^+ \quad (4.1)$$

$$CO_2 + 2R_2NH \leftrightarrow R_2NCOO^- + R_2NH_2^+ \quad (4.2)$$

$$CO_2 + R_2NH + R'NH_2 \leftrightarrow R_2NCOO^- + R'NH_3^+ \quad (4.3)$$

Two moles of amino groups interact with one mole of CO_2 to form ammonium carbamate. However, with the presence of moisture, one mole of CO_2 can be captured by one mole of amino group to form ammonium bicarbonate. The relative reactions are listed as follows [167]:

$$2RNH_2 + CO_2 \leftrightarrow RNH_3^+ + RNHCOO^- \quad (4.4)$$

$$RNHCOO^- + H_2O \leftrightarrow RNH_2 + HC0_3^- \quad (4.5)$$

$$2R_2NH + CO_2 \leftrightarrow R_2NH_2^+ + R_2NCOO^- \quad (4.6)$$

$$R_2NCOO^- + H_2O \leftrightarrow R_2NH + HC0_3^- \quad (4.7)$$

$$R_3N + H_2O \rightarrow R_3NH^+ + OH^- \quad (4.8)$$

$$CO_2 + OH^- \rightarrow HC0_3^- \quad (4.9)$$

It can be easily explained that the promotion on CO_2 adsorption capacity with the presence of moisture is due to the increase in stoichiometry of CO_2 to amino groups. The equations listed above suggested that the CO_2 adsorption capacity can potentially increase by a factor of 2 with the presence of moisture participating into the reactions. It can be seen from Eqs.(4.1)-(4.3) and Eqs. (4.4)-(4.9) that the maximum amine efficiency (mmol CO_2/ mmol N ratio) under dry and humid conditions should be 0.5 and 1.0, respectively. However, in our cases, the improved CO_2 adsorption capacity did not achieve that level as suggested.

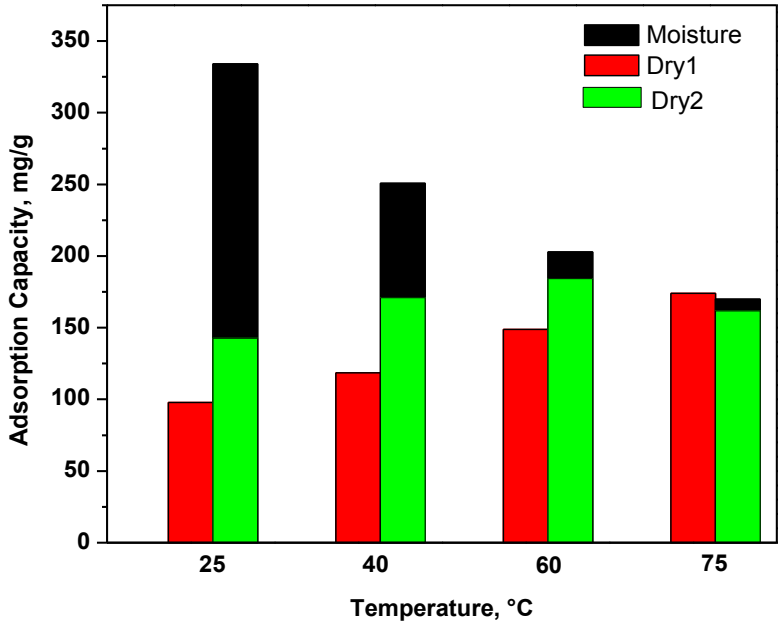

Figure 4.23 Adsorption capacity of 70 wt% PEI-MCFs in humid and dry conditions at various adsorption temperatures in 10% CO_2/90% N_2 gas mixture (adsorption time of 10 min).

Table 4.10 presents the values of CO_2 adsorption capacity and amine efficiency of 70 wt% PEI-MCFs under dry and humid conditions. It can be observed that the amine efficiency increased as adsorption temperature increases in dry conditions. With the presence of moisture in gas

mixture, the amine efficiency improved in adsorption temperature below 75 °C. However, the change in amine efficiency is not comparable with the potential change in amine efficiency. It is probably because in the humid condition, the CO_2 molecules not only interact with amines to form ammonium bicarbonate, but also ammonium carbamate. The formation of carbamate, especially with primary and secondary amines, is faster than the formation of bicarbonate, which is supported by data presented in Figure 4.24.

Table 4.10 CO_2 adsorption capacity and amine efficiency of 70 wt% PEI-MCFs at various adsorption temperatures in dry and humid 10% CO_2/90% N_2 gas mixture.

T_{Ads}		25 °C		40 °C		60 °C		75 °C	
		Dry	Humid	Dry	Humid	Dry	Humid	Dry	Humid
t_{Ads} = 10 min	q_t	2.22	3.27	2.69	3.88	3.38	4.19	3.95	3.67
	η	0.137	0.200	0.165	0.238	0.208	0.257	0.243	0.226
t_{Ads} = 1 hour	q_t	2.49	4.14	2.85	4.69	3.41	4.39	3.95	3.51
	η	0.153	0.254	0.175	0.288	0.209	0.270	0.243	0.215

q_t : CO_2 adsorption capacity in mmol/g;
η : Amine efficiency in mmol CO_2/mmol N.

Figure 4.24 compares the adsorption kinetics of 70 wt% PEI-MCFs in humid and dry conditions with10% CO_2/90% N_2 gas mixture at 60 °C. The moisture adsorption capacity is very low compared with the CO_2 adsorption capacity. The kinetics for CO_2 adsorption reduced with the presence of moisture. However, the CO_2 adsorption capacity improved with the presence of moisture. This would explain why the amine efficiency is less than 1.0. Another possible reason for this is because the equilibrium is not achieved in 10 minutes. From Table 4.10, it can be seen that as adsorption time increase up to 1 hour, the amine efficiency improved. A higher CO_2 adsorption capacity and higher amine efficiency would be obtained if longer adsorption time is applied. Besides, moisture volume is also another possible factor contributable to low amine efficiency. The humid gas mixture used in our case only contains 3 vol% moisture, which is

pretty low to achieve high CO_2 adsorption capacity in 10 minutes. The CO_2 adsorption capacity and amine efficiency slightly decrease at adsorption temperature of 75 °C in humid compared to those in dry conditions. It is probably due to the increased amount of heat released in humid gas mixture during the adsorption process at 75 °C, resulting in desorption of CO_2.

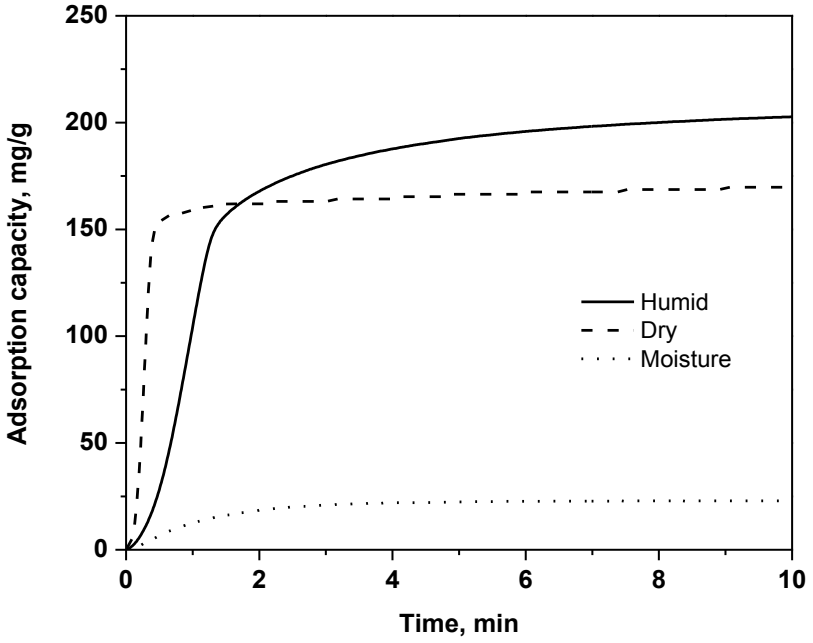

Figure 4.24 Comparison of adsorption capacity in humid and dry conditions for 70 wt% PEI-MCFs at 60 °C.

4.2.7 Stability of cyclic adsorption/desorption performance

In order to investigate the multi-cycle stability of PEI-impregnated MCFs, multi-cycle adsorption/desorption tests were conducted in dry and humid 10%CO_2/90% N_2 gas mixture at atmospheric pressure. Figure 4.25 presents 10 adsorption/desorption cycles using 70 wt% PEI-MCFs in dry 10% CO_2/ 90% N_2 gas mixture at atmospheric pressure. Each cycle is comprised of 10 min adsorption in dry 10% CO_2/ 90% N_2 gas mixture at adsorption temperature of 75 °C and

10 min desorption at either 90 °C or 105 °C in pure N_2 gas. A good stability of multi-cycle adsorption/desorption process of PEI-MCFs can be observed. Table 4.11 summarizes CO_2 adsorption capacity of 10 cycles in both cases. For multi-cycle test with desorption temperature of 105 °C, the first cycle and 10^{th} cycle CO_2 adsorption capacity is 4.33 mmol/g and 4.04 mmol/g, respectively. For multi-cycle test with desorption temperature of 90 °C, the first cycle and 10^{th} cycle CO_2 adsorption capacity was 4.2 mmol/g and 4.06 mmol/g, respectively. The decrease in CO_2 adsorption capacity after multi-cycle runs is due to the amine leaching at high desorption temperature. The capacity drop in multi-cycle test with desorption temperature of 90 °C is 3.3%, which is less than that in multi-cycle test with desorption temperature of 105 °C (6.7%). This indicates that lower desorption temperature results in less amine losses during multi-cycle adsorption/desorption process.

Table 4.11 10 multi-cycle CO_2 adsorption capacities in dry 10% CO_2/ 90% N_2 gas mixture at atmospheric pressure.

T_{Des}	Cycle number										Loss
(°C)	1	2	3	4	5	6	7	8	9	10	%
105	4.33	4.31	4.27	4.2	4.19	4.16	4.12	4.12	4.11	4.04	6.7
90	4.2	4.12	4.12	4.14	4.11	4.1	4.1	4.07	4.1	4.06	3.3

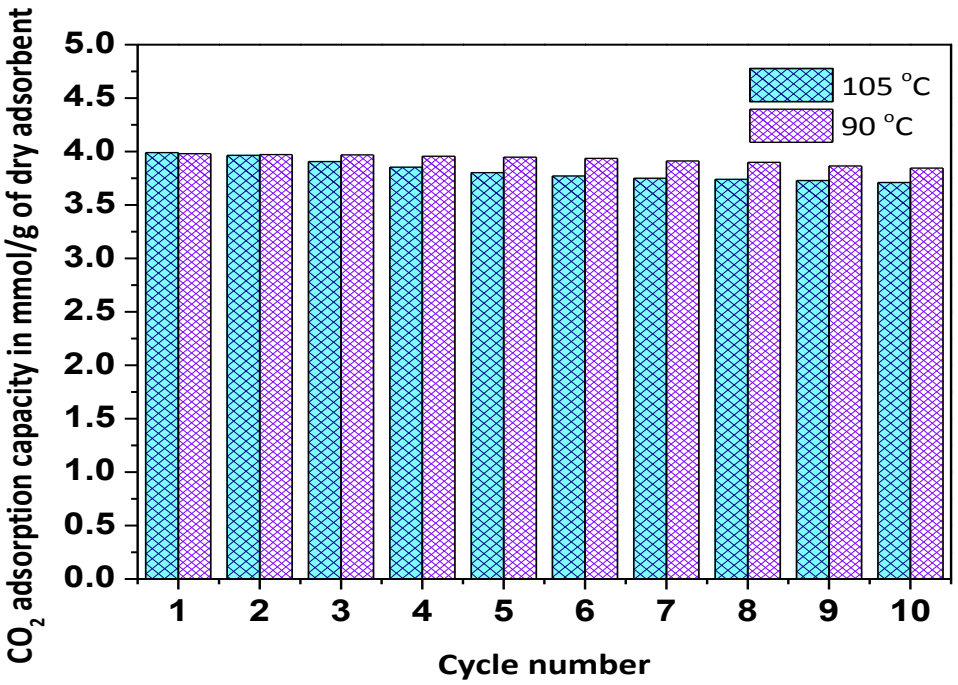

Figure 4.25 10 cycles of adsorption/desorption of 70 wt% PEI-MCFs with 10% CO_2/90% N_2 under dry conditions (adsorption at 75 °C and desorption at 105 °C /90 °C).

The effect of moisture in 10% CO_2/90% N_2 gas mixture on the stability and CO_2 adsorption performance in multi-cycle adsorption/desorption of PEI-MCFs was investigated. Figure 4.26 illustrates 50 multi-cycle adsorption/desorption for CO_2 capture in humid 10% CO_2/ 90% N_2 gas mixture. Each cycle is comprised of 10 min adsorption in humid 10% CO_2/ 90% N_2 gas mixture at adsorption temperature of 60 °C or 75 °C and 10 min desorption at desorption temperature of 105 °C in pure N_2 gas. It can be observed from Figure 4.26, the adsorption capacity in humid 10% CO_2/ 90% N_2 gas mixture for both adsorption temperatures dropped suddenly after first cycle, then maintained quite stable afterwards. The adsorption capacity in humid gas mixtures improved compared to that in dry conditions due to the presence of moisture. For multi-cycle test with adsorption temperature of 60 °C, the first cycle and 50th cycle CO_2 adsorption capacity is

190.01 mg/g and 178.21 mg/g, respectively. The drop in adsorption capacity is around 6.2%. For multi-cycle test with adsorption temperature of 75 °C, the first cycle and 50th cycle CO_2 adsorption capacity is 174 mg/g and 153.93 mg/g, respectively. The drop in adsorption capacity is around 11.5%. The used samples after 50 multi-cycle adsorption/desorption process were then heated up to 600 °C to burn off all the organics. The weight change before and after heating of adsorbents refers to the weight of amines loaded onto the support. It can be calculated that the weight loss of amines after 50 cycles is 2.3% and 6.6% with adsorption temperature of 60 °C and 75 °C, respectively.

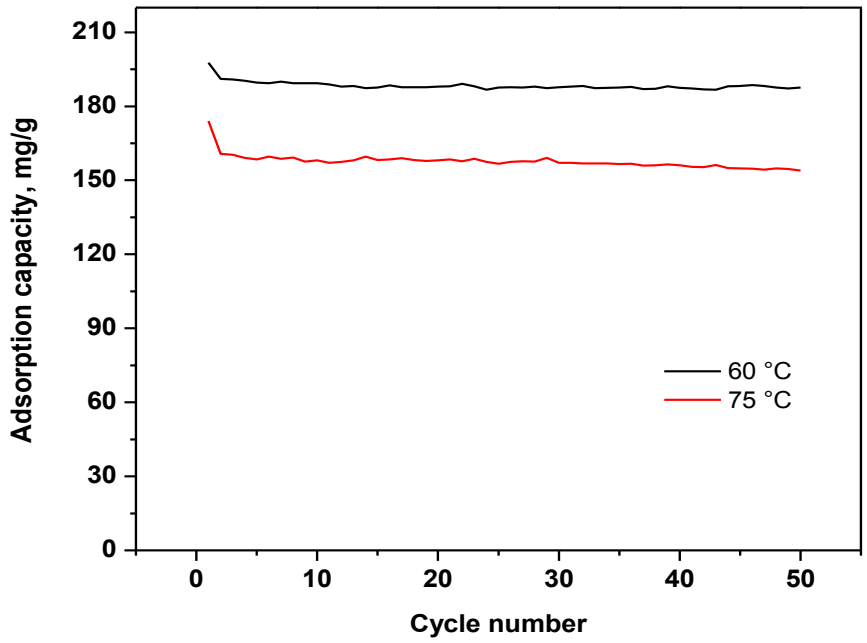

Figure 4.26 Comparison of 50 cycles of adsorption capacities using 70 wt% PEI-MCFs with 10% CO_2/90% N_2 under humid conditions (adsorption at 60°C and 75 °C and desorption at 105 °C).

In order to compare the CO_2 adsorption capacity at two adsorption temperatures in humid gas mixture, the moisture adsorption capacity was deducted from the total adsorption capacity for

each cycle. It is assumed that the moisture adsorption capacity stayed the same throughout the entire multi-cycle adsorption/desorption runs and that its value is approximately equal to the one in humid pure N_2 gas under the same adsorption temperatures. The resulted CO_2 adsorption capacities of 50 multi-cycle adsorption/desorption were plotted in Figure 4.27.

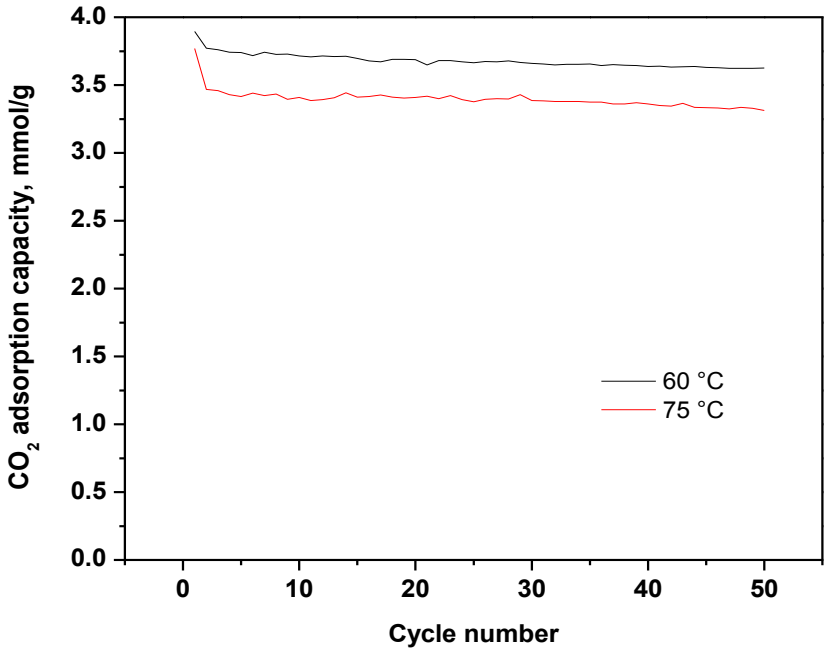

Figure 4.27 Comparison of 50 cycles of CO_2 adsorption capacities using 70 wt% PEI-MCFs with 10% CO_2/90% N_2 under humid conditions (adsorption at 60°C and 75 °C and desorption at 105 °C).

Figure 4.28 compares the CO_2 adsorption capacities in 50 multi-cycle adsorption /desorption in humid 10% CO_2/ 90% N_2 gas mixture at adsorption temperature of 60 °C and desorption temperature of 90 °C and 105 °C. The drop in CO_2 adsorption capacity is around 6.89% and 5.67% with desorption temperature of 105 °C and 90 °C, respectively. It can be concluded that

the lower desorption temperature provides a better stability in multi-cycle adsorption/desorption process with less amine losses.

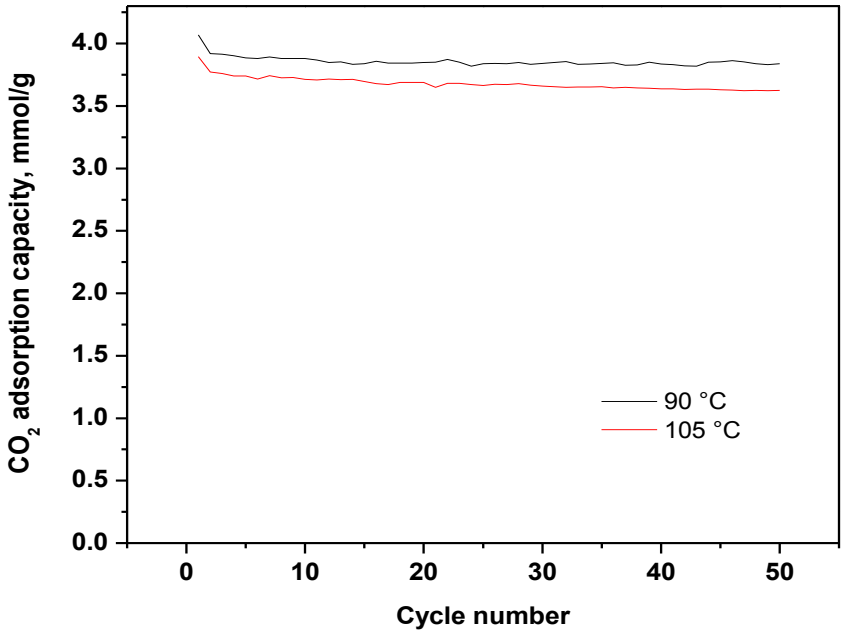

Figure 4.28 Comparison of 50 cycles of CO_2 adsorption capacities using 70 wt% PEI-MCFs with 10% CO_2/90% N_2 under humid conditions (adsorption at 60°C and desorption at 90 °C and 105 °C).

Chapter 5

Adsorption Equilibrium Modeling

5.1 Adsorption equilibrium model

In order to evaluate the CO_2 adsorption performance for novel adsorbents, it is important to develop optimum adsorption equilibrium correlations for predicting adsorption parameters and quantitative comparison of adsorbent performance under different experimental conditions [168, 169]. In our case, an adsorption isotherm describes how CO_2 interacts with the amine-functionalized mesoporous silica at a desired constant temperature. The adsorption equilibrium is achieved when sufficient time is provided to allow the gaseous CO_2 to contact with the solid surface. In order to obtain the equilibrium CO_2 adsorption capacity (q_e), the CO_2 adsorption process was monitored using TGA (TA Instruments Q500 SDT). Different partial pressures of CO_2 were used for CO_2 adsorption measurements at a given temperature. The sample was first properly grinded into uniform particle sizes. Around 5 mg of 70 wt% PEI impregnated MCFs was loaded for each run. The sorbent was heated up to 105 °C at a heating rate of 10 °C /min under pure N_2 with a flow rate of 100 cm^3/min to remove all the moisture and adsorbed CO_2. After being isothermal for 30 minutes, the temperature was then adjusted to the desired adsorption temperatures (e.g. 60 °C, 75 °C, 90 °C). Once the temperature was equilibrated with the target temperature, the gas was switched from pure N_2 to CO_2/N_2 gas mixtures with different CO_2 concentrations (e.g. 10% CO_2, 15% CO_2, 30% CO_2, 50% CO_2, 75% CO_2, 95% CO_2) with a flow rate of 100 cm^3/min. The adsorption process started and the temperature was kept isothermal at desired adsorption temperature for long enough time till the equilibrium status was

achieved. We assumed that the equilibrium was obtained when the weight change of the sample in the last 60 minutes was less than 1% of the overall weight change. A wide variety of equilibrium isotherm models have been developed. Here, different adsorption isotherms, including Langmuir, Freundlich, Temkin, Redlich-Peterson (R-P), Dubinin-Radushkevich (D-R), Sips, Toth, Koble-Corrigan (K-C), Khan, and Radke-Prausnitz (R-P) isotherms were explored and investigated to describe the CO_2 adsorption behavior with PEI-functionalized MCFs.

5.1.1 Langmuir adsorption isotherm

Langmuir developed a theoretical equilibrium isotherm relating the amount of adsorbed gas on the surface of the adsorbent to the gas pressure. It is the most widely used isotherm and produced a good agreement with experimental data [168, 170, 171]. In order to have a deeper understanding of the adsorption phenomena examined by thermal instruments, the Langmuir isotherm equation, which described quantitatively the formation of a monolayer adsorbate on the surface of the adsorbent, was used. This choice is due to the fact that the experimental adsorption isotherms from TGA are type I isotherm. This isotherm was valid based on the assumptions that all the adsorption sites are homogeneous and equivalent; each site can hold at most one molecule of the adsorbate; there are no interactions between the adsorbate molecules on adjacent sites; the energies of adsorption are uniform and there is no transmigration of adsorbate in the plane of the surface [166, 172] . It is described as follows:

$$q_e = q_{max} \frac{k_L p}{1+k_L p} \tag{5.1}$$

Where, q_{max} represents the maximum monolayer coverage capacity in mmol/g of dry adsorbents, and k_L is the adsorption rate constant. The parameter of the Langmuir isotherm k_L, is in general dependent on temperature.

5.1.2 Langmuir separation factor

The Langmuir separation factor, R_L, is defined as

$$R_L = \frac{1}{1+k_L p_0} \tag{5.2}$$

Where, p_0 is the initial partial pressure of CO_2. The value of R_L indicates the adsorption to be either unfavorable ($R_L > 1$), linear (if R_L=1), favorable (if 0<R_L<1) or irreversible (if R_L=0).

5.1.3 Freundlich adsorption isotherm

Freundlich proposed the earliest known sorption isotherm equation in 1906. This empirical model is commonly used to describe the non-ideal adsorption on heterogeneous surfaces as well as multilayer sorption [168, 172]. This isotherm represents in the following form:

$$q_e = K_F C_{CO_2}^{1/n} \tag{5.3}$$

Where, K_F and n are empirical constants for each pair of adsorbent-adsorbate at given temperatures. K_F is defined as the adsorption capacity of the adsorbent [173, 174]. 1/n is a function of the strength of adsorption in the adsorption process [171]. If 1/n = 0, it indicates that the partition between two phases are independent of the concentration. If 1/n < 1, it corresponds to a normal L-type Langmuir isotherm. If 1/n > 1, it indicates a cooperative sorption involving strong interactions between the molecules. The value of 1/n ranging from 0 to 1 also indicates the surface heterogeneity, with a more heterogeneous surface as 1/n gets closer to zero [175].

5.1.4 Temkin adsorption isotherm

The Temkin isotherm describes the behavior of adsorption systems on heterogeneous surfaces. This isotherm contains a factor that explicitly taking into the account of adsorbent–adsorbate interactions [166, 171]. This isotherm is valid based on the assumptions that the heat of adsorption of all molecules in the layer would decrease linearly rather than logarithmic with coverage due to adsorbent–adsorbate interactions, and that the adsorption is characterized by a uniform distribution of binding energies, up to some maximum binding energy [4, 6-7]. The model is given by the following equation [4]:

$$q_e = \frac{RT}{b} \ln(k_T C_{CO_2}) \tag{5.4}$$

$$B = \frac{RT}{b} \tag{5.5}$$

$$q_e = B \ln(k_T C_{CO_2}) \tag{5.6}$$

Where, k_T = Temkin isotherm equilibrium binding constant

b = Temkin isotherm constant

R = universal gas constant (8.314 J/mol/K)

B = constant related to heat of sorption

5.1.5 Dubinin–Radushkevich adsorption isotherm

The Dubinin–Radushkevich (D–R) isotherm is commonly used to describe adsorption on heterogeneous surfaces with a Gaussian energy distribution [166, 171, 176]. The D–R equation is shown as follows:

$$q_e = q_m e^{-\lambda \omega^2} \tag{5.7}$$

The parameter ω is the Polanyi potential that is related to the equilibrium by

$$\omega = \mathrm{RTln}(1 + \frac{1}{C_{co_2}}) \quad (5.8)$$

where, R is the gas constant and T is the absolute temperature. The mean free energy adsorbed per molecule adsorbate can be computed using the relationship [166, 168]

$$\mathrm{E} = \frac{1}{\sqrt{2\lambda}} \quad (5.9)$$

The values of E are useful for estimating the mechanism of the adsorption process. If E < 8 kJ/mol, it indicates that physical forces dominate the adsorption. If E is in the range of 8–16 kJ/mol, it indicates adsorption is governed by ion exchange mechanism. If E > 16 kJ/ mol, particle diffusion dominates [166].

5.1.6 Redlich-Peterson isotherm

This isotherm contains three parameters and combines the characteristics of the Langmuir and Freundlich isotherms [168, 170]. It is presented as follows:

$$q_e = \frac{A\, C_{co_2}}{1 + B\, {C_{co_2}}^g} \quad (5.10)$$

Where; A, B and g (0<g<1) are the three isotherm constants.

5.1.7 Sips isotherm

Sips isotherm is an equation that combines the Langmuir and Freundlich isotherms. It is used for predicting the heterogeneous adsorption system. At low adsorbate concentrations, it reduces to Freundlich isotherm; while at high concentrations, it predicts a monolayer adsorption capacity characteristic of Langmuir isotherm. The Sips isotherm is presented in the following form:

$$q_e = \frac{K_s C_e^{\beta_s}}{1 + \alpha_s C_e^{\beta_s}} \quad (5.11)$$

Where α_s = Sips isotherm model constant (L/mg)

K_s = Sips isotherm model constant (L/g)

β_s = Sips isotherm model exponent

C_e = equilibrium constant

q_e = amount of adsorbate in the adsorbent at equilibrium (mg/g)

5.1.8 Toth isotherm

Toth isotherm was originally proposed by Toth for monolayer adsorption. Now this equation is used as it gives a more extensive range of fit than the Langmuir or Freundlich isotherm equations when applied to Type IV isotherms for porous adsorbents. The Toth equation has the advantage over the Sips equation because it appears to satisfy both limits of the isotherm, at $c_e \rightarrow 0$ and $c_e \rightarrow \infty$ [169]. It is presented in the following form:

$$q_e = \frac{K_T c_e}{(a_T + c_e)^{1/t}} \tag{5.12}$$

Where K_T = Toth isotherm constant (mg/g)

c_e = equilibrium concentration (mg/L)

a_T = Toth isotherm constant (L/mg)

t = Toth isotherm constant

q_e = amount of adsorbate in the adsorbent at equilibrium (mg/g)

5.1.9 Koble-Corrigan isotherm

Koble- Corrigan isotherm combines the Langmuir and Freundlich isotherms for representing the equilibrium adsorption data. The isotherm constants A, B and n are evaluated from the linear plot using a trial and error optimization. The isotherm equation is shown as follows:

$$q_e = \frac{AC_e^n}{1+BC_e^n} \tag{5.13}$$

Where c_e = equilibrium concentration (mg/L)

q_e = amount of adsorbate in the adsorbent at equilibrium (mg/g)

A = Koble-Corrigan isotherm constant ($L^n mg^{1-n}/g$)

B = Koble-Corrigan isotherm constant $(L/mg)^n$

n = adsorption intensity

5.1.10 Khan isotherm

$$q_e = \frac{q_s b_K c_e}{(1+b_K c_e)^{a_K}} \tag{5.14}$$

Where c_e = equilibrium concentration (mg/L)

q_e = amount of adsorbate in the adsorbent at equilibrium (mg/g)

q_s = theoretical isotherm saturation capacity (mg/g)

a_K = Khan isotherm model exponent

b_K = Khan isotherm model exponent

5.1.11 Radke-Prausnitz isotherm

The correlation of Radke-Prausnitz isotherm is usually predicted well by the high RMSE and chi-square values. Its model exponent is represented by β_R, where α_R and γ_R are referred to the model constants. Radke-Prausnitz isotherm is presented as follows:

$$q_e = \frac{\alpha_{RP}\gamma_R c_e^{\beta_R}}{\alpha_{RP}+\gamma_R c_e^{\beta_R-1}} \tag{5.15}$$

Where c_e = equilibrium concentration (mg/L)

q_e = amount of adsorbate in the adsorbent at equilibrium (mg/g)

α_{RP} = Radke-Prausnitz isotherm model constant

γ_R = Radke-Prausnitz isotherm model constant

β_R = Radke-Prausnitz isotherm model exponent

5.2 Results and discussions

The equilibrium experimental data for CO_2 adsorption using 70 wt% PEI-impregnated MCFs was analyzed by applying Langmuir, Freundlich, Temkin isotherm, Redlich-Peterson and Dubinin-Radushkevich, Sips, Toth, Koble-Corrigan, Khan and Radke-Prausnitz isotherms. The values of isotherm constants for different models were obtained using curve fitting tools available in MATLAB. The isotherm constants for different equilibrium models obtained from MATLAB are listed in Table 5.1. The coefficient of determination (R^2) represents the fitting degree between the experimental data and the isotherm curves. As can be seen from Table 5.1, the Langmuir isotherm did not fit well at low temperature. The R^2 value is only 0.9274 at 60 °C. At higher temperatures, the Langmuir isotherm fits the experimental data much better. This indicates a more homogeneous surface at high temperatures. This result is consistent with the

JMA kinetic model which can be considered as a pseudo-first order reaction with b value approaching to unity at high temperatures. The R^2 value of 0.993 of CO_2 adsorption data on PEI-impregnated MCFs at 90 °C is best fitted to the Langmuir adsorption isotherm model.

Table 5.1 Isotherm constants values obtained from MATLAB for different equilibrium models.

Langmuir			
T (°C)	k_L (bar^{-1})	q_m (mmol/g)	R^2
60	54.09	4.978	0.9274
75	19.61	5.708	0.946
90	6.971	5.869	0.993
Freundlich			
T (°C)	1/n	k_F(mmol/g)$(dm^3/mg)^{1/n}$	R^2
60	0.0664	4.977	0.9996
75	0.1533	5.622	0.9818
90	0.3016	5.357	0.9764
Temkin			
T (°C)	k_T (dm^3/mg)	B (kJ/mol)	R^2
60	1360000	0.3555	0.9564
75	2159	0.7279	0.9836
90	83.95	1.189	0.9932
Dubinin-Radushkevich			
T (°C)	q_m (mmol/g)	E (J/mol)	R^2
60	4.967	11600	0.9449
75	5.618	7870	0.9537
90	5.449	5646	0.9894
Redlich-Peterson			
T (°C)	A (dm^3/g)	B $(dm^3/mg)^g$	g	R^2
60	2345	470.9	0.9402	0.9815
75	522.4	92.4	0.8738	0.9837
90	51.88	8.971	0.9133	0.9958
Sips				
T (°C)	a_s	k_s	β_s	R^2
60	0.481	7.383	0.0964	0.979
75	0.9206	10.78	0.2623	0.9816
90	3.272	22.36	0.7553	0.9967
Toth				
T (°C)	a_T	k_T	t	R^2
60	0.001326	4.985	1.067	0.9793
75	0.006285	5.649	1.158	0.9818

90	0.081	5.613	1.151	0.9961
		Koble-Corrigan		
T (°C)	A	B	n	R^2
60	7.386	0.4825	0.09644	0.979
75	10.78	0.9207	0.2626	0.9816
90	22.36	3.272	0.7553	0.9967
		Khan		
T (°C)	a_k	b_k	q_s	R^2
60	0.9373	754	3.29	0.9793
75	0.8635	159.1	2.827	0.9818
90	0.8691	12.35	4.04	0.9961
		Radke-Prausnitz		
T (°C)	β_R	a_{RP}	r_R	R^2
60	0.06254	3301	4.987	0.9792
75	0.1337	650.1	5.667	0.9818
90	0.107	54.93	5.797	0.9963

In Freundlich adsorption isotherm, the values of 1/n represents the adsorption intensity of CO_2 for the PEI-impreganted MCFs. The values of $1/n$ range from 0 to 1, indicating a L-type Langmuir adsorption isotherm. This is consistent with the L-shape experimental curve. It also indicates that the CO_2 adsorption using the amine modified mesoporous silica adsorbent is favorable. It can be observed that the values of $1/n$ increase as temperature increases. The increase in $1/n$ value indicates that the interactions involved are enhanced. This is because that higher temperature facilitates CO_2 adsorption by overcoming barrier of diffusion into multilayer of amines, resulting in better accessibility of amine active sites and therefore, results in higher CO_2 adsorption capacity. In addition, $1/n$ value is getting far from zero as temperature increases, indicating a more homogenous surface at higher temperatures. This result is also in a good agreement of that from Langmuir. For Temkin model, it is assumed that the binding energy decreases linearly with increasing amounts of CO_2 adsorbed on the surface. In our case, the

distribution of binding energy resulted from CO_2 adsorption to active sites can be explained by two parts: a favorable energy from the specific CO_2-to-surface contacts ('intrinsic binding energy') and an unfavorable energy required to match each binding site and CO_2 to make contacts ('rearrangement energy') [177]. The CO_2 molecules will adsorb on the active sites with highest binding energy. Some rearrangement would be required for less optimal patterns of functional groups to obtain the same number of interactions, which will lead to a lower net binding energy. From Table 5.1, it can be seen that Temkin isotherm model fitted better with experimental data at high temperatures. For both Temkin and D-R model, the energy related constants B and E values are in the range of phsisorption process, which is not reflected the real reaction mechanism of the CO_2 adsorption process. The parameter of g from R-P isotherm model is very close to 1 at all the temperatures, resulting in the reduction of R-P model to Langmuir adsorption isotherm model. Other models are the combination of Langmuir and Fruendlich isotherms in different forms. All of them present high R^2 for all three temperatures over the entire experiments. Figure 5.1-5.3 show the comparison of the experimental data of equilibrium CO_2 adsorption capacity with various isotherms as a function of CO_2 partial pressures at 60°C, 75°C and 90°C. In summary, CO_2 adsorption using PEI-impregnated MCFs was a function of temperature. At low temperatures, the Freundlich isotherm model was best fitted with the experimental data. This isotherm model indicates that the CO_2 uptake using this kind of adsorbent was favorable. At higher temperatures, all the isotherm models rather than Freundlich isotherm model are better fitted with the experimental data.

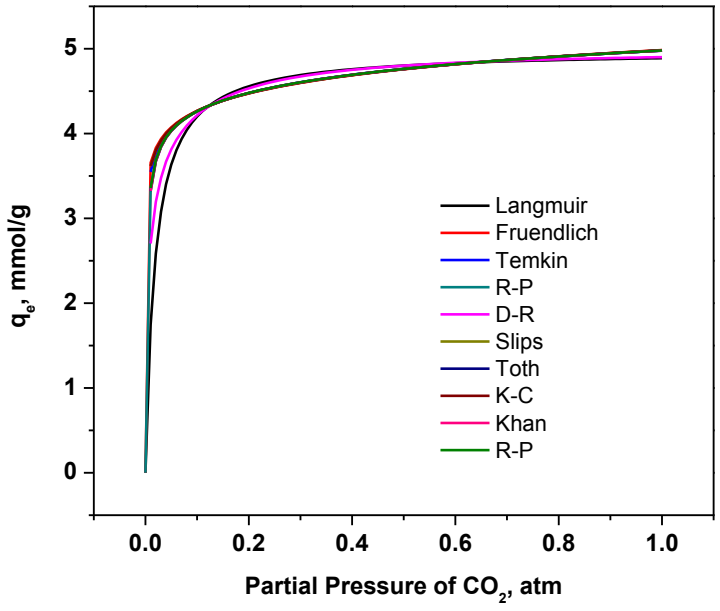

Figure 5.1 Adsorption isotherms using experimental data from TGA under different CO_2 concentrations at 60 °C.

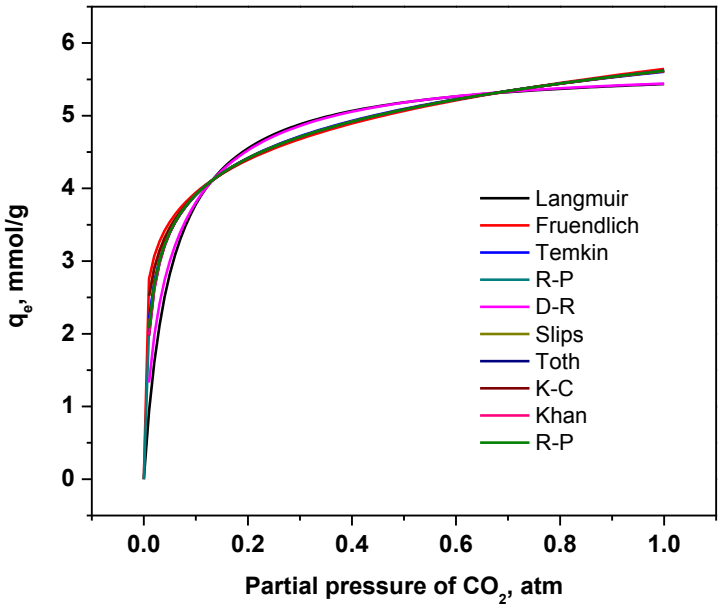

Figure 5.2 Adsorption isotherms using experimental data from TGA under different CO_2 concentrations at 75 °C.

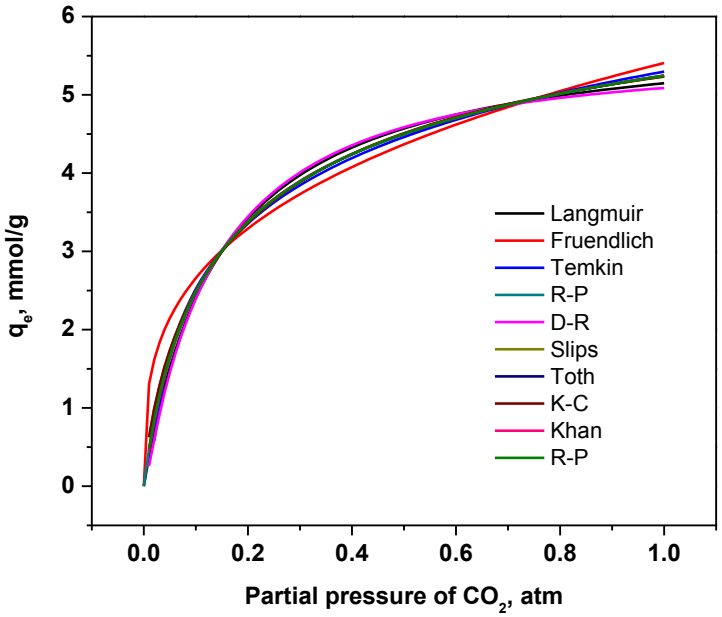

Figure 5.3 Adsorption isotherms using experimental data from TGA under different CO_2 concentrations at 90 °C.

Langmuir separation factor, R_L, can classify different shapes of Langmuir adsorption isotherms. Figure 5.4 shows the Langmuir separation factor as a function of different partial pressures of CO_2 at given temperatures. It can be seen that the values of R_L are in the range of 0 to 1 indicating that CO_2 adsorption performance was favorable using PEI impregnated MCFs. The values of R_L decreased at higher concentrations of CO_2 indicating that the adsorption was less reversible at higher CO_2 concentrations. It also can be seen that higher temperatures are not favorable for CO_2 adsorption at lower CO_2 concentrations. It is probably because that the reaction itself is exothermic. There would be a higher potential for the reactions in the reverse direction at high temperatures. Thereby a loss in CO_2 adsorption capacity was observed at higher

temperatures. It was also observed that an increase in CO_2 concentrations enhanced the CO_2 adsorption process.

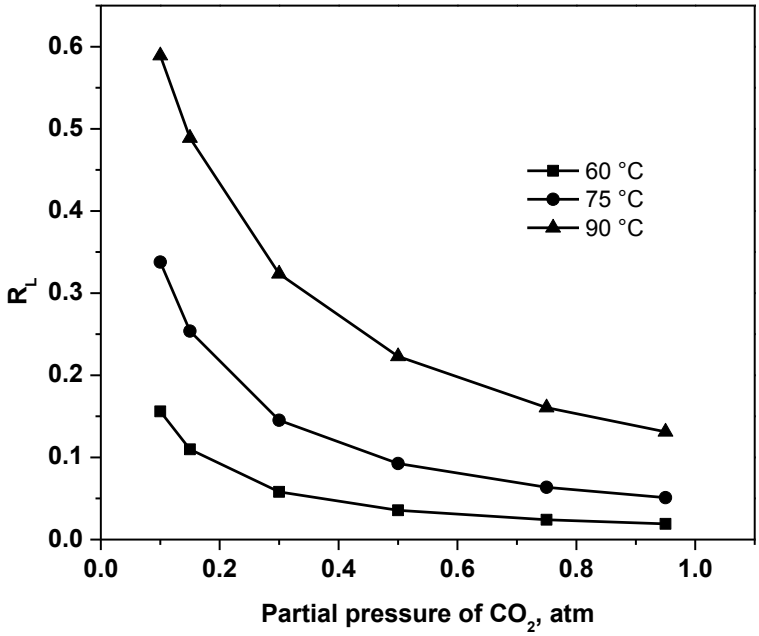

Figure 5.4 Langmuir separation factor under different temperatures.

Chapter 6

John-Mehl-Avrami (JMA) model

6.1 John-Mehl-Avrami (JMA) model

John-Mehl-Avrami (JMA) model is frequently used for the description of crystallization process involving nucleation and growth [178, 179]. It describes the time dependence of fractional extent of crystallization. The JMA model is usually written in the following form [166, 178]:

$$X(t) = 1 - e^{-at^b} \tag{6.1}$$

Where X refers to the fractional extent of crystallization, a is the scale parameter and b is the shape parameter. This equation can be used to describe the transformation kinetic of solid-state processes under isothermal conditions.

According to the nucleation and growth model [166], a is described as a cluster of numerical and growth constants, while b is considered as the kinetic exponent. The decrease in a will increase the slope of curve, resulting in longer time to reach steady state. The shape factor, b, reflects how the nucleation rate changes under isothermal conditions. The increase in b will lead to a steeper uptake curve. The characteristic values of b in diffusion controlled growth process [180] are listed in Table 6.1.

Table 6.1 Values of kinetic exponent for diffusion controlled growth in isothermal conditions [180].

Increasing nucleation rate	>2.5
Constant nucleation rate	=2.5
Decreasing nucleation rate	1.5-2.5
Zero nucleation rate	<1.5

According to JMA model, the gas-solid reactions proceed initially by nucleation, followed by the nuclei growth. There is a delay or induction period for the formation of nuclei [166]. In this case, CO_2 molecules diffuse through the particles and then randomly interact with the amino groups and occupy amine active sites. Once the local concentration of occupied sites exceeds the critical concentration of saturation, the nuclei of carbamate start to form. The formed nuclei will grow larger during the reaction process. Since the CO_2 adsorption process can be described in a manner analogous to the formation of nuclei, JMA model is used to study the kinetics of CO_2 adsorption behavior using PEI-impregnated MCFs.

6.2 Results and discussions

Figure 6.1 shows the experimental CO_2 uptake and its corresponding simulated CO_2 uptake at different temperatures using 10% CO_2/90% N_2. The symbol profiles in different colors refer to the experimental CO_2 uptake at different temperatures. The solid lines in different colors refer to the predicted CO_2 uptake from JMA model. The JMA model constants a and b were obtained by curve fitting with the experimental data using CurveFittingTools available from MATLAB. The corresponding values of a and b in different conditions are summarized in Table 6.2. The values of shape parameter, b, range from 1.7-2.0 for the all the temperatures below 90 °C. At high temperature (90 °C), the value of b decreases approaching unity. When b equals to 1, Eq. (6.1) can be reduced to pseudo-first order model. The significantly higher R^2 value suggests the higher association and thus the applicability of JMA model in the kinetic analysis of CO_2 adsorption. Figure 6.3 presents the experimental CO_2 uptake and simulated CO_2 uptake at different CO_2

concentrations at 75 °C. Again, the degree of agreement is good throughout the entire experiments.

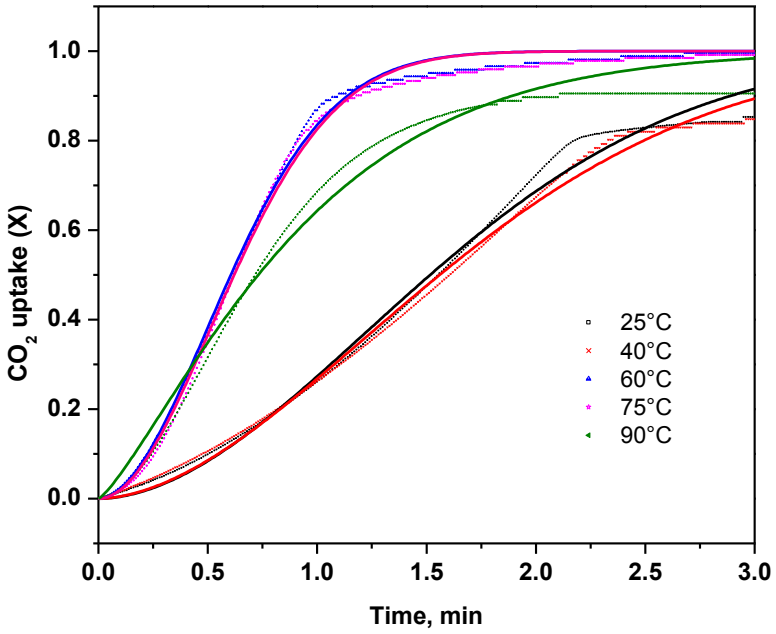

Figure 6.1 Experimental fractional uptake of CO_2 adsorption using 10%CO_2/90%N_2.

Table 6.2 Values of JMA model constants at different temperatures.

Parameters	25 °C	40 °C	60 °C	75 °C	90 °C
a	0.3193	0.3116	1.8	1.744	1.03
b	1.862	1.798	1.901	1.936	1.263
R^2	0.992	0.995	0.996	0.995	0.979

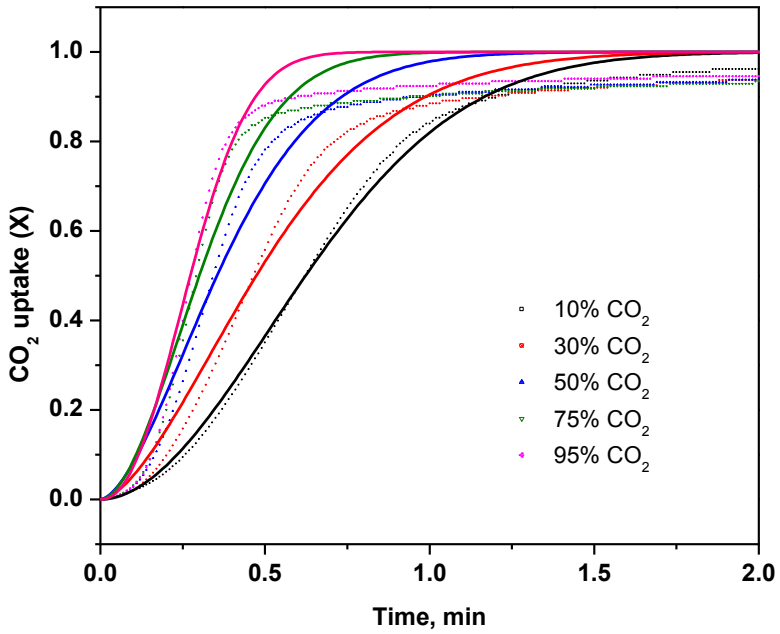

Figure 6.2 Experimental fractional uptake of CO_2 adsorption at different CO_2 concentrations for 75 °C.

Table 6.3 Values of JMA model constants at different CO_2 concentrations.

Parameters	10% CO_2	30% CO_2	50% CO_2	75% CO_2	95% CO_2
a	1.713	0.7617	2.35	3.84	6.372
b	1.914	1.641	1.663	1.649	1.845
R^2	0.994	0.999	0.972	0.950	0.925

Chapter 7

Adsorption kinetics modeling

7.1 Adsorption kinetics models

In this study, for investigating kinetics of CO_2 adsorption using PEI-impregnated MCFs, three commonly used kinetic models, namely Lagergren's pseudo-first order represented by Eq. (7.1) and pseudo-second order represented by Eq. (7.2) and modified fractional-order kinetic model represented by Eq. (7.3) were applied [164, 181, 182].

$$\frac{\partial q_t}{\partial t} = k(q_e - q_t) \tag{7.1}$$

$$\frac{\partial q_t}{\partial t} = k(q_e - q_t)^2 \tag{7.2}$$

$$\frac{\partial q_t}{\partial t} = k_n t^{m-1}(q_e - q_t)^n \tag{7.3}$$

Where,

q_e = adsorption capacity at equilibrium

q_t = adsorption capacity at time *t*

k = rate constant for both pseudo-first order and pseudo-second order models

k_n, *m* and *n* are the model constants for fractional-order model.

After integration and applying the boundary conditions:

at $t = 0$, $q_t = 0$

at $t = \infty$, $q_t = q_e$

The integrated forms of the above three equations become:

$$q_t = q_e(1 - e^{-kt}) \tag{7.4}$$

$$q_t = q_e - \frac{q_e}{1+ktq_e} \tag{7.5}$$

$$q_t = q_e - \left(q_e^{1-n} + \frac{n-1}{m} k_n t^m\right)^{\frac{1}{1-n}} \tag{7.6}$$

The least squares criterion was applied in deducing the characteristic parameters of each model for modeling and optimization in MATLAB. The average absolute percentage deviations (AAPD) presented by Eq. (7.7) was used to determine the agreement degree in fitness between the experimental and predicted adsorption profiles.

$$\text{AAPD\%} = \frac{\sum_{i=1}^{N} \left| \left(q_{e_{exp}} - q_{e_{pred}} \right) / q_{e_{exp}} \right|}{N} \times 100 \tag{7.7}$$

Where

N = total number of experimental points.

q_{exp} = experimental adsorption capacity

q_{cal} = calculated adsorption capacity

7.2 Results and discussions

Figure 7.1-7.5 shows the CO_2 adsorption capacity as a function of time at different adsorption temperatures (e.g. 25 °C, 40 °C, 60 °C, 75 °C, and 90 °C) with a gas mixture of 10% CO_2/90% N_2 and the predicted CO_2 adsorption behavior by pseudo-first, pseudo-second and fractional order models. The optimized parameters for each kinetic model are listed in Table 7.1. As can be seen from Figure 7.1-7.5, the factional order kinetic model is fitted with the experimental data better than the pseudo-first order and pseudo-second order kinetic models. For pseudo-first order and pseudo-second order kinetic models, the CO_2 adsorption capacity at first few minutes is overestimated. It takes some time to adjust to the trend of the experimental profile. After that,

both of the models underestimate the CO_2 adsorption capacity. For fractional-order kinetic model at low temperatures, the CO_2 adsorption behavior using PEI-impregnated MCFs is underestimated. It quickly responded to adjust its predictions approaching to experimental data. Once its prediction is overestimated, it then responds fast to bring it back to near-reality values. At high adsorption temperatures, the fractional-order kinetic model presents the experimental adsorption data more accurately. The extremely low value of AAPD% indicates that the fractional-order kinetic model can describe the CO_2 adsorption behavior using PEI-impregnated MCFs much better compared to the other two models.

Table 7.1 Parametric values of corresponding kinetic models.

Kinetic models	Parameters	25°C	40 °C	60 °C	75 °C	90 °C
Pseudo-first	$k\ (s^{-1})$	0.4003	0.4491	1.2032	1.3618	1.4343
	$q_e(mmol/g)$	2.3747	2.7251	3.5864	3.9835	2.7073
	$AAPD\%$	66.963	66.906	28.269	33.041	23.897
	R^2	0.8690	0.8590	0.8047	0.7436	0.7377
Pseudo-second	$k\ (s^{-1})$	0.2527	0.2534	0.5006	0.5591	0.9535
	$q_e(mmol/g)$	2.5224	2.8783	3.8274	4.2039	2.8341
	$AAPD\%$	35.37	52.062	45.589	97.968	70.945
	R^2	0.9514	0.9416	0.9230	0.8615	0.7846
Fractional	$k_n(mmol^{1-m}g^{m-1}s^{-n})$	0.0071	0.0223	1.3209	3.3658	3.0739
	$q_e(mmol/g)$	2.5626	2.8505	3.6547	3.9681	2.6820
	m	5.3877	4.4703	3.8830	2.8352	1.8619
	n	8.7872	6.1472	4.0177	1.8796	0.9954
	$AAPD\%$	15.715	20.143	7.6524	0.7245	0.6056
	R^2	0.9784	0.9774	0.9871	0.9990	0.9982

From Table 7.1, it can be seen that as adsorption temperature increases beyond 75 °C, the model constant parameter, n, is likely to approach 1, which indicates that it is a near-pseudo-first order reaction influenced by the $(m-1)^{th}$ power of adsorption time. The value of model constant, m, also decreased as temperature increases, which means that the adsorption kinetics is less

dependent on adsorption time at high temperatures. It is probably because at high temperatures, the control of the sorption shifts from diffusion kinetic regime to thermodynamic regime. The increase in temperature facilitates the CO_2 adsorption uptake by overcoming the kinetic barrier for diffusion.

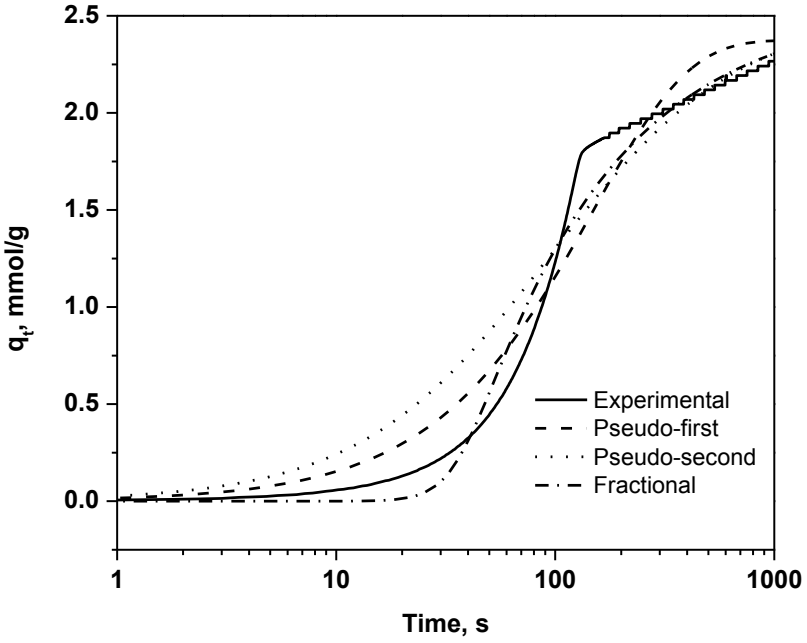

Figure 7.1 Adsorption behavior predicted by different kinetic models at 25 °C.

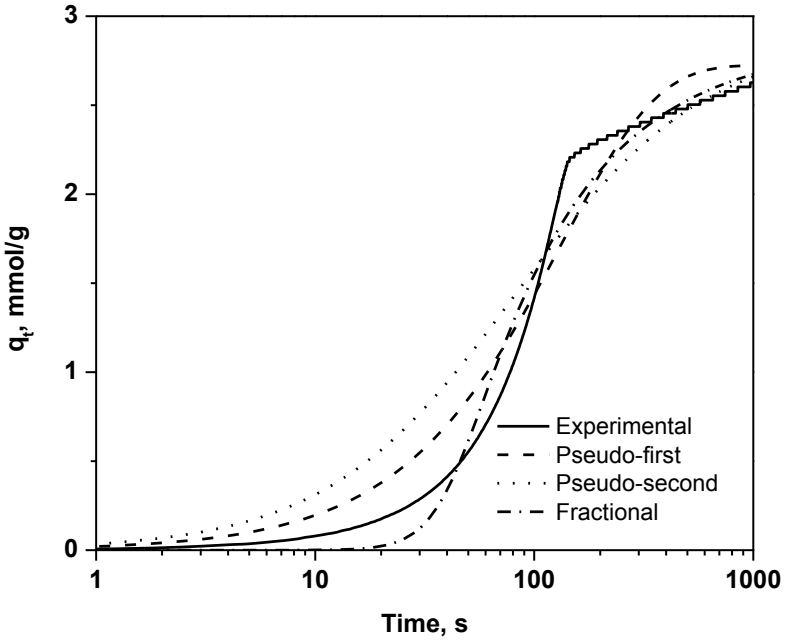

Figure 7.2 Adsorption behavior predicted by different kinetic models at 40 °C.

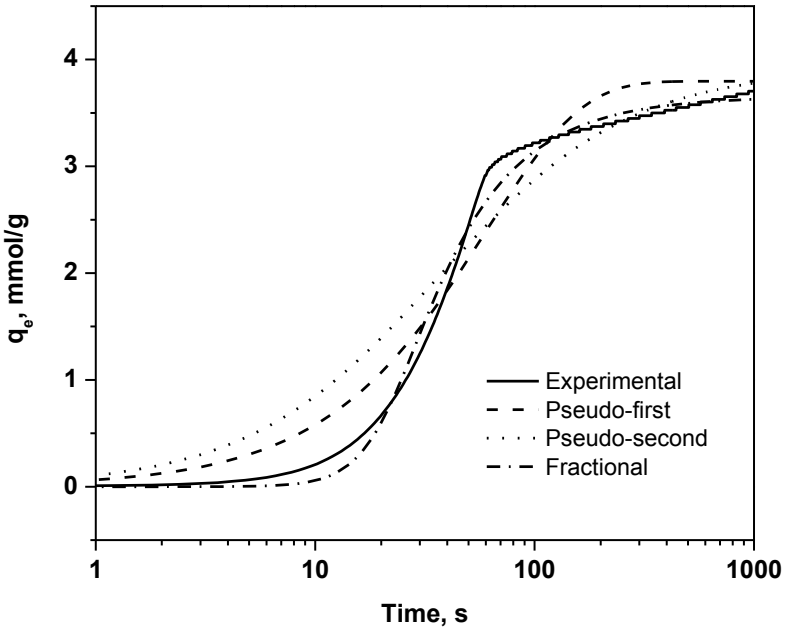

Figure 7.3 Adsorption behavior predicted by different kinetic models at 60 °C.

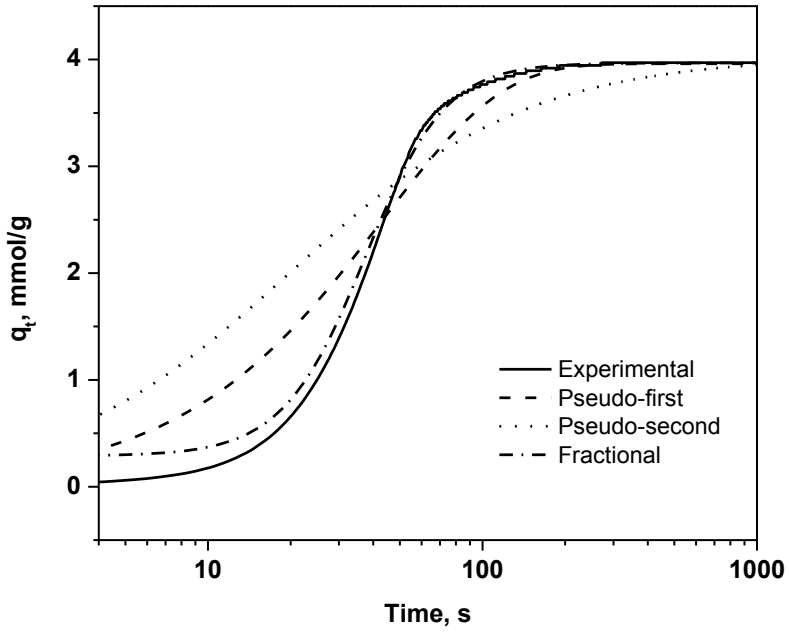

Figure 7.4 Adsorption behavior predicted by different kinetic models at 75 °C.

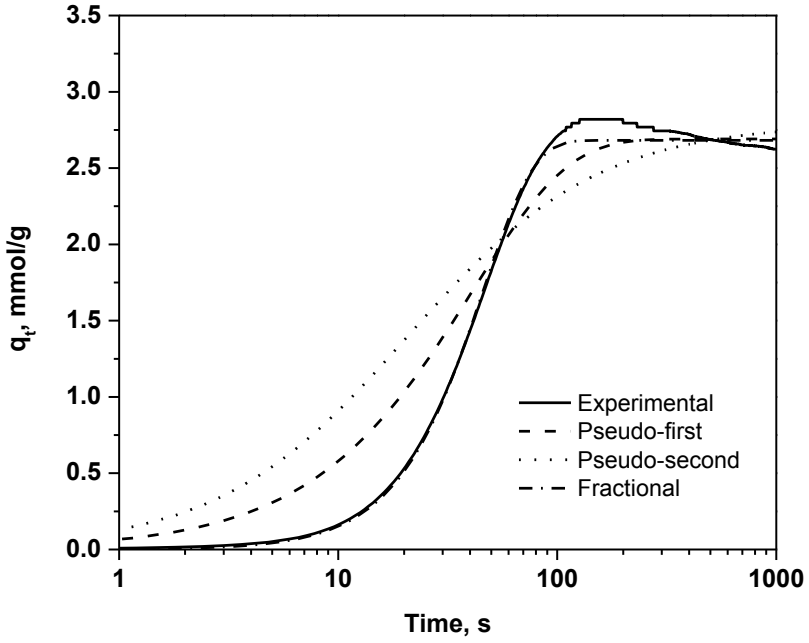

Figure 7.5 Adsorption behavior predicted by different kinetic models at 90 °C.

Chapter 8

Heat of Adsorption

8.1 Heat of adsorption

By applying the Langmuir isotherm, it is possible to establish an expression for the isosteric heat of adsorption in terms of the ratio of the infinitesimal change in the adsorbate enthalpy to the infinitesimal change in the amount adsorbed, as a function of the fractional coverage of the adsorbent $\theta = {}^{q}/_{q_{max}}$ [183]. Eq. (8.1) shows the expression of Langmuir isotherm model.

$$q_e = q_{max} \frac{k_L p}{1+k_L p} \tag{8.1}$$

where q_{max} represents the maximum monolayer coverage capacity in mmol/g of dry adsorbents, and k_L is the adsorption rate constant. The parameter of the Langmuir isotherm k_L, in general is dependent on temperature. Its dependence on temperature can be expressed as follows:

$$k_L = k_0 \exp\left[\frac{Q}{RT_0}\left(\frac{T_0}{T} - 1\right)\right] \tag{8.2}$$

Where k_0 is the value of k_L at the reference temperature T_0, R is the gas constant (8.314 J/mol/K), and Q is a measure of the adsorption heat. It was reported that the following exponential function can be used to describe the dependence of q_{max} on temperature:

$$q_{max} = q_{max,0} \exp\left[\chi\left(1 - \frac{T_0}{T}\right)\right] \tag{8.3}$$

Where $q_{max,0}$ is the value of q_{max} at T_0, χ is an adimensional parameter [183].

It was reported that the isosteric heat of adsorption can be calculated from the Van't Hoff equation :

$$\frac{\Delta H}{RT^2} = -(\frac{\partial lnp}{\partial T})_q \quad (8.4)$$

The heat of adsorption $-\Delta H$ can be obtained by rearranging Eq. (8.1) in terms of p as a function of q, substituting Eq. (8.2) and Eq. (8.3) into it and then taking the derivative of its natural logarithm with respect to T. The resulting heat of adsorption can be displayed in the following expression:

$$-\Delta \mathrm{H} = \mathrm{Q} - \chi RT_0 \frac{q_{max}}{q_{max}-q} \quad (8.5)$$

Since the fractional coverage of the adsorbent can be expressed as follows:

$$\theta = \frac{q}{q_{max}} \quad (8.6)$$

Substituting Eq. (8.6) into Eq. (8.5), it can be obtained as:

$$-\Delta \mathrm{H} = \mathrm{Q} - \frac{\chi RT_0}{1-\theta} \quad (8.7)$$

In order to plot the heat of adsorption as a function of the fractional coverage as shown in Eq. (8.7), it was important to obtain the values of Q and χ. The values of parameters (e.g. $q_{max,0}$, k_0, Q, and χ) from Eqs. (8.2)-(8.3) can be calculated by using the MATLAB with the experimental data of the equilibrium CO_2 adsorption capacity of 70 wt% PEI-impregnated MCFs under different CO_2 concentrations at different temperatures.

8.2 Results and discussions

Table 8.1 displays the calculated values of the four parameters at T_0 = 25 °C using MATLAB.

Table 8.1 Parameters for CO_2 adsorption on 70 wt% PEI with MCFs.

Parameters	$q_{max,0}$ (mol/kg)	k_0 (kPa^{-1})	Q (J/mol)	χ
value	3.561	3319	87268.305	3.08

Figure 8.1 shows the plot of heat of adsorption as a function of fractional coverage of the adsorbent using the best fitting values of χ and Q from MATLAB. It can be observed that the heat of adsorption decreases as the fractional coverage of the adsorbent increases. The heat of adsorption reached zero as the fractional coverage was around 0.91. For higher values of the fractional coverage up to 1, the heat of adsorption becomes negative.

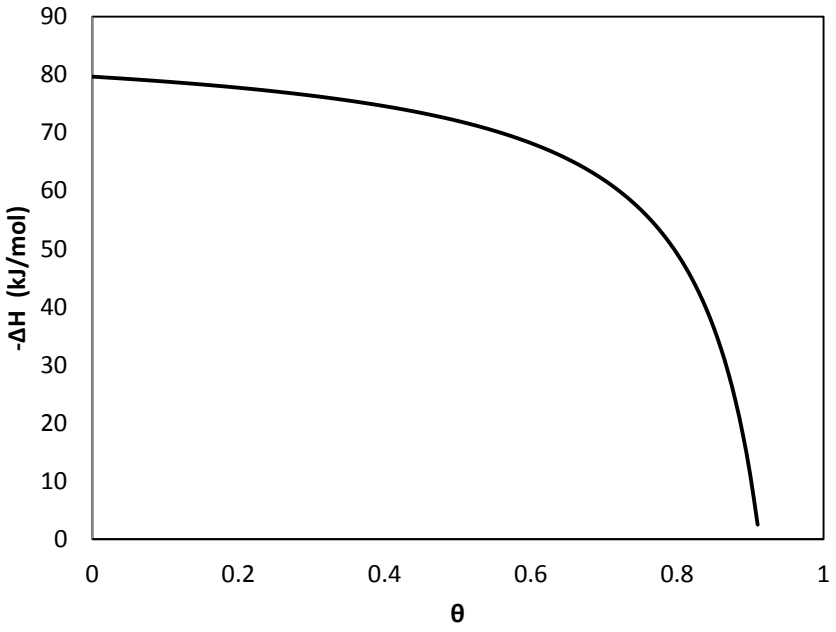

Figure 8.1 Heat of adsorption for CO_2 uptake on 70 wt% PEI with MCFs as a function of fractional coverage of the adsorbent

Chapter 9

Conclusions and Future Work

9.1 Conclusions

In this study, PEI-impregnated MCFs as the solid adsorbents for post-combustion CO_2 capture were synthesized and its performance were evaluated. The findings can be summarized as follows:

1. Calcined MCFs possess a unique 3-D interconnected structure with a high surface area, a large pore volume and pore diameters with narrow pore size distributions.
2. The textural properties of calcined MCFs can be affected by many factors, such as synthesis temperature, amount of TMB, presence of NH_4F, and stirring time.
3. The optimal PEI loading was found to be 70 wt% with maximum CO_2 adsorption capacity of 4 mmol/g in 10% CO_2/ 90% N_2 gas mixture and 5 mmol/g in 95% CO_2/ 5% N_2 gas mixture.
4. The optimal adsorption temperature of PEI-impregnated MCFs was found to be 75 °C with highest CO_2 adsorption and fast kinetics. The low adsorption temperature resulted in a higher kinetic barrier for diffusion. The low CO_2 adsorption capacity at high adsorption temperatures (e.g. 90 °C) is due to the exothermic nature of the reaction.
5. The CO_2 adsorption capacity was observed to increase with partial pressure of CO_2. The CO_2 adsorption capacity increased fast at lower CO_2 partial pressures and then increased slowly at high CO_2 partial pressures.
6. The kinetics of CO_2 adsorption using PEI-impregnated MCFs was observed to be fast. The adsorption process reached equilibrium within first few minutes of adsorption.

7. The heat of adsorption of PEI-impregnated MCFs for CO_2 adsorption obtained from DSC was found to be higher than 60 kJ/mol, which indicates that the chemisorption is dominant.
8. The adsorption capacities of PEI-impregnated MCFs in humid gas mixtures were observed to be much higher than those in dry conditions, especially at low adsorption temperatures. The enhancement of adsorption capacity can be contributed to two parts: moisture adsorption capacity and improved CO_2 adsorption capacity in the presence of moisture. The presence of moisture in the simulated flue gas enhanced the CO_2 adsorption performance at adsorption temperatures no higher than 60 °C. The CO_2 adsorption capacity decreased slightly at adsorption temperature of 75 °C in humid conditions.
9. The regenerability and stability of PEI-impregnated MCFs in 50 multi-cycle CO_2 adsorption/desorption process was found to be good.
10. Various adsorption equilibrium isotherms were applied to study the CO_2 adsorption behavior of PEI-impregnated MCFs. At low temperatures, the Freundlich isotherm model was best fitted with the experimental data. At higher temperatures, all the isotherm models rather than Freundlich isotherm model were better fitted with the experimental data.
11. John-Mehl-Avrami (JMA) model was found to be another way to describe the CO_2 adsorption kinetics using PEI-impregnated MCFs under isothermal conditions.
12. The factional order kinetic model was observed to be fitted with the experimental data better than the pseudo-first order and pseudo-second order kinetic models.
13. The isosteric heat of adsorption using PEI-impregnated MCFs as a function of fractional coverage of the adsorbent was obtained.

9.2 Contribution to original knowledge

The preparation method of MCFs was proposed by Schmidt-Winkel et al. in early 2000. Then after, modifying MCFs with polyamines as solid adsorbents for post-combustion CO_2 capture has been explored by a few researchers. The contributions of the present study in advancing the knowledge in terms of CO_2 adsorption performance of PEI-impregnated MCFs are listed as follows:

1. Synthesized MCFs in this research possess larger pore volume (2.8-3.5 cc/g) compared to those reported in the literature.
2. High CO_2 adsorption capacity of 5 mmol/g in 95% CO_2/5% N_2 gas mixture and 4mmol/g in 10% CO_2/90% N_2 gas mixture and good stability in multi-cycle adsorption/desorption were achieved.
3. Higher CO_2 adsorption capacity with presence of moisture at lower adsorption temperatures was obtained.
4. Equilibrium and kinetic studies on CO_2 adsorption using PEI-impregnated MCFs were explored, which explained the experimental observations.
5. Heat of adsorption of PEI-impregnated MCFs for CO_2 capture was calculated, which is rarely available in literature.

9.3 Future work

Based on the work done so far, there are still some further studies to be investigated as part of the systematic study of CO_2 capturing with PEI-impregnated MCFs for post-combustion process. The details are as follows:

1. Study the methods of improving stability of sorbents for multi-cycle adsorption/ desorption process for CO_2 capture, such as using PEI with larger molecular weight.
2. Explore the effect of SO_x and NO_x in flue gas mixture on the CO_2 adsorption performance of PEI-impregnated MCFs.
3. Investigate the thermal stability and CO_2 adsorption performance of PEI-impregnated MCFs in presence of moisture after multi-cycle adsorption/desorption process in packed bed.

References

[1]. M. Yamaguchi, in Climate Change Mitigation, Springer, **2012**, pp. 7-42.

[2]. IPCC, Climate Change 2013: The Physical Science Basis. Contribution of Working Group I to the Fifth Assessment Report of the Intergovernmental Panel on Climate Change, Cambridge University Press, Cambridge, United Kingdom and New York, NY, USA, **2013**.

[3]. U. S. Briefing, International Energy Outlook 2013, *U.S. Energy Information Administration*, **2013**.

[4]. I. Statistics, CO2 emissions from fuel combustion-highlights, *IEA, Paris http://www. iea. org/co2highlights/co2highlights. pdf. Cited July*, **2011**.

[5]. W. A. W. A. K. Ghani, A. Mohd, G. da Silva, et al., Biochar production from waste rubber-wood-sawdust and its potential use in C sequestration: Chemical and physical characterization, *Industrial Crops and Products*, **2013**, 44 (0): 18-24.

[6]. E. Rubin and H. De Coninck, IPCC special report on carbon dioxide capture and storage, *UK: Cambridge University Press. TNO (2004): Cost Curves for CO2 Storage, Part*, **2005**, 2.

[7]. M. G. Plaza, C. Pevida, B. Arias, et al., A comparison of two methods for producing CO_2 capture adsorbents, *Energy Procedia*, **2009**, 1 (1): 1107-1113.

[8]. M. G. Plaza, C. Pevida, B. Arias, et al., Development of low-cost biomass-based adsorbents for postcombustion CO_2 capture, *Fuel*, **2009**, 88 (12): 2442-2447.

[9]. R. Azargohar and A. K. Dalai, Steam and KOH activation of biochar: Experimental and modeling studies, *Microporous and Mesoporous Materials*, **2008**, 110 (2–3): 413-421.

[10]. J. M. Rosas, J. Bedia, J. Rodríguez-Mirasol, et al., On the preparation and characterization of chars and activated carbons from orange skin, *Fuel Processing Technology*, **2010**, 91 (10): 1345-1354.

[11]. H. Demiral, İ. Demiral, B. Karabacakoğlu, et al., Production of activated carbon from olive bagasse by physical activation, *Chemical Engineering Research and Design*, **2011**, 89 (2): 206-213.

[12]. M. M. Maroto-Valer, Z. Tang and Y. Zhang, CO_2 capture by activated and impregnated anthracites, *Fuel Processing Technology*, **2005**, 86 (14–15): 1487-1502.

[13]. M. G. Plaza, C. Pevida, J. J. Pis, et al., Evaluation of the cyclic capacity of low-cost carbon adsorbents for post-combustion CO_2 capture, *Energy Procedia*, **2011**, 4 (0): 1228-1234.

[14]. M. G. Plaza, C. Pevida, C. F. Martin, et al., Developing almond shell-derived activated carbons as CO_2 adsorbents, *Sep Purif Technol*, **2010**, 71 (1): 102-106.

[15]. A. C. Lua and J. Guo, Activated carbon prepared from oil palm stone by one-step CO_2 activation for gaseous pollutant removal, *Carbon*, **2000**, 38 (7): 1089-1097.

[16]. A. Arami-Niya, W. M. A. W. Daud and F. S. Mjalli, Using granular activated carbon prepared from oil palm shell by $ZnCl_2$ and physical activation for methane adsorption, *Journal of Analytical and Applied Pyrolysis*, **2010**, 89 (2): 197-203.

[17]. W. M. A. W. D. a. F. S. M. A. Arami-Niya, Production of Palm Shell-Based Activated Carbon with More Homogeniouse Pore Size Distribution, *Journal of Applied Sciences*, **2010**, 10: 3361-3366.

[18]. M. Radosz, X. Hu, K. Krutkramelis, et al., Flue-Gas Carbon Capture on Carbonaceous Sorbents: Toward a Low-Cost Multifunctional Carbon Filter for "Green" Energy Producers†, *Industrial & Engineering Chemistry Research*, **2008**, 47 (10): 3783-3794.

[19]. L. K. C. de Souza, N. P. Wickramaratne, A. S. Ello, et al., Enhancement of CO_2 adsorption on phenolic resin-based mesoporous carbons by KOH activation, *Carbon*, **2013**, 65 (0): 334-340.

[20]. M. Balsamo, T. Budinova, A. Erto, et al., CO_2 adsorption onto synthetic activated carbon: Kinetic, thermodynamic and regeneration studies, *Sep Purif Technol*, **2013**, 116 (0): 214-221.

[21]. X.-L. Zhu, P.-Y. Wang, C. Peng, et al., Activated carbon produced from paulownia sawdust for high-performance CO_2 sorbents, *Chinese Chemical Letters* (0).

[22]. S. Deng, H. Wei, T. Chen, et al., Superior CO_2 adsorption on pine nut shell-derived activated carbons and the effective micropores at different temperatures, *Chemical Engineering Journal* (0).

[23]. S.-Y. Lee, H.-M. Yoo, S. W. Park, et al., Preparation and characterization of pitch-based nanoporous carbons for improving CO_2 capture, *Journal of Solid State Chemistry*, **2014**, 215 (0): 201-205.

[24]. A. Heidari, H. Younesi, A. Rashidi, et al., Adsorptive removal of CO_2 on highly microporous activated carbons prepared from Eucalyptus camaldulensis wood: Effect of chemical activation, *Journal of the Taiwan Institute of Chemical Engineers*, **2014**, 45 (2): 579-588.

[25]. K. Berlier and M. Frere, Adsorption of CO_2 on microporous materials. 1. On activated carbon and silica gel, *Journal of Chemical & Engineering Data*, **1997**, 42 (3): 533-537.

[26]. B.-K. Na, K.-K. Koo, H.-M. Eum, et al., CO_2 recovery from flue gas by PSA process using activated carbon, *Korean J. Chem. Eng.*, **2001**, 18 (2): 220-227.

[27]. K. T. Chue, J. N. Kim, Y. J. Yoo, et al., Comparison of Activated Carbon and Zeolite 13X for CO_2 Recovery from Flue Gas by Pressure Swing Adsorption, *Industrial & Engineering Chemistry Research*, **1995**, 34 (2): 591-598.

[28]. C. Lu, H. Bai, B. Wu, et al., Comparative Study of CO_2 Capture by Carbon Nanotubes, Activated Carbons, and Zeolites, *Energy & Fuels*, **2008**, 22 (5): 3050-3056.

[29]. Z. Zhang, M. Xu, H. Wang, et al., Enhancement of CO_2 adsorption on high surface area activated carbon modified by N_2, H_2 and ammonia, *Chemical Engineering Journal*, **2010**, 160 (2): 571-577.

[30]. D. Bezerra, R. Oliveira, R. Vieira, et al., Adsorption of CO_2 on nitrogen-enriched activated carbon and zeolite 13X, *Adsorption*, **2011**, 17 (1): 235-246.

[31]. H. C. Foley, Carbogenic molecular sieves: synthesis, properties and applications, *Microporous Materials*, **1995**, 4 (6): 407-433.

[32]. T. D. Burchell, R. R. Judkins, M. R. Rogers, et al., A novel process and material for the separation of carbon dioxide and hydrogen sulfide gas mixtures, *Carbon*, **1997**, 35 (9): 1279-1294.

[33]. S. W. Rutherford and D. D. Do, Adsorption dynamics of carbon dioxide on a carbon molecular sieve 5A, *Carbon*, **2000**, 38 (9): 1339-1350.

[34]. J. Alcañiz-Monge, J. P. Marco-Lozar and M. Á. Lillo-Ródenas, CO_2 separation by carbon molecular sieve monoliths prepared from nitrated coal tar pitch, *Fuel Processing Technology*, **2011**, 92 (5): 915-919.

[35]. S. Cho, H.-R. Yu, K.-D. Kim, et al., Surface characteristics and carbon dioxide capture characteristics of oxyfluorinated carbon molecular sieves, *Chemical Engineering Journal*, **2012**, 211–212 (0): 89-96.

[36]. A. Wahby, J. Silvestre-Albero, A. Sepúlveda-Escribano, et al., CO_2 adsorption on carbon molecular sieves, *Microporous and Mesoporous Materials*, **2012**, 164 (0): 280-287.

[37]. J. Zhao, A. Buldum, J. Han, et al., Gas molecule adsorption in carbon nanotubes and nanotube bundles, *Nanotechnology*, **2002**, 13 (2): 195.

[38]. M. Bienfait, P. Zeppenfeld, N. Dupont-Pavlovsky, et al., Thermodynamics and structure of hydrogen, methane, argon, oxygen and carbon dioxide adsorbed on single wall carbon nanotube bundles, *Physica B: Condensed Matter*, **2004**, 350 (1–3, Supplement): E423-E426.

[39]. G. P. Lithoxoos, A. Labropoulos, L. D. Peristeras, et al., Adsorption of N_2, CH_4, CO and CO_2 gases in single walled carbon nanotubes: A combined experimental and Monte Carlo molecular simulation study, *The Journal of Supercritical Fluids*, **2010**, 55 (2): 510-523.

[40]. S. S. Razavi, S. M. Hashemianzadeh and H. Karimi, Modeling the adsorptive selectivity of carbon nanotubes for effective separation of CO_2/N_2 mixtures, *Journal of molecular modeling*, **2011**, 17 (5): 1163-1172.

[41]. A. I. Skoulidas, D. S. Sholl and J. K. Johnson, Adsorption and diffusion of carbon dioxide and nitrogen through single-walled carbon nanotube membranes, *The Journal of Chemical Physics*, **2006**, 124 (5): -.

[42]. M. Cinke, J. Li, C. W. Bauschlicher Jr, et al., CO_2 adsorption in single-walled carbon nanotubes, *Chemical Physics Letters*, **2003**, 376 (5–6): 761-766.

[43]. S.-C. Hsu, C. Lu, F. Su, et al., Thermodynamics and regeneration studies of CO_2 adsorption on multiwalled carbon nanotubes, *Chemical Engineering Science*, **2010**, 65 (4): 1354-1361.

[44]. F. Su, C. Lu, W. Cnen, et al., Capture of CO_2 from flue gas via multiwalled carbon nanotubes, *Science of The Total Environment*, **2009**, 407 (8): 3017-3023.

[45]. Q. Sun, M. Wang, Z. Li, et al., CO_2 capture and gas separation on boron carbon nanotubes, *Chemical Physics Letters*, **2013**, 575 (0): 59-66.

[46]. L. Wang, Z. Liu, P. Li, et al., Experimental and modeling investigation on post-combustion carbon dioxide capture using zeolite 13X-APG by hybrid VTSA process, *Chemical Engineering Journal*, **2012**, 197 (0): 151-161.

[47]. W. Won, S. Lee and K. S. Lee, Modeling and parameter estimation for a fixed-bed adsorption process for CO_2 capture using zeolite 13X, *Sep Purif Technol*, **2012**, 85 (0): 120-129.

[48]. R. Krishna and J. M. van Baten, A comparison of the CO_2 capture characteristics of zeolites and metal–organic frameworks, *Sep Purif Technol*, **2012**, 87 (0): 120-126.

[49]. B. J. Maring and P. A. Webley, A new simplified pressure/vacuum swing adsorption model for rapid adsorbent screening for CO_2 capture applications, *International Journal of Greenhouse Gas Control*, **2013**, 15 (0): 16-31.

[50]. X. Li, J. E. Remias, J. K. Neathery, et al., NF/RO faujasite zeolite membrane-ammonia absorption solvent hybrid system for potential post-combustion CO_2 capture application, *Journal of Membrane Science*, **2011**, 366 (1–2): 220-228.

[51]. L. Wang, Y. Yang, W. Shen, et al., Experimental evaluation of adsorption technology for CO_2 capture from flue gas in an existing coal-fired power plant, *Chemical Engineering Science*, **2013**, 101 (0): 615-619.

[52]. E. I. Gkanas, T. A. Steriotis, A. K. Stubos, et al., A complete transport validated model on a zeolite membrane for carbon dioxide permeance and capture, *Applied Thermal Engineering* (0).

[53]. F. Akhtar, L. Andersson, N. Keshavarzi, et al., Colloidal processing and CO_2 capture performance of sacrificially templated zeolite monoliths, *Applied Energy*, **2012**, 97 (0): 289-296.

[54]. E. Ruiz, J. M. Sánchez, M. Maroño, et al., CO_2 capture from PCC power plants using solid sorbents: Bench scale study on synthetic gas, *Fuel*, **2013**, 114 (0): 143-152.

[55]. L. Yu, J. Gong, C. Zeng, et al., Synthesis of binderless zeolite X microspheres and their CO_2 adsorption properties, *Sep Purif Technol*, **2013**, 118 (0): 188-195.

[56]. O. Cheung, Z. Bacsik, Q. Liu, et al., Adsorption kinetics for CO_2 on highly selective zeolites NaKA and nano-NaKA, *Applied Energy*, **2013**, 112 (0): 1326-1336.

[57]. J. Zhang, N. Burke, S. Zhang, et al., Thermodynamic analysis of molecular simulations of CO_2 and CH4 adsorption in FAU zeolites, *Chemical Engineering Science*, **2014**, 113 (0): 54-61.

[58]. H. V. Thang, L. Grajciar, P. Nachtigall, et al., Adsorption of CO_2 in FAU zeolites: Effect of zeolite composition, *Catalysis Today*, **2014**, 227 (0): 50-56.

[59]. M. T. Snider and H. Verweij, Gas sorption studies on Zeolite Y membrane materials for post-combustion CO_2 capture in coal-fired plants, *Microporous and Mesoporous Materials*, **2014**, 192 (0): 3-7.

[60]. Y. H. Ma and C. Mancel, Diffusion studies of CO_2, NO, NO_2, and SO_2 on molecular sieve zeolites by gas chromatography, *AIChE Journal*, **1972**, 18 (6): 1148-1153.

[61]. V. R. Choudhary, S. Mayadevi and A. P. Singh, Sorption isotherms of methane, ethane, ethene and carbon dioxide on NaX, NaY and Na-mordenite zeolites, *Journal of the Chemical Society, Faraday Transactions*, **1995**, 91 (17): 2935-2944.

[62]. V. G. Gomes and K. W. Yee, Pressure swing adsorption for carbon dioxide sequestration from exhaust gases, *Sep Purif Technol*, **2002**, 28 (2): 161-171.

[63]. T. Inui, Y. Okugawa and M. Yasuda, Relationship between properties of various zeolites and their carbon dioxide adsorption behaviors in pressure swing adsorption operation, *Industrial & Engineering Chemistry Research*, **1988**, 27 (7): 1103-1109.

[64]. D. Ko, R. Siriwardane and L. T. Biegler, Optimization of a Pressure-Swing Adsorption Process Using Zeolite 13X for CO_2 Sequestration, *Industrial & Engineering Chemistry Research*, **2002**, 42 (2): 339-348.

[65]. E. Díaz, E. Muñoz, A. Vega, et al., Enhancement of the CO_2 retention capacity of X zeolites by Na- and Cs-treatments, *Chemosphere*, **2008**, 70 (8): 1375-1382.

[66]. P. J. E. Harlick and F. H. Tezel, An experimental adsorbent screening study for CO_2 removal from N2, *Microporous and Mesoporous Materials*, **2004**, 76 (1–3): 71-79.

[67]. Q. Jiang, J. Rentschler, G. Sethia, et al., Synthesis of T-type zeolite nanoparticles for the separation of CO_2/N_2 and CO_2/CH_4 by adsorption process, *Chemical Engineering Journal*, **2013**, 230 (0): 380-388.

[68]. C. Chen and W.-S. Ahn, CO2 adsorption on LTA zeolites: Effect of mesoporosity, *Applied Surface Science* (0).

[69]. C. Chen, D.-W. Park and W.-S. Ahn, CO_2 capture using zeolite 13X prepared from bentonite, *Applied Surface Science*, **2014**, 292 (0): 63-67.

[70]. N. Konduru, P. Lindner and N. M. Assaf-Anid, Curbing the greenhouse effect by carbon dioxide adsorption with Zeolite 13X, *AIChE Journal*, **2007**, 53 (12): 3137-3143.

[71]. A. Zukal, J. Mayerová and M. Kubů, Adsorption of Carbon Dioxide on High-Silica Zeolites with Different Framework Topology, *Top Catal*, **2010**, 53 (19-20): 1361-1366.

[72]. M. Katoh, T. Yoshikawa, T. Tomonari, et al., Adsorption Characteristics of Ion-Exchanged ZSM-5 Zeolites for CO_2/N_2 Mixtures, *Journal of Colloid and Interface Science*, **2000**, 226 (1): 145-150.

[73]. S. Cavenati, C. A. Grande and A. E. Rodrigues, Adsorption Equilibrium of Methane, Carbon Dioxide, and Nitrogen on Zeolite 13X at High Pressures, *Journal of Chemical & Engineering Data*, **2004**, 49 (4): 1095-1101.

[74]. Z. Zhang, W. Zhang, X. Chen, et al., Adsorption of CO_2 on zeolite 13X and activated carbon with higher surface area, *Separation Science and Technology*, **2010**, 45 (5): 710-719.

[75]. R. Hernández-Huesca, L. Díaz and G. Aguilar-Armenta, Adsorption equilibria and kinetics of CO_2, CH_4 and N_2 in natural zeolites, *Sep Purif Technol*, **1999**, 15 (2): 163-173.

[76]. S. Pakseresht, M. Kazemeini and M. M. Akbarnejad, Equilibrium isotherms for CO, CO_2, CH_4 and C_2H_4 on the 5A molecular sieve by a simple volumetric apparatus, *Sep Purif Technol*, **2002**, 28 (1): 53-60.

[77]. R. V. Siriwardane, M.-S. Shen and E. P. Fisher, Adsorption of CO_2, N_2, and O_2 on Natural Zeolites, *Energy & Fuels*, **2003**, 17 (3): 571-576.

[78]. R. V. Siriwardane, M.-S. Shen, E. P. Fisher, et al., Adsorption of CO_2 on Zeolites at Moderate Temperatures, *Energy & Fuels*, **2005**, 19 (3): 1153-1159.

[79]. J. Zhang, R. Singh and P. A. Webley, Alkali and alkaline-earth cation exchanged chabazite zeolites for adsorption based CO_2 capture, *Microporous and Mesoporous Materials*, **2008**, 111 (1–3): 478-487.

[80]. O. M. Yaghi, M. O'Keeffe, N. W. Ockwig, et al., Reticular synthesis and the design of new materials, *Nature*, **2003**, 423 (6941): 705-714.

[81]. S. Saha, S. Chandra, B. Garai, et al., Carbon dioxide capture by metal organic frameworks, *Indian Journal of Chemistry-Part A InorganicPhysical Theoretical and Analytical*, **2012**, 51 (9): 1223.

[82]. R. Banerjee, H. Furukawa, D. Britt, et al., Control of Pore Size and Functionality in Isoreticular Zeolitic Imidazolate Frameworks and their Carbon Dioxide Selective Capture Properties, *Journal of the American Chemical Society*, **2009**, 131 (11): 3875-3877.

[83]. A. Ö. Yazaydın, A. I. Benin, S. A. Faheem, et al., Enhanced CO_2 Adsorption in Metal-Organic Frameworks via Occupation of Open-Metal Sites by Coordinated Water Molecules, *Chemistry of Materials*, **2009**, 21 (8): 1425-1430.

[84]. A. O. z. r. Yazaydın, R. Q. Snurr, T.-H. Park, et al., Screening of metal− organic frameworks for carbon dioxide capture from flue gas using a combined experimental and modeling approach, *Journal of the American Chemical Society*, **2009**, 131 (51): 18198-18199.

[85]. J. Liu, Y. Wang, A. I. Benin, et al., CO_2/H_2O Adsorption Equilibrium and Rates on Metal−Organic Frameworks: HKUST-1 and Ni/DOBDC, *Langmuir*, **2010**, 26 (17): 14301-14307.

[86]. Q. Yang, S. Vaesen, F. Ragon, et al., A Water Stable Metal–Organic Framework with Optimal Features for CO_2 Capture, *Angewandte Chemie International Edition*, **2013**, 52 (39): 10316-10320.

[87]. Y. Zhao, Y. Cao and Q. Zhong, CO_2 Capture on Metal-Organic Framework and Graphene Oxide Composite Using a High-Pressure Static Adsorption Apparatus, *Journal of Clean Energy Technologies*, **2014**, 2 (1).

[88]. H. Hayashi, J. Taniuchi, N. Furuyashiki, et al., Efficient Recovery of Carbon Dioxide from Flue Gases of Coal-Fired Power Plants by Cyclic Fixed-Bed Operations over K2CO3-on-Carbon, *Industrial & Engineering Chemistry Research*, **1998**, 37 (1): 185-191.

[89]. V. Sharonov, A. Okunev and Y. Aristov, Kinetics of carbon dioxide sorption by the composite material K_2CO_3 in Al_2O_3, *Reaction Kinetics and Catalysis Letters*, **2004**, 82 (2): 363-369.

[90]. A. G. Okunev, V. E. Sharonov, A. V. Gubar, et al., Sorption of carbon dioxide by the composite sorbent "potassium carbonate in porous matrix", *Russian Chemical Bulletin*, **2003**, 52 (2): 359-363.

[91]. S. Lee, B. Choi, C. Ryu, et al., The effect of water on the activation and the CO_2 capture capacities of alkali metal-based sorbents, *Korean J. Chem. Eng.*, **2006**, 23 (3): 374-379.

[92]. C. Zhao, X. Chen, C. Zhao, et al., Carbonation and hydration characteristics of dry potassium-based sorbents for CO_2 capture, *Energy & Fuels*, **2009**, 23 (3): 1766-1769.

[93]. C. Zhao, X. Chen and C. Zhao, Effect of crystal structure on CO_2 capture characteristics of dry potassium-based sorbents, *Chemosphere*, **2009**, 75 (10): 1401-1404.

[94]. C. W. Zhao, X. P. Chen and C. S. Zhao, in Proceedings of the 20th International Conference on Fluidized Bed Combustion, eds. G. Yue, H. Zhang, C. Zhao, et al., Springer Berlin Heidelberg, **2010**, pp. 562-568.

[95]. C. Zhao, X. Chen and C. Zhao, CO_2 absorption using dry potassium-based sorbents with different supports, *Energy & Fuels*, **2009**, 23 (9): 4683-4687.

[96]. C. Zhao, X. Chen and C. Zhao, Study on CO_2 capture using dry potassium-based sorbents through orthogonal test method, *International Journal of Greenhouse Gas Control*, **2010**, 4 (4): 655-658.

[97]. C. Zhao, Y. Guo, C. Li, et al., Removal of low concentration CO_2 at ambient temperature using several potassium-based sorbents, *Applied Energy*, **2014**, 124 (0): 241-247.

[98]. C. Zhao, X. Chen, E. J. Anthony, et al., Capturing CO_2 in flue gas from fossil fuel-fired power plants using dry regenerable alkali metal-based sorbent, *Progress in Energy and Combustion Science*, **2013**, 39 (6): 515-534.

[99]. J. B. Lee, T. H. Eom, B. S. Oh, et al., CO_2 capture from flue gas using potassium-based dry regenerable sorbents, *Energy Procedia*, **2011**, 4 (0): 1494-1499.

[100]. Y. C. Park, S.-H. Jo, C. K. Ryu, et al., Long-term operation of carbon dioxide capture system from a real coal-fired flue gas using dry regenerable potassium-based sorbents, *Energy Procedia*, **2009**, 1 (1): 1235-1239.

[101]. S. C. Lee, Y. M. Kwon, S. Y. Jung, et al., Excellent thermal stability of potassium-based sorbent using ZrO_2 for post combustion CO_2 capture, *Fuel*, **2014**, 115 (0): 97-100.

[102]. S. Lee and J. Kim, Dry Potassium-Based Sorbents for CO_2 Capture, *Catal Surv Asia*, **2007**, 11 (4): 171-185.

[103]. S. C. Lee, H. J. Chae, S. J. Lee, et al., Novel regenerable potassium-based dry sorbents for CO_2 capture at low temperatures, *Journal of Molecular Catalysis B: Enzymatic*, **2009**, 56 (2–3): 179-184.

[104]. J. B. Lee, C. K. Ryu, J.-I. Baek, et al., Sodium-Based Dry Regenerable Sorbent for Carbon Dioxide Capture from Power Plant Flue Gas, *Industrial & Engineering Chemistry Research*, **2008**, 47 (13): 4465-4472.

[105]. N. Pojananukij, N. Runruksa, S. Neramittagapong, et al., Synthesis of Alkali Metal/CaO Sorbent for CO_2 Capture Low at Low Temperature, *International Transaction Journal of Engineering, Management & Applied Sciences & Technologies*, **2014**, 5 (1).

[106]. S. C. Lee, B. Y. Choi, T. J. Lee, et al., CO_2 absorption and regeneration of alkali metal-based solid sorbents, *Catalysis Today*, **2006**, 111 (3–4): 385-390.

[107]. C. Ryu, J. Lee, T. Eom, et al., Proceedings of the Fourth Annual Conference on Carbon Capture and Sequestration DOE/NETL, Alexandria, Virginia, USA, **2005**.

[108]. R. R. Kondakindi, G. McCumber, S. Aleksic, et al., Na_2CO_3-based sorbents coated on metal foil: CO_2 capture performance, *International Journal of Greenhouse Gas Control*, **2013**, 15 (0): 65-69.

[109]. C. Pevida, M. G. Plaza, B. Arias, et al., Surface modification of activated carbons for CO_2 capture, *Applied Surface Science*, **2008**, 254 (22): 7165-7172.

[110]. M. G. Plaza, C. Pevida, A. Arenillas, et al., CO_2 capture by adsorption with nitrogen enriched carbons, *Fuel*, **2007**, 86 (14): 2204-2212.

[111]. M. Mercedes Maroto-Valer, Z. Lu, Y. Zhang, et al., Sorbents for CO_2 capture from high carbon fly ashes, *Waste Management*, **2008**, 28 (11): 2320-2328.

[112]. J. Przepiórski, M. Skrodzewicz and A. W. Morawski, High temperature ammonia treatment of activated carbon for enhancement of CO_2 adsorption, *Applied Surface Science*, **2004**, 225 (1–4): 235-242.

[113]. R. J. J. Jansen and H. van Bekkum, Amination and ammoxidation of activated carbons, *Carbon*, **1994**, 32 (8): 1507-1516.

[114]. P. Vinke, M. van der Eijk, M. Verbree, et al., Modification of the surfaces of a gasactivated carbon and a chemically activated carbon with nitric acid, hypochlorite, and ammonia, *Carbon*, **1994**, 32 (4): 675-686.

[115]. B. Stöhr, H. P. Boehm and R. Schlögl, Enhancement of the catalytic activity of activated carbons in oxidation reactions by thermal treatment with ammonia or hydrogen cyanide and observation of a superoxide species as a possible intermediate, *Carbon*, **1991**, 29 (6): 707-720.

[116]. S. Biniak, G. Szymański, J. Siedlewski, et al., The characterization of activated carbons with oxygen and nitrogen surface groups, *Carbon*, **1997**, 35 (12): 1799-1810.

[117]. C. Pevida García, M. González Plaza, B. Arias Rozada, et al., Nitrogen enriched solid sorbents for CO_2 capture, **2007**.

[118]. Z. Tang, Y. Zhang and M. M. Maroto-Valer, Study of the CO_2 adsorption capacities of modified activated anthracites, *Prepr. Pap.-Am. Chem. Soc., Div. Fuel Chem*, **2004**, 49 (1): 308.

[119]. M. L. Gray, Y. Soong, K. J. Champagne, et al., CO_2 capture by amine-enriched fly ash carbon sorbents, *Sep Purif Technol*, **2004**, 35 (1): 31-36.

[120]. I. Zinnen; Hermann A. (Evanston, Oroskar; Anil R. (Downers Grove, IL), Chang; Chin-Hsiung (Palatine, IL), Carbon dioxide removal using aminated carbon molecular sieves,*US Pat.*, **1989**.

[121]. Y. Zhang, M. M. Maroto-Valer and Z. Tang, Microporous activated carbons produced from unburned carbon in fly ash and their application for CO_2 capture.

[122]. A. Arenillas, K. M. Smith, T. C. Drage, et al., CO_2 capture using some fly ash-derived carbon materials, *Fuel*, **2005**, 84 (17): 2204-2210.

[123]. E. P. Dillon, C. A. Crouse and A. R. Barron, Synthesis, Characterization, and Carbon Dioxide Adsorption of Covalently Attached Polyethyleneimine-Functionalized Single-Wall Carbon Nanotubes, *ACS Nano*, **2008**, 2 (1): 156-164.

[124]. M. G. Plaza, S. García, F. Rubiera, et al., Evaluation of ammonia modified and conventionally activated biomass based carbons as CO_2 adsorbents in postcombustion conditions, *Sep Purif Technol*, **2011**, 80 (1): 96-104.

[125]. S. H. Khalil, M. K. Aroua and W. M. A. W. Daud, Study on the improvement of the capacity of amine-impregnated commercial activated carbon beds for CO_2 adsorbing, *Chemical Engineering Journal*, **2012**, 183 (0): 15-20.

[126]. M. M. Gui, Y. X. Yap, S.-P. Chai, et al., Multi-walled carbon nanotubes modified with (3-aminopropyl)triethoxysilane for effective carbon dioxide adsorption, *International Journal of Greenhouse Gas Control*, **2013**, 14 (0): 65-73.

[127]. D. J. Babu, M. Lange, G. Cherkashinin, et al., Gas adsorption studies of CO_2 and N_2 in spatially aligned double-walled carbon nanotube arrays, *Carbon*, **2013**, 61 (0): 616-623.

[128]. Q. Liu, Y. Shi, S. Zheng, et al., Amine-functionalized low-cost industrial grade multi-walled carbon nanotubes for the capture of carbon dioxide, *Journal of Energy Chemistry*, **2014**, 23 (1): 111-118.

[129]. F. Su, C. Lu, A.-J. Chung, et al., CO_2 capture with amine-loaded carbon nanotubes via a dual-column temperature/vacuum swing adsorption, *Applied Energy*, **2014**, 113 (0): 706-712.

[130]. Z. Zhang, B. Wang, Q. Sun, et al., A novel method for the preparation of CO_2 sorption sorbents with high performance, *Applied Energy*, **2014**, 123 (0): 179-184.

[131]. P. D. Jadhav, R. V. Chatti, R. B. Biniwale, et al., Monoethanol Amine Modified Zeolite 13X for CO_2 Adsorption at Different Temperatures, *Energy & Fuels*, **2007**, 21 (6): 3555-3559.

[132]. J. C. Fisher, J. Tanthana and S. S. C. Chuang, Oxide-supported tetraethylenepentamine for CO_2 capture, *Environmental Progress & Sustainable Energy*, **2009**, 28 (4): 589-598.

[133]. F. Su, C. Lu, S.-C. Kuo, et al., Adsorption of CO_2 on Amine-Functionalized Y-Type Zeolites, *Energy & Fuels*, **2010**, 24 (2): 1441-1448.

[134]. K. Kim, S. Lee, J. H. Ryu, et al., An improved CO_2 adsorption efficiency for the zeolites impregnated with the amino group: A molecular simulation approach, *International Journal of Greenhouse Gas Control*, **2013**, 19 (0): 350-357.

[135]. D. Aruldoss, R. Saigoanker, J. D. Savarimuthu, et al., Amine-grafted zeolites-mesoporous ceramics: Synthesis and adsorption characteristics, *Ceramics International*, **2014**, 40 (5): 7583-7587.

[136]. S. Satyapal, T. Filburn, J. Trela, et al., Performance and Properties of a Solid Amine Sorbent for Carbon Dioxide Removal in Space Life Support Applications, *Energy & Fuels*, **2001**, 15 (2): 250-255.

[137]. P. Li, S. Zhang, S. Chen, et al., Preparation and adsorption properties of polyethylenimine containing fibrous adsorbent for carbon dioxide capture, *Journal of applied polymer science*, **2008**, 108 (6): 3851-3858.

[138]. P. Li, B. Ge, S. Zhang, et al., CO_2 capture by polyethylenimine-modified fibrous adsorbent, *Langmuir*, **2008**, 24 (13): 6567-6574.

[139]. C. Pevida, T. C. Drage and C. E. Snape, Silica-templated melamine–formaldehyde resin derived adsorbents for CO_2 capture, *Carbon*, **2008**, 46 (11): 1464-1474.

[140]. D. H. Jo, H. Jung, D. K. Shin, et al., Effect of amine structure on CO_2 adsorption over tetraethylenepentamine impregnated poly methyl methacrylate supports, *Sep Purif Technol*, **2014**, 125 (0): 187-193.

[141]. X. Xu, C. Song, J. M. Andresen, et al., Novel Polyethylenimine-Modified Mesoporous Molecular Sieve of MCM-41 Type as High-Capacity Adsorbent for CO_2 Capture, *Energy & Fuels*, **2002**, 16 (6): 1463-1469.

[142]. X. Xu, C. Song, J. M. Andrésen, et al., Preparation and characterization of novel CO_2 "molecular basket" adsorbents based on polymer-modified mesoporous molecular sieve MCM-41, *Microporous and Mesoporous Materials*, **2003**, 62 (1–2): 29-45.

[143]. X. Xu, C. Song, B. G. Miller, et al., Adsorption separation of carbon dioxide from flue gas of natural gas-fired boiler by a novel nanoporous "molecular basket" adsorbent, *Fuel Processing Technology*, **2005**, 86 (14–15): 1457-1472.

[144]. X. Xu, C. Song, R. Wincek, et al., Separation of CO_2 from Power Plant Flue Gas Using a Novel CO_2 "Molecular Basket" Adsorbent.

[145]. X. Xu, C. Song, B. G. Miller, et al., Influence of moisture on CO_2 separation from gas mixture by a nanoporous adsorbent based on polyethylenimine-modified molecular sieve MCM-41, *Industrial & engineering chemistry research*, **2005**, 44 (21): 8113-8119.

[146]. X. Xu, B. Graeffe and C. Song, Effect of Type of Polymers Loaded in Mesoporous Carbon Dioxide "Molecular Basket" Adsorbent on Carbon Dioxide Separation from Gas Mixtures, *Prepr. Pap.-Am. Chem. Soc., Div. Fuel Chem*, **2004**, 49 (1): 259.

[147]. X. Ma, X. Wang and C. Song, "Molecular Basket" Sorbents for Separation of CO_2 and H_2S from Various Gas Streams, *Journal of the American Chemical Society*, **2009**, 131 (16): 5777-5783.

[148]. W.-J. Son, J.-S. Choi and W.-S. Ahn, Adsorptive removal of carbon dioxide using polyethyleneimine-loaded mesoporous silica materials, *Microporous and Mesoporous Materials*, **2008**, 113 (1–3): 31-40.

[149]. C. Chen, S.-T. Yang, W.-S. Ahn, et al., Amine-impregnated silica monolith with a hierarchical pore structure: enhancement of CO_2 capture capacity, *Chemical Communications*, **2009** (24): 3627-3629.

[150]. M. B. Yue, Y. Chun, Y. Cao, et al., CO_2 Capture by As-Prepared SBA-15 with an Occluded Organic Template, *Advanced Functional Materials*, **2006**, 16 (13): 1717-1722.

[151]. M. B. Yue, L. B. Sun, Y. Cao, et al., Promoting the CO_2 adsorption in the amine-containing SBA-15 by hydroxyl group, *Microporous and Mesoporous Materials*, **2008**, 114 (1–3): 74-81.

[152]. M. B. Yue, L. B. Sun, Y. Cao, et al., Efficient CO_2 Capturer Derived from As-Synthesized MCM-41 Modified with Amine, *Chemistry – A European Journal*, **2008**, 14 (11): 3442-3451.

[153]. A. Goeppert, S. Meth, G. S. Prakash, et al., Nanostructured silica as a support for regenerable high-capacity organoamine-based CO_2 sorbents, *Energy & Environmental Science*, **2010**, 3 (12): 1949-1960.

[154]. N. Gargiulo, D. Caputo and C. Colella, in Studies in Surface Science and Catalysis, eds. Z. G. J. C. Ruren Xu and Y. Wenfu, Elsevier, **2007**, vol. Volume 170, pp. 1938-1943.

[155]. R. S. Franchi, P. J. E. Harlick and A. Sayari, Applications of Pore-Expanded Mesoporous Silica. 2. Development of a High-Capacity, Water-Tolerant Adsorbent for CO_2, *Industrial & Engineering Chemistry Research*, **2005**, 44 (21): 8007-8013.

[156]. G. Qi, Y. Wang, L. Estevez, et al., High efficiency nanocomposite sorbents for CO_2 capture based on amine-functionalized mesoporous capsules, *Energy & Environmental Science*, **2011**, 4 (2): 444-452.

[157]. G. D. Pirngruber, S. Cassiano-Gaspar, S. Louret, et al., Amines immobilized on a solid support for postcombustion CO_2 capture–A preliminary analysis of the performance in a VSA or TSA process based on the adsorption isotherms and kinetic data, *Energy Procedia*, **2009**, 1 (1): 1335-1342.

[158]. A. Arenillas de la Puente, T. C. Drage, K. M. Smith, et al., Thermal stability of polyethylenimine based carbon dioxide adsorbents and its influence on selection of regeneration strategies, **2008**.

[159]. X. Wang, X. Ma, C. Song, et al., Molecular basket sorbents polyethylenimine–SBA-15 for CO_2 capture from flue gas: Characterization and sorption properties, *Microporous and Mesoporous Materials*, **2013**, 169 (0): 103-111.

[160]. E. S. Sanz-Pérez, M. Olivares-Marín, A. Arencibia, et al., CO_2 adsorption performance of amino-functionalized SBA-15 under post-combustion conditions, *International Journal of Greenhouse Gas Control*, **2013**, 17 (0): 366-375.

[161]. C. Chen and W.-S. Ahn, CO_2 capture using mesoporous alumina prepared by a sol–gel process, *Chemical Engineering Journal*, **2011**, 166 (2): 646-651.

[162]. W. Cai, L. Tan, J. Yu, et al., Synthesis of amino-functionalized mesoporous alumina with enhanced affinity towards Cr(VI) and CO_2, *Chemical Engineering Journal*, **2014**, 239 (0): 207-215.

[163]. P. Schmidt-Winkel, W. W. Lukens, P. Yang, et al., Microemulsion templating of siliceous mesostructured cellular foams with well-defined ultralarge mesopores, *Chemistry of Materials*, **2000**, 12 (3): 686-696.

[164]. A. Heydari-Gorji and A. Sayari, CO_2 capture on polyethylenimine-impregnated hydrophobic mesoporous silica: Experimental and kinetic modeling, *Chemical Engineering Journal*, **2011**, 173 (1): 72-79.

[165]. G. Fagerlund, Determination of specific surface by the BET method, *Mat. Constr.*, **1973**, 6 (3): 239-245.

[166]. E. R. Monazam, L. J. Shadle, D. C. Miller, et al., Equilibrium and kinetics analysis of carbon dioxide capture using immobilized amine on a mesoporous silica, *AIChE Journal*, **2013**, 59 (3): 923-935.

[167]. D. J. N. Subagyono, M. Marshall, G. P. Knowles, et al., CO_2 adsorption by amine modified siliceous mesostructured cellular foam (MCF) in humidified gas, *Microporous and Mesoporous Materials*, **2014**, 186 (0): 84-93.

[168]. Y. Ho, J. Porter and G. McKay, Equilibrium isotherm studies for the sorption of divalent metal ions onto peat: copper, nickel and lead single component systems, *Water, Air, and Soil Pollution*, **2002**, 141 (1-4): 1-33.

[169]. K. Y. Foo and B. H. Hameed, Insights into the modeling of adsorption isotherm systems, *Chemical Engineering Journal*, **2010**, 156 (1): 2-10.

[170]. J. He, S. Hong, L. Zhang, et al., Equilibrium and thermodynamic parameters of adsorption of methylene blue onto rectorite, *Fresenius Environmental Bulletin*, **2010**, 19 (11): 2651-2656.

[171]. A. Dada, A. Olalekan, A. Olatunya, et al., Langmuir, Freundlich, Temkin and Dubinin–Radushkevich Isotherms Studies of Equilibrium Sorption of Zn^{2+} Unto Phosphoric Acid Modified Rice Husk, *IOSR Journal of Applied Chemistry*, **2012**, 3 (1): 38-45.

[172]. R. I. Masel, Principles of Adsorption and Reaction on Solid Surfaces, 1st edn., Wiley-Interscience, **1996**.

[173]. R. I. Yousef, B. El-Eswed and A. a. H. Al-Muhtaseb, Adsorption characteristics of natural zeolites as solid adsorbents for phenol removal from aqueous solutions: Kinetics, mechanism, and thermodynamics studies, *Chemical Engineering Journal*, **2011**, 171 (3): 1143-1149.

[174]. I. Tan, B. Hameed and A. Ahmad, Equilibrium and kinetic studies on basic dye adsorption by oil palm fibre activated carbon, *Chemical Engineering Journal*, **2007**, 127 (1): 111-119.

[175]. F. Haghseresht and G. Lu, Adsorption characteristics of phenolic compounds onto coal-reject-derived adsorbents, *Energy & Fuels*, **1998**, 12 (6): 1100-1107.

[176]. S. SRISUDA and B. VIROTE, Adsorption of formaldehyde vapor by amine-functionalized mesoporous silica materials, *Journal of Environmental Sciences*, **2008**, 20 (3): 379-384.

[177]. R. D. Johnson and F. H. Arnold, The temkin isotherm describes heterogeneous protein adsorption, *Biochimica et Biophysica Acta (BBA) - Protein Structure and Molecular Enzymology*, **1995**, 1247 (2): 293-297.

[178]. J. Málek, The applicability of Johnson-Mehl-Avrami model in the thermal analysis of the crystallization kinetics of glasses, *Thermochimica Acta*, **1995**, 267 (0): 61-73.

[179]. Z.-j. YAN, S.-e. DANG, X.-h. WANG, et al., Applicability of Johnson-Mehl-Avrami model to crystallization kinetics of $Zr_{60}Al_{15}Ni_{25}$ bulk amorphous alloy, *Transactions of Nonferrous Metals Society of China*, **2008**, 18 (1): 138-144.

[180]. J. W. Christian, The Theory of Transformations in Metals and Alloys, 2nd edn., *Pergamon*, **1975**.

[181]. Y.-S. Ho, Review of second-order models for adsorption systems, *Journal of Hazardous Materials*, **2006**, 136 (3): 681-689.

[182]. M. Delavar, A. Asghar Ghoreyshi, M. Jahanshahi, et al., Equilibria and kinetics of natural gas adsorption on multi-walled carbon nanotube material, *RSC Advances*, **2012**, 2 (10): 4490-4497.

[183]. N. Gargiulo, F. Pepe and D. Caputo, Modeling carbon dioxide adsorption on polyethylenimine-functionalized TUD-1 mesoporous silica, *Journal of Colloid and Interface Science*, **2012**, 367 (1): 348-354.